

Superconducting Magnets for CLAS12

R. Fair^{a,1}, J. Ballard^b, N. Baltzell^a, R. Banchimanchi^a, G. Biallas^c, V. Burkert^a, G. Cheng^a, L. Elouadrhiri^a, B. Eng^a, P. K. Ghoshal^a, V. Hagen-Gates^c, D. Hampshire^f, L. Harwood^a, J. Hogan^a, D. Insley^a, V. Kashikhin^d, D. Kashy^a, S. Krave^d, O. Kumar^a, M. Laney^a, R. Legg^g, A. Lung^a, C. Luongo^h, A. Makarov^d, F. Martin^b, J. Matalevich^a, M. Mestayer^a, R. Miller^a, W. Moore^a, F. Nobrega^d, W. Oren^a, O. Pastor^b, S. Philip^a, L. Quettierⁱ, R. Rajput-Ghoshal^a, V. Rao Ganni^j, B. Reinhart^a, C. Rode^b, N. Sandoval^a, W. Schneider^c, S. Spiegel^a, E. Stallworth^a, M. Stirbet^a, J. Szal^d, D. Tilles^c, K. Tremblay^a, G. Velev^d, C. Wiggins^a, T. Willard^b, C. Wilson^a, M. Wiseman^a, G. R. Young^c, M. Zarecky^c

^a Thomas Jefferson National Accelerator Facility (TJNAF), Newport News, VA, 23606, USA

^b Previously with Thomas Jefferson National Accelerator Facility (TJNAF), Newport News, VA, 23606, USA

^c Thomas Jefferson National Accelerator Facility, Newport News, VA, 23606, USA (Retired)

^d Fermi National Accelerator Laboratory (FNAL), Batavia, IL, USA

^e University of Houston, Texas, USA (Previously with TJNAF)

^f University of Durham, Durham, UK

^g SLAC National Accelerator Laboratory, Stanford, CA, USA (Previously with TJNAF)

^h International Thermonuclear Experimental Reactor Organization (ITER), St. Paul-lez-Durance 13067, France (Previously with TJNAF)

ⁱ CEA Saclay, France

^j Michigan State University, East Lansing, MI, USA (Previously with TJNAF)

ARTICLE INFO

Keywords:

Superconducting, magnets, torus, solenoid, quench, mapping , toroid

ABSTRACT

As part of the Jefferson Lab 12 GeV upgrade, the Hall B CLAS12 system requires two superconducting iron-free magnets – a torus and a solenoid. The physics requirements to maximize space for the detectors guided engineers towards particular coil designs for each of the magnets which, in turn, led to the choice of using conduction cooling. The torus consists of 6 trapezoidal NbTi coils connected in series with an operating current of 3770 A. The solenoid is an actively shielded 5 T magnet consisting of 5 NbTi coils connected in series operating at 2416 A. Within the hall, the two magnets are located in close proximity to each other and are completely covered both inside and outside by particle detectors. Stringent size limitations were imposed for both magnets and introduced particular design and fabrication challenges. This paper describes the design, construction, installation, commissioning, and operation of the two magnets.

¹ The Manuscript received XXXXXX.

This work was supported by Jefferson Science Associates, LLC, under U.S. DOE Contract DE-AC05-06OR23177. The U.S. Government retains a non-exclusive, paid-up, irrevocable, world-wide license to publish or reproduce this manuscript for U.S. Government purposes.

Corresponding author: R Fair (e-mail: rfair@jlab.org)

Color versions of one or more of the figures in this paper are available online at XXXXXXXX

Digital Object Identifier (inserted by Publisher)

I. PHYSICS REQUIREMENTS AND TECHNICAL SPECS

The CEBAF Large Acceptance Spectrometer for 12 GeV (CLAS12) is a new detector system within Hall B at Jefferson Laboratory (JLab) designed to measure **electron**-induced reactions over a broad kinematic phase space. It consists of two large superconducting magnets, a 6-coil torus and a 5-coil solenoid. The solenoid magnet is located upstream of the torus magnet and provides a field to bend low energy (300 MeV to 1.5 GeV) charged particles. The field also provides focusing and shielding for Moeller electrons, which allows the detector system to run at high data rates. A homogeneous field at the magnet center is needed for polarized targets. The torus provides a bending field for high energy (0.5 GeV to 10 GeV) charged particles and mechanical support for 3 regions of drift chambers.

Tables I and II summarize the physics requirements for the torus and solenoid superconducting magnets, respectively, while **Table III** provides a summary of the key design parameters for the two magnets. **Figure 1** shows photographs of the two magnets.

TABLE I
CLAS12 HALL B - TORUS PHYSICS REQUIREMENTS

Parameters	Requirement
Angular coverage	$\Theta = 5^\circ - 40^\circ$ $\Delta\Theta = 50\text{-}90\%$ of 2π
$\int B \cdot dl$ @ nominal current	2.83 T.m @ $\Theta = 5^\circ$ 0.6-1.0 T.m @ $\Theta = 40^\circ$
Access	Open access to field volume on either side of beamline
Uniformity of B-field in Θ	Limit distortions from toroidal field

TABLE II
CLAS12 HALL B – SOLENOID PHYSICS REQUIREMENTS

Parameters	Requirement
B_0	5 T
$L=1/B_0 \int B dl$	$L = 1$ to 1.4 m
Field uniformity in target Area	$\Delta B/B_0 < 10^{-4}$ in cylinder 0.04 m length x 0.025 m (100 ppm)
Field at HTCC PMTs	$B < 35$ G (for the four HTCC PMT locations) [Ref?]
Field at TOF PMTs	$B < 1200$ G (for the two CTOF PMT locations) [Ref?]

TABLE III
CLAS12 HALL B - SOLENOID AND TORUS MAGNET PARAMETERS

PARAMETER	DESIGN VALUE	
	SOLENOID	TORUS
Number of Coils	4 + 1	6
Coil structure	Layer wound	Double pancake potted in aluminum case
Total number of turns	5096 (2 x 840 + 2 x 1012+1392)	1404 (117 x 2 x 6)
NbTi Rutherford cable	SSC 36 strands	SSC 36 strands
Nominal current (A)	2416	3770
Central field (T)	5	N/A
Conductor peak field (T)	6.56	3.6
Field homogeneity in	1×10^{-4}	N/A

$\phi 25\text{mm} \times L40\text{ mm}$ cylinder		
Inductance (H)	5.89	2
Stored energy (MJ)	17	14
Warm bore (mm)	780	124
Outer diameter x length	2.16 m x1.8 m	N/A
Inner bore length /opening angle	0.897 m/41°	N/A
Coil case thickness	-	Originally 100mm changed to 125mm
Total weight (KG)	18800	25500
Cooling mode	Conduction cooled	Conduction cooled
Supply temperature (K)	4.5	4.5
Temperature margin	1.5	1.5
Stabilized conductor	W17 mm x T2.5 mm copper channel	W20 mm x T2.5 mm copper channel
Turn to turn insulation	0.004" glass tape $\frac{1}{2}$ Lap	0.003" glass tape $\frac{1}{2}$ lap
Heat shield cooling	Helium boil-off	LN ₂ thermo-siphon

The torus magnet, the Torus Service Tower (TST) and Cryogenic Distribution Box (DBX), were designed and assembled at JLab, while the coils were fabricated at the Fermi National Accelerator Laboratory (FNAL), USA [2,3]. The solenoid magnet was designed and fabricated by Everson Tesla Inc., USA (ETI), while the Solenoid Service Tower (SST) and cryogenics were designed and fabricated by JLab. The magnets differ in their cooling schemes from that of more conventional bath-cooled superconducting magnets by using conduction-cooling methodology in order to comply with tight physical space requirements. These requirements imposed certain size limitations on the design of the torus and solenoid magnet coils, which led to each magnet having their own unique issues for design, fabrication and installation [4]. Leftover NbTi Rutherford superconductor cable from the Superconducting Super Collider (SSC) project (which was terminated in 1993) was modified by soldering the cable into a C-shaped copper channel and then used to wind the coils for both the torus and solenoid.

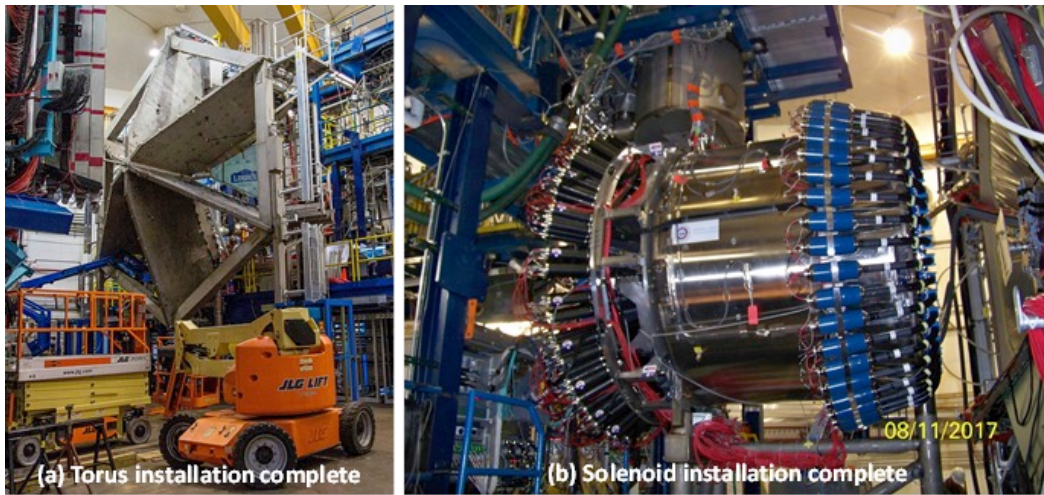


Fig.1 Magnets installed in Hall B – (a) Torus (before drift chambers were installed between the coils), (b) Solenoid (with some detectors installed).

II. PROJECT MANAGEMENT AND RISK MITIGATION APPROACH

The Hall B torus and solenoid magnets were part of the JLab 12 GeV Upgrade project, which included an upgrade to the accelerator and three of the four experimental halls B, C, and D. The project involved the fabrication, installation, and commissioning of a total of 8 superconducting magnet systems [1]. A Magnet Task Force was set up at JLab in order to provide consistency in the

management of the various activities and to promote the sharing of lessons learned between the different magnet systems and halls. The task force leader had overall technical responsibility for all the magnets, including the Hall B torus and solenoid magnets, and oversaw the timely completion of all tasks. Key procurements (for example individual magnets and magnet power supplies) were overseen by the respective Subcontract Officers from the JLab Procurement Department with technical assistance being provided by Subcontract Officer Technical Representatives (SOTRs). Multiple design and manufacturing reviews were held for each magnet and other key components, most of which were face to face. Progress tracking, problem-solving meetings, and teleconference calls were held with the various vendors on either a regular schedule or on an as needed basis. JLab staff also provided oversight at the vendors' premises, especially during key manufacturing stages.

All critical tasks and systems of the magnets of the CLAS12 system, both torus and solenoid, were subjected to a detailed Risk Assessment and Mitigation (RAM) process. The process was used to evaluate the overall magnet design and the robustness of its protection system and commissioning process. The magnet risk assessments were developed via a series of electromagnetic and electromechanical analyses, which included induced eddy currents, Lorentz forces, thermal loading, magnet-to-magnet interactions, and an assessment of magnet performance while in proximity to ferromagnetic structures. The assessments also included things like loss of control power, loss of main power, loss of cryogenic supply, and loss of vacuum. The risk mitigation approach was based on a Failure Modes and Effects Analysis (FMEA) carried out for each phase of the project: design, fabrication, installation, and commissioning [5]. FMEA is a tool used to eliminate or mitigate known potential failures, problems, and errors within systems. A failure mode is defined as the way a component could fail to meet its performance requirements or to function. More than 400 risk items were identified, categorized, and ranked; mitigation avenues were investigated for all risks, and implemented when warranted, either because the risk was deemed to be high, or implementation was easily achieved.

The potential failure modes were evaluated based on a Risk Priority Number (RPN), which is the product of three factors: the Severity ranking (S), the probability of Occurrence (O), and the probability of Detection (D). The RPN was used as a measure of overall risk and helped to identify and rank the risks of the potential failure modes. The end results of failures that lead to unsafe conditions or significant losses in functionality were rated high in severity. Larger RPNs indicated the need for corrective action or failure resolution. The FMEA process was used to assist in identifying potential failure modes early in the design phase.

Several of the key risks for the torus and solenoid (indicated by larger RPNs) are listed below and were addressed during the project:

- The system does not satisfy the physics requirements
- Defects in the build and manufacture of thermal insulation (e.g. standoffs, multi-layer insulation)
- Insufficient helium mass flow in the cooling channel
- Vacuum vessel cannot maintain required vacuum

- Breakdown of the electrical insulation of magnet system
- Loss of control of the magnet power supply system
- Loss of magnet protection due to a fault in the quench detection and protection system

Some of the mitigation actions stemming from the FMEA included:

- Extensive use of mock-ups and practice builds for all quality-critical activities (e.g. conductor soldering into channel, conductor splices, distortion of vacuum jackets during welding, connection of hex beams to coils, mounting of instrumentation)
- Development of written procedures, before and in conjunction with the practice builds
- Safety and risk-awareness meetings prior to each critical operation
- Extensive use of in-process quality assurance (QA) checks
- Detailed weekly and daily planning of installation activities in the hall
- Vendor oversight by JLab staff

Safety reviews, as well as Director's Reviews, Magnet Advisory Group Meetings, and Department of Energy Reviews, played a crucial role in developing the RAM process at JLab as well as to guide the technical path, verify resources, and check project progress. Safety reviews in particular comprised two key sub-reviews - Pressure System Reviews (which checked against relevant design codes like ASME and also ensured all relevant documentation was in place), and Experimental Readiness Reviews (Cool down and Power-up reviews) before the magnet systems were signed over to the JLab Physics Division for operation.

III. DESIGN AND ANALYSIS

The coils for the two magnets utilized surplus Superconducting Collider (SSC) outer dipole conductor consisting of 36 strands of 0.6 mm diameter multi-filament NbTi superconductor with a Cu:Sc ratio of 1.8 : 1, manufactured as a keystone Rutherford cable and soldered into a nominally dimensioned 2.5 mm × 20 mm OFHC copper channel for the torus and a 2.5mm x 17 mm channel for the solenoid (see [Figure 2 and Table IV](#) for details). This Rutherford conductor had been in storage for many years, so sample lengths of conductor from each spool were tested to check for any degradation in performance. The superconductor for the magnets has a tested short sample performance of better than 11000 A at 4.2 K at 5 T and showed no discernable degradation when compared to its original specifications.

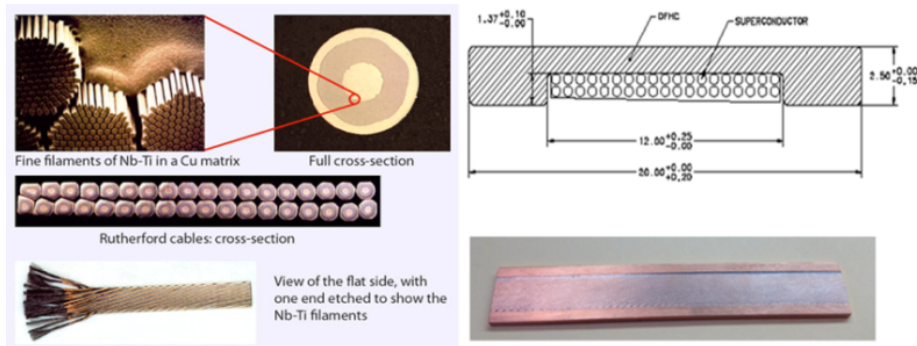


Fig 2. SSC Outer Dipole NbTi Rutherford Cable and cross-sectional view of the conductor with critical dimensions.

TORUS

Torus Magnet Design

TABLE IV
TORUS CONDUCTOR SPECIFICATION

Parameter	Details
Rutherford type of cable (Superconductor)	NbTi
Conductor material (NbTi + Cu)	Cu-(NbTi) in Cu channel
Number of strands in the cable	36
Number of NbTi filaments in each strand	4600
Strand bare diameter (mm)	0.648
Copper to non-copper ratio	1.8
Twist pitch (mm)	15
Conductor size (bare) (mm x mm)	20 x 2.5
Conductor size (insulated) (mm x mm)	20.2 x 2.7
Short sample current at 4.22 K, 5 T (kA)	11
RRR Cu (Cu-NbTi) – Strand	100
RRR Cu stabilizer (design)	200 (70)

(a)

- Cold Mass (4 and 80 K) = 11,000 Kg
- Heat Load analysis summary
 - 4K load on magnet proper = 46 W
 - 80K load on magnet proper = 794 W
 - 4K total load = 69 W
 - 80K total load = 890 W
 - 4K load for ANALYSIS & DESIGN on magnet = 80W
 - 80K Load for ANALYSIS & DESIGN on magnet = 1200 W

(b)

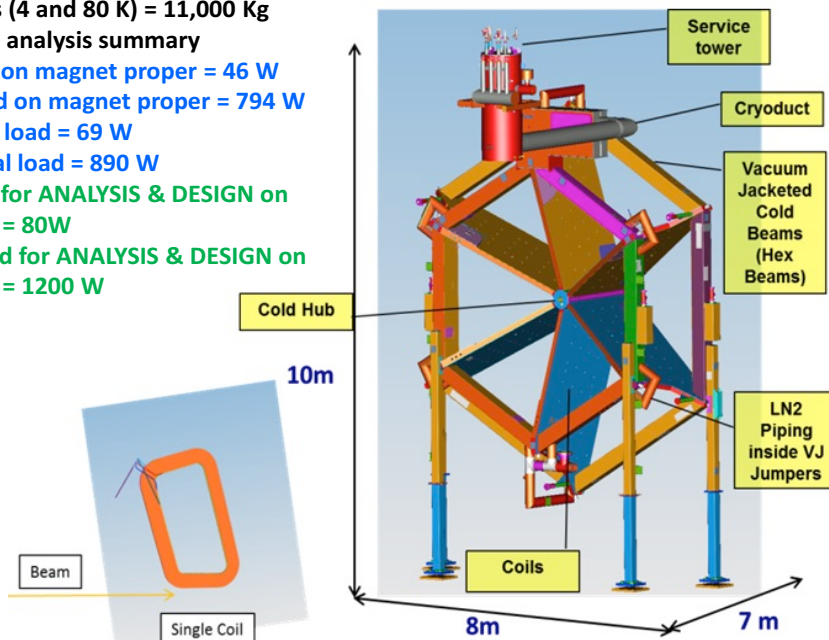


Fig 3. The torus magnet (a) design heat loads, (b) key features and dimensions.

The torus magnet has 6 double-pancake, trapezoidal-shaped coils wound with copper-stabilized NbTi Rutherford cable, which were vacuum impregnated with epoxy, wrapped with copper cooling sheets, assembled in aluminum cases, and then epoxy-impregnated a second time, to produce a coil cold mass (CCM) which operates at 4.5 K. Pre-formed multi-layer insulation (MLI) blankets were fitted to each CCM. Aluminum thermal shields, (cooled to 80 K by a liquid nitrogen thermo-siphon), surround each CCM and themselves were covered with additional MLI blankets. The whole assembly is enclosed within a welded stainless steel vacuum jacket. The 6 independent CCMs are mechanically held together at a cold hub positioned along the axis of the torus. The CCMs are connected to each other on their outer extremities via 12 hex beams, which are conduction cooled to 4.5 K. There are two hex beams per sector, upstream and downstream (see [Figure 3](#)). The six coils are electrically connected in series using soldered joints (splices). The system has three hydraulic circuits all supplied by the Torus Service Tower (TST) – supercritical helium to indirectly cool the coils, atmospheric helium running through the re-coolers and a liquid-nitrogen circuit for the thermal shields. A liquid-filled (4.5 K, 1.4 atmosphere) helium re-cooler (tube in shell heat exchanger) is mounted to each upstream hex beam. The coil to coil splices are mounted to and cooled by these re-coolers. The re-coolers remove heat input at each coil before entering the next coil and thus maintain equal helium inlet temperatures to each coil. A small fraction of the boiloff from the re-coolers is used to cool the magnet's vapor-cooled current leads, the rest is sent back to the refrigerator. All six coils share a common vacuum space with two vacuum pumping systems being operated continuously - at the top and bottom of the torus magnet. A single distribution box (DBX) supplies both the torus and the solenoid magnets.

Torus Superconducting Coil Design

The torus magnet coils generate a toroidal magnetic field. [Figure 4a](#) illustrates the magnetic field distribution on the coil surface. The peak field of 3.6 T is located at the coil inner bore surface and is almost half this value at the coil's outer radius. [Figure 4b](#) indicates the temperature distribution across the coil, with the ‘warmest’ part of coil having the highest thermal radiation heat load near the lead exit due to the extended surface of the coil case at the hex rings.

[Figure 5](#) summarizes the performance of the superconducting Rutherford cable used for both the torus and solenoid magnets in the form of a set of critical current curves at varying operating temperatures. The load lines for the torus and solenoid magnets are displayed as straight lines labeled I_{coil} .

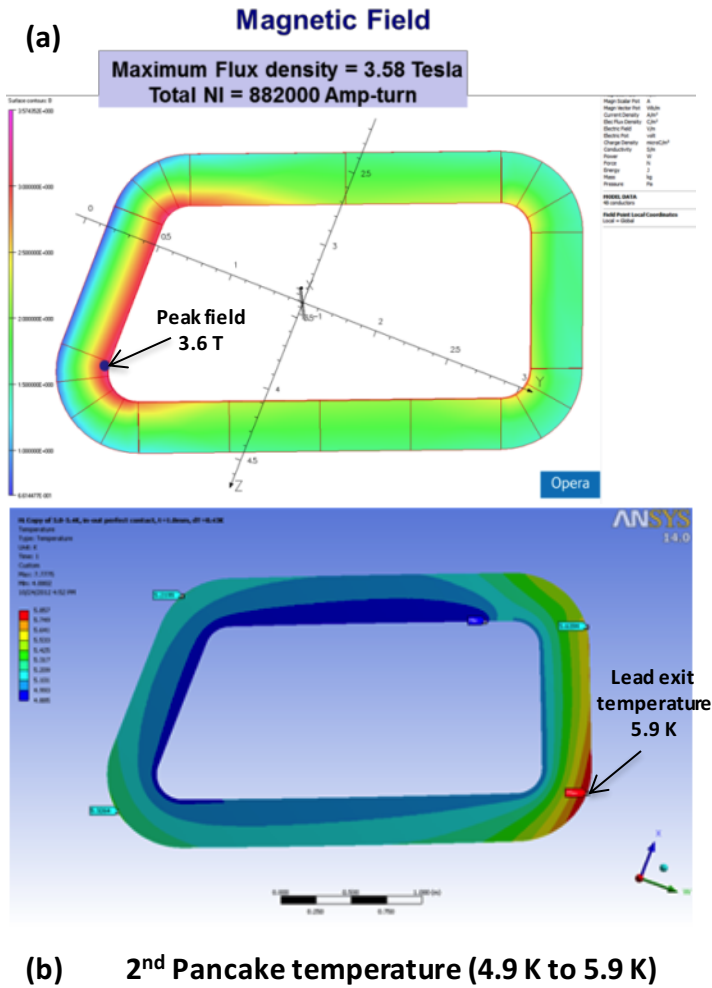
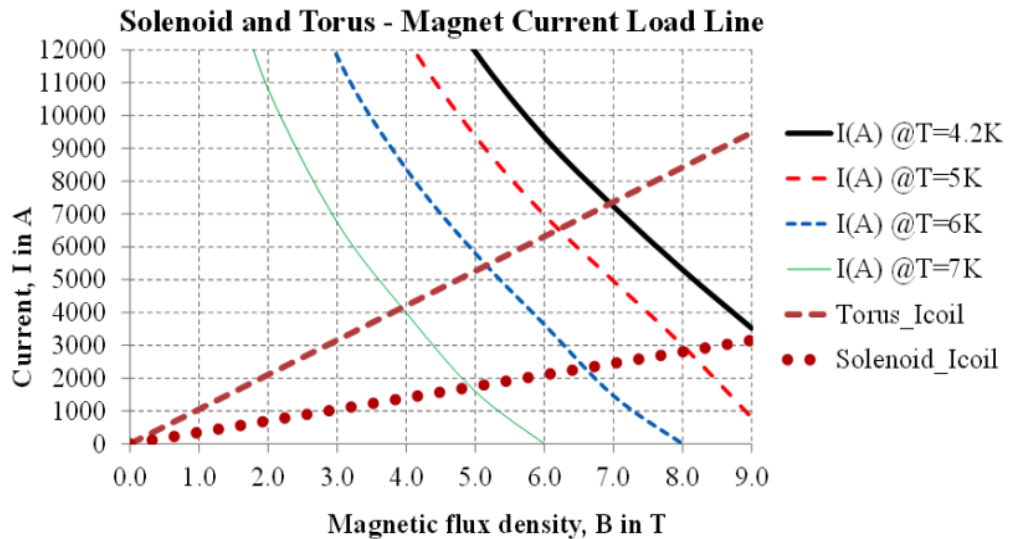
(b) 2nd Pancake temperature (4.9 K to 5.9 K)

Fig 4 (a) Magnetic field distribution on the torus coil surface with the magnet at 3770 A, (b) Steady state temperature distribution on the torus coil surface (assuming 3x design heat load).

**Fig.5** Superconducting Rutherford cable critical current – solenoid and torus magnet load lines (I_{coil}).

An assessment of the conductor stability for the torus is summarized in **Table V**.

TABLE V
SUMMARY OF TORUS CONDUCTOR STABILITY ASSESSMENT [6]

Operating Scenario (Hall B Torus)		
Conductor temperature_ T_{op} (K)	5.3	K
Maximum field in the coil_ B_{max} (T)	3.58	T
Operating current_ I_{op} (A)	3770	A
I_c (at B_{max}) (A) at T_{op}	9836	
Summary		
Short sample performance (SSP)	< 40%	38.33%
Stable for T_{cs} value (Margin)	Yes	>1.5 K
Stable for Beta (Adiabatic stability)	Yes	
Adiabatic flux jump stability	Yes	
Dynamic stability	Yes	
Adiabatic self-field stability	Yes	
Stable in term of twist pitch	Yes	
Stable for finite element size	Yes	

As can be seen from **Figure 5** and **Table VI**, the torus coil design has a more than adequate temperature margin ΔT , which in all cases exceeds the usual design guidance of 1.5 K, strongly suggesting that the magnet coils are tolerant to temperature variations.

- Case #1: Operating temperature (T_{op}) 4.7 K (1st pancake), B_{max}
- Case #2: $T_{op}=4.9$ K (2nd pancake), B_{max}
- Case #3: $T_{op}=5.3$ K (2nd pancake), B_{max}
- Case #4: $T_{op}=5.3$ K (2nd pancake), B_{max} (2 lost strands)
- Case #5: $T_{op}=5.9$ K (2nd pancake), $B = 1.5$ T (lead exit)

TABLE VI
TORUS MAGNET MARGIN AND SSP

Case	B_{max} (T)	I_c (at B_{max}) (A) at T_{op}	I_{op} (A)	% SSP	T_{op} (K)	T_c (K)	T_g (K)	ΔT (K) = T_g (K) – T_{op} (K)
1	3.58	12076	3770	31.22	4.7	7.86	6.87	2.17
2	3.58	11332	3770	33.27	4.9	7.86	6.88	1.98
3	3.58	9836	3770	38.33	5.3	7.86	6.88	1.58
4	3.58	9285	3770	40.60	5.3	7.86	6.82	1.52
5	1.5	11467	3770	32.88	5.9	8.75	7.81	1.91

The magnet coils are protected via an externally located dump resistor that is permanently connected across the magnet terminals. This resistor has a center tap that then feeds a ground-fault indicator. The presence of this center tap produces an expected maximum voltage across the magnet during a typical quench scenario of 250 V. However, in the unlikely event that the center tap is lost, the voltage across the magnet terminals could increase to a peak of 500 V and this value together with a safety factor was used to determine the overall design for the coil turn insulation, pancake-to-pancake insulation and the Turn-to-Ground insulation (see **Figure 6** and **Table VII**) [6]. A similar approach was used to define the solenoid coil insulation.

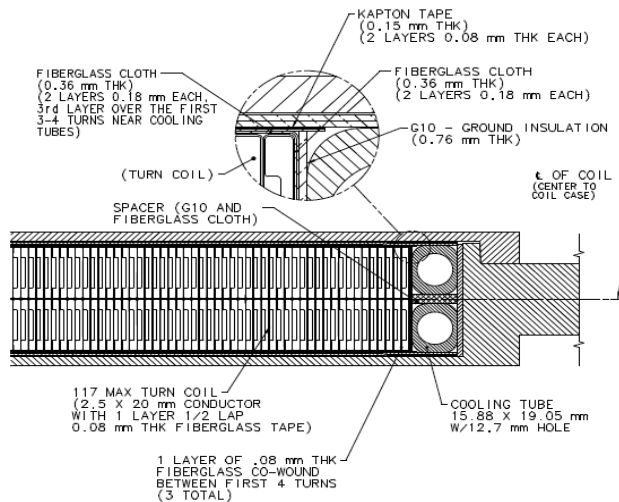


Fig. 6 Partial construction detail for the torus coils, showing the conduction cooling mechanism and coil winding details. The coil cross section inside of the aluminum case is 353 x 45 mm.

TABLE VII
TORUS COIL ELECTRICAL INSULATION BREAKDOWN VOLTAGE [6]

Material	E-Glass with Epoxy	G10	Kapton
Insulation Region	Thickness (mm)	Thickness (mm)	Thickness (mm)
Turn to Turn Insulation (T-T)	0.3048	0	0
Turn to Turn Insulation (P-P)	0.3048	0.38	0
Turn to Ground (GND)	0.508	0	0.1524
Location	Turn to Turn	Pancake- Pancake	Turn to GND
Breakdown Voltage (kV) - calculated	7.01	15.75 kV	21.74 kV
Factor of safety	10	10	5
Breakdown voltage (kV) with safety factor used for design	0.7	1.58	4.35
Torus magnet 12 GeV (V) expected	< 10	< 120	< 250 (500*)

* Rare fault case resulting in 500V

Additional analyses were carried out to ensure that the coil pack and coil case stresses were within acceptable limits during normal operation (see Table VIII) [5], [6-11].

TABLE VIII
TORUS STRESS SUMMARY

Component	Primary Limit (MPa)	Primary + Secondary Limit(MPa)	EM+Gravity [Primary] (MPa)		Cool down+EM [Primary+Secondary] (MPa)	
			Peak	General	Peak	General
Case	184	552	350	70	380	300
Cover	184	552	130	45	430	350
Conductor	94	282	-	68	-	-181
Coil Pack Shear	15	45	5	13	40	20
Coil Pack Radial	94	282	-	-30	-	-120

Primary stresses were limited to the lesser of 2/3 times the yield strength or 1/3 times the ultimate tensile strength. Primary plus secondary stresses were limited to 3 times the primary stress allowable.

Torus Splice Design

The magnet consists of six trapezoidal (race track) coils connected in series, with an operating current of 3770 A. The magnet coils are cooled by 4.6 K supercritical helium, whereas the joints connecting the coils (splices) are all conduction-cooled by 4.6 K liquid helium [12].

The key drivers for the splice design were minimization of contact resistance and adequate quench protection. All conductors that are not within the main coil winding, (splices between the individual superconducting magnet coils, conductors between coils and current leads, and long runs of superconducting bus bar), have additional copper stabilizer to manage temperature rises during a quench event. The conductors that enter and exit the coil case also have stabilizer that runs to the outermost turn of each pancake. To design a ‘quench-tolerant’ splice, the amount of copper has to be large enough to minimize peak temperatures during a quench event but also small enough to allow the development of a resistive voltage that can be detected and used to trip the fast dump interlocks to prevent the superconductor from burning out. This ‘balancing act’ is a critical part of the design of the quench protection system of any superconducting magnet. The Oxygen Free High Conductivity (OFHC) copper stabilizer bars extend over the entire splice length and are soldered to the assembly in the same operation that solders the splice.

The splice has been designed for low temperature operation at about 5 K to allow for some margin. Each splice was required to have a resistance of no higher than $7 \times 10^{-9} \Omega$, thus imposing a joule heating limit of no more than 100 mW [12]. This resistance corresponds to an operating current of 3770 A at 4.6 K with a background magnetic field in the region of 0.3 T, allowing for the magnetoresistance in copper. Splices are cooled via copper braids soldered to the helium re-cooler units located inside the upstream cold hex beams. The splice design was also constrained by the available space on the re-cooler units and electrical insulation requirements (similar to the coils).

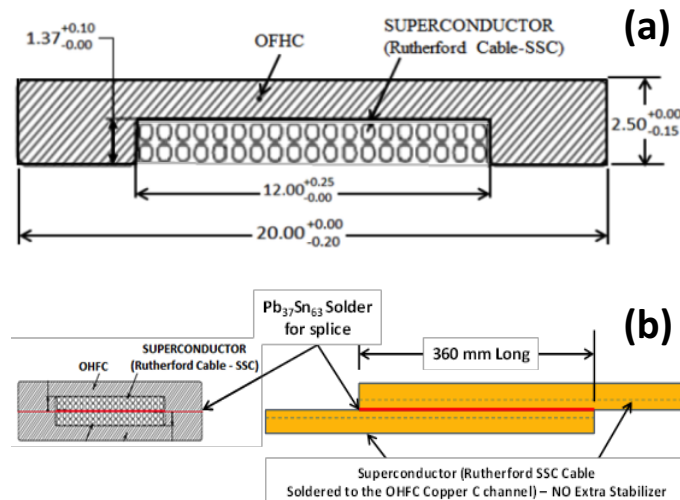


Fig. 7 (a) Torus conductor - SSC outer cable soldered into a copper channel (dimensions in mm), (b) Typical layout of the test splice for joint resistance evaluation (without additional copper stabilizer).

The key risk to the joint is the lack of even solder distribution and the inadvertent creation of voids within the solder and between the cables being joined. The cables are placed with the SSC cables facing each other and the keystone edges of the mating conductors lying on opposite sides of the joint to ensure a minimum gap between the cables. Several splice mock-ups were made and destructively tested to qualify the soldering fixture and fabrication procedure. A portion of the lip of the copper channel along the mating surfaces of the two conductors was removed to reduce the likelihood of void formation since the groove in the channel is deeper than the thickness of the Rutherford cable (see [Figure 7](#)).



[Fig 8 \(a\)](#) Temperature controlled aluminum block splicing rig. Cut-outs in the side of the rig allowed for visual inspection of solder flow, (b) Splice mock-up end-on view of the sectioned splice cut lengthwise showing void-free construction. NbTi strands and solder can be seen in the copper matrix. The outer-wrap is polyimide film and epoxy.

$\text{Sn}_{60}\text{Pb}_{40}$ solder was used to bond the Rutherford cable into the copper channel. It has a liquidus of 188 °C to 190 °C (and melts above 200 °C). Soft solder paste $\text{Sn}_{63}\text{Pb}_{37}$ (with an eutectic melting point of 183 °C) was used for the splice. Delamination of the Rutherford cable from the copper channel was avoided by careful control of the temperature during the soldering process using thermocouples for monitoring. The design of the soldering rig shown in [Figure 8](#) included open zones for direct viewing of the conductors during soldering, which allowed visual inspection of solder flow during the splicing operation.

The splice insulation system is designed to accommodate a 2.5 kV standoff to ground using polyimide film and a minimum tracking length of 1/2 inch. For improved thermal performance, any physical gaps in the assembly were filled with two-part blue Stycast 2850 FT epoxy. The assembly was hi-Pot tested (conductor to ground) to 1 kV in air to validate electrical isolation and integrity.

Test splices with 360 mm-long soldered joints were prepared at JLab and critical current (I_C), n-value and V-I data measurements were carried out at the University of Durham, UK up to 2000 A in one of two 15 T magnet systems (see [Table IX](#)). Due to a limitation of the measurement set up that could not accommodate the full length of the splice in the magnet, the resistance across the splice was also measured at a lower current and in an elevated magnetic field at LHe temperature. This measurement was carried out in order to characterize splices that would be located in higher fields (up to 4 T) for the Hall B solenoid magnet system, which employs similar conductor and splices. Typical resistances measured for sample DR4686 are given in [Table X](#).

TABLE IX
 CRITICAL CURRENT AND N-VALUE DATA FOR JLAB SPLICE SAMPLE# DR4562

<i>Critical Current data</i>		10.5 T	10.0 T	9.5 T
100 μ V/m		254 A	851 A	1708 A
10 μ V/m		165 A	656 A	1415 A
<i>n-Value</i>		5	9	12
10-100 μ V/m				

TABLE X
 RESISTANCE MEASURED FOR DR4686 AT VARYING MAGNETIC FIELD AT 4.2 K

Joint Length (mm)	Field at Field Centre (T)	Field at the top of the Joint (T)	Joint Resistance ($\times 10^{-9} \Omega$)
260	0	0	≤ 0.1
	0.5	0.13	0.70
	1	0.25	0.66
	2	0.50	0.68
	3	0.75	0.68
	4	1	0.7

The resistance of the splices measured at elevated magnetic fields was less than 1 n Ω in LHe (4.2 K), the maximum allowed design value was 7.0 n Ω .

Torus Quench Protection Design

Various quench scenarios were analyzed utilizing the Vector Fields (Cobham) quench codes that incorporate the ELEKTRA 3D (transient analysis) and TEMPO 3D (thermal analysis) software modules [13]. The analyses involved the examination of eddy currents generated during a quench event within the coils themselves, as well as in any nearby electrically conductive components such as the aluminum coil cases and aluminum thermal shields and any subsequent forces produced by these eddy currents (see Figure 9). These generated eddy currents can produce a phenomenon known as ‘quench-back’ – i.e. the eddy currents produce a heating effect that then reflects back into the superconducting coils, thus speeding up the quenching of the coils – in effect providing a secondary form of quench protection.

The torus magnet is protected via an externally located dump resistor that is permanently connected across the magnet terminals. This resistor has a center tap that then feeds a ground-fault indicator (see Figure 10). Quench detection is via voltage taps located on either side of the splices between coils, thus allowing voltage detection across individual coils, splices, and long runs of bus bar.

At the operating current of 3770 A and with a total inductance of about 2 H, the torus magnet has a stored energy of 14.2 MJ. With the 0.124 Ω dump resistor in circuit, any current decay under non-quench conditions will have a time constant of 16.7 s, with the magnet therefore running down to almost zero amps in about 5 time constants or 83.5 s. It should be noted that even during a ‘normal’ fast discharge of current into the dump resistor (for example an interlock activating due a non-quench event) sufficient eddy current heating can be produced, which in turn would initiate a quench-back event that could then initiate a quench in one or all of the coils. During the quench event nonlinear superconductor normal zone growth and induced eddy currents in the aluminum cases and shields will decrease the effective discharge time due to the increase in effective resistance in the overall magnet circuit.

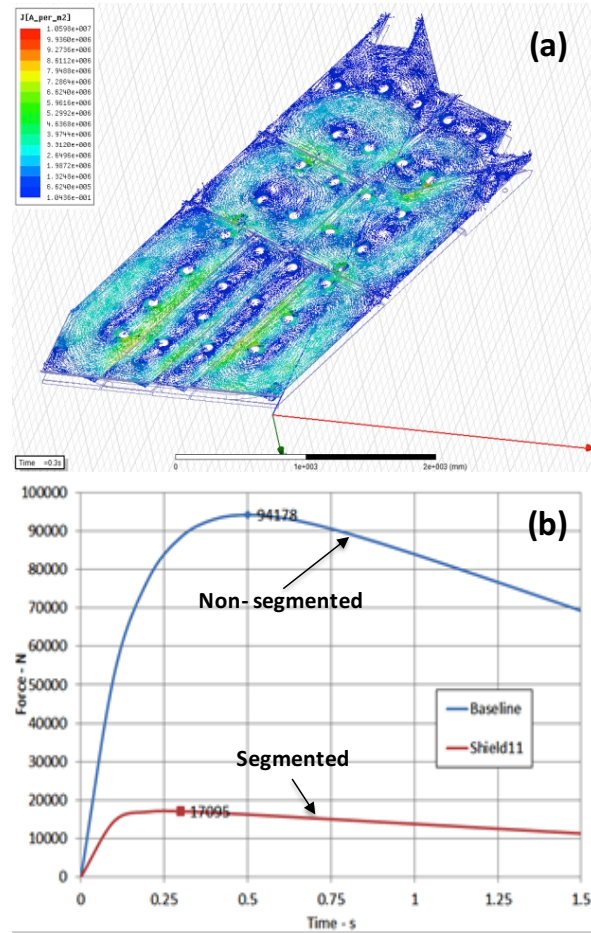


Fig 9 Torus segmented thermal shield performance during quench event – (a) current density vector plot, (b) Total force vs. time during a fast dump. Force reduction in segmented is about 1/5th of non-segmented shield design.

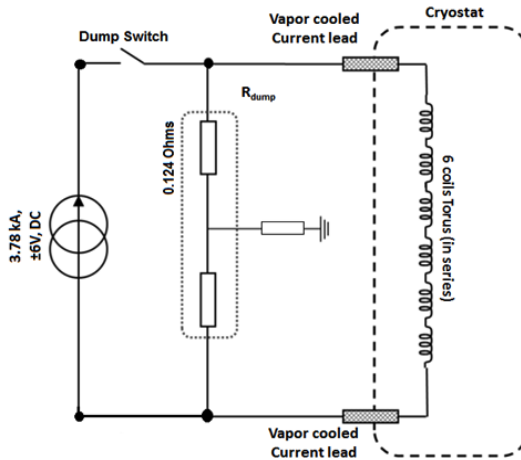


Fig. 10 Torus magnet protection circuit.

Quenches normally start from the peak magnetic field region within a coil, (which is the inner bore coil surface for the torus), and then propagate through the coil to the outer radius, causing the current in the series-connected coils to decay very rapidly. This rapid current decay in turn induces large eddy currents and therefore large forces in the aluminum coil cases and thermal shields. Initial analysis suggested that the forces on the thermal shield would cause excessive deflection and permanent bending of the shield.

Multiple iterations of segmentation were analyzed to reduce the eddy currents developed during a quench. Figure 9a shows the final segmentation employed for the shield and Figure 9b shows the total force on the shield. The segmentation reduced the force by a factor of more than 5 [14].

Based on the quench and normal operation scenario analysis, the observed results and mitigating actions are summarized in **Table XI** [6,14].

TABLE XI
TORUS - ANALYZED QUENCH AND NORMAL OPERATING SCENARIOS

	Quench Scenario	Results from Analysis	Mitigation
1	Normal magnet current decay from 3770 A with dump resistor connected across magnet terminals	The magnet system's 'normal' decay via the dump resistor (i.e. without a quench) will initiate a "quench back" after about 0.3 s, which will then cause all the coils to quench. The thermal shield can experience high forces due to the induced eddy currents during a quench.	This has been mitigated at the design stage by slotting or segmenting the shield in multiple locations and using a combination of two different grades of aluminum in its construction – one to preserve mechanical strength and the other to improve thermal conductivity. Bumpers between the shield and the coil case and vacuum jacket have also been incorporated in the design. The segmentation of the shields reduces the current density from 9.5×10^6 to 2.5×10^6 A/m ² ; with a corresponding reduction of out-of-plane forces from 94 kN to 17 kN.
2	One coil quench from 3770 A with full stored energy being dissipated amongst all 6 coils	Coil peak hot spot temperature = 53 K	None necessary as typical conservative design guidelines limit this peak hot spot temperature to no higher than 150 K.
3	One coil quench from 3770 A with full stored energy being dissipated in only one coil	Coil peak hot spot temperature = 75 K	None necessary as typical conservative design guidelines limit this peak hot spot temperature to no higher than 150 K.
4	A short in one coil that then causes the coil to quench (includes thermal stresses from cooling (395 K to 4 K), Lorentz forces due to a quench resulting from a single coil to ground short, and 110% gravity loading.	A single coil short followed by a quench will disrupt the symmetry of the magnetic field, which can result in out-of-balance forces between the coils. The out of plane load generated by this load case is ~129 kN.	Damage to the cold mass that potentially could be caused by these non-symmetric forces has been mitigated by incorporating "coil case-vacuum vessel" bumpers. The vacuum vessel has also been designed to be capable of withstanding these forces.
5	Cool-down stresses from 395 K to 4 K (includes stresses due to epoxy curing at 122°C).	The results from this analysis suggest that the coils are preloaded (compression) at room temperature. All stresses due to cool-down are secondary stresses (self-limiting). Refer to Table IX.	
6	Normal operation (includes cool-down stresses from 395K to 4 K, Lorentz forces due to energization and 110% static gravity loading to allow for earthquake loads). Assumes perfect coil symmetry with no out of plane forces due to electromagnetic loads.	The stresses from this load case are both primary (EM and gravity) and secondary (cool-down). Refer to Table VIII.	
7	Current imbalance (includes thermal stresses from cooling (395 K to 4 K), Lorentz forces due to a current imbalance condition, and 110% gravity loading). The current imbalance includes Lorentz forces from a 10% reduction of current (equivalent to losing ~12 turns in each pancake) in a single coil.	This current imbalance generates a ~70 kN out of plane force on the coil. This analysis is also used to verify stresses due to out of plane EM forces resulting from imperfect coil locations. The maximum out of plane force due to imperfect coil locations is ~7 kN.	

SOLENOID

Solenoid Magnet Design

The solenoid is an actively shielded 5 T magnet designed and built by the Tesla Ltd. Group of companies. The magnet was designed by Tesla Engineering Ltd. (TEL), Storrington, U.K. and built by Everson Tesla Inc. (ETI) Pennsylvania, USA. The solenoid magnet has five coils in series (also wound with copper-stabilized NbTi Rutherford cable but with a slightly narrower copper channel, 17 mm instead of 20 mm as for the torus). The two main inner coils (Coils 1 and 2) are shrunk-fit inside a thick-walled

stainless steel bobbin, another two intermediate coils (Coils 3 and 4) are wound into separate pockets milled into the outer surface of the same bobbin and one long thin shield coil (see [Figure 11](#)). The shield coil is wound onto its own bobbin but electrically connected in reverse to the other four coils as an “active shield” to limit the extent of the magnet’s stray field. This is important as there are many detectors mounted in close proximity to the solenoid that are sensitive to magnetic fields (see [Figure 12](#)). Using two split-pair coils and one solenoidal coil allowed the required field strength and homogeneity to be obtained in a compact magnet volume that also satisfied the placement and location of the various physics detector packages [15].

All coils are supported via 8 radial and 8 axial supports and are conduction-cooled via copper cooling strips, which are potted with the coils and connected to a centrally located annular helium cooling channel. The magnet is cooled by a helium thermo-siphon connected to the magnet reservoir. Gas generated by the magnet is used to cool the thermal shield and also the magnet’s vapor-cooled current leads before being exhausted via the Solenoid Service Tower (SST).

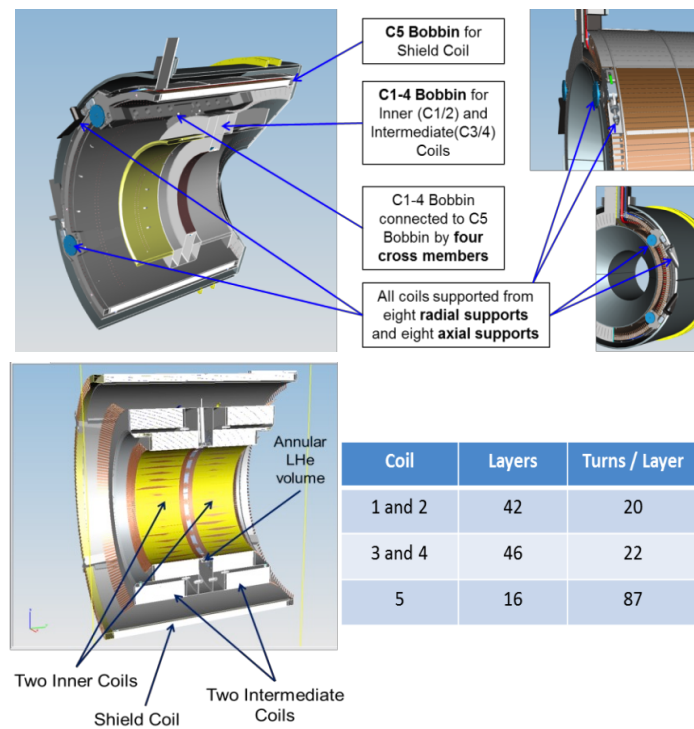


[Fig. 11](#) Cross-sectional views of the internal construction of the solenoid together with the coil winding details.

Coils “sticking and slipping” against their formers during current ramp-up, can cause spurious quenching, and necessitated the incorporation of slip planes consisting of Kapton and Mylar sheets placed between Coils 3, 4, and 5 and their respective bobbins to mitigate this problem. Forces and stresses encountered within the thermal radiation shield during quench events have been mitigated by slotting the shield. Temperature margins for each coil were quantified and resulted in improvements to the design and operation of the overall cryogenic cooling scheme.

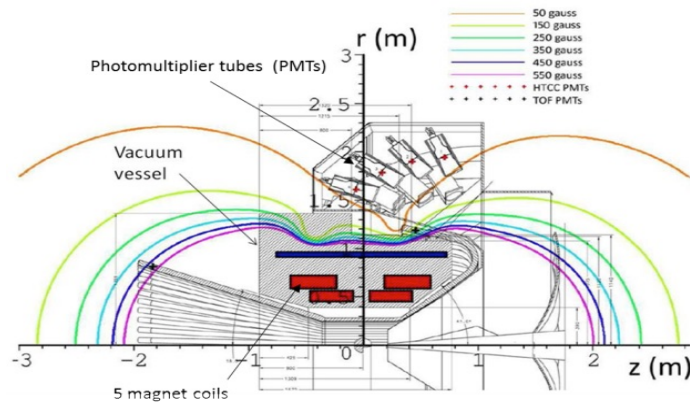


Fig. 12 Cross-sectional view through the side of the solenoid showing the location of the PMTs and the stray field lines.

Coil manufacturing variations can degrade the magnetic field homogeneity from its required value of < 100 ppm (peak-to-peak) within a cylindrical volume of 25 mm diameter \times 40 mm length located at the geometric center of the magnet. This homogeneous magnetic field region will be required for polarized target experiments in the near future and a solution being developed is to incorporate small superconducting shims (Z1, Z2, X, and Y) on the 1 K shield that surrounds the target within the bore of the magnet. To quantify manufacturing variations for the solenoid coils and to check on the effectiveness of the winding and epoxy impregnation processes, a half-size practice coil was successfully wound, potted, and dissected.

Electromagnetic and cryogenic interactions exist between the torus and the solenoid magnet systems and had to be considered during the design stage.

Solenoid Superconducting Coil Design

The initial design of the coils indicated that the innermost Coils 1 and 2 had the smallest temperature margin (1.117 K), whereas design guidelines suggest at least 1.5 K for better stability (see [Figure 13](#) and [Table XII](#)). As a result, JLab made plans to enable operation of the magnet at sub-atmospheric pressures in order to obtain additional temperature margin and the complete magnet system was designed for this lower operating pressure. As it turned out, in practice the cooling of the coils was predicted properly and there were no unaccounted for heat loads, thus the sub-atmospheric mode of operation was not needed.

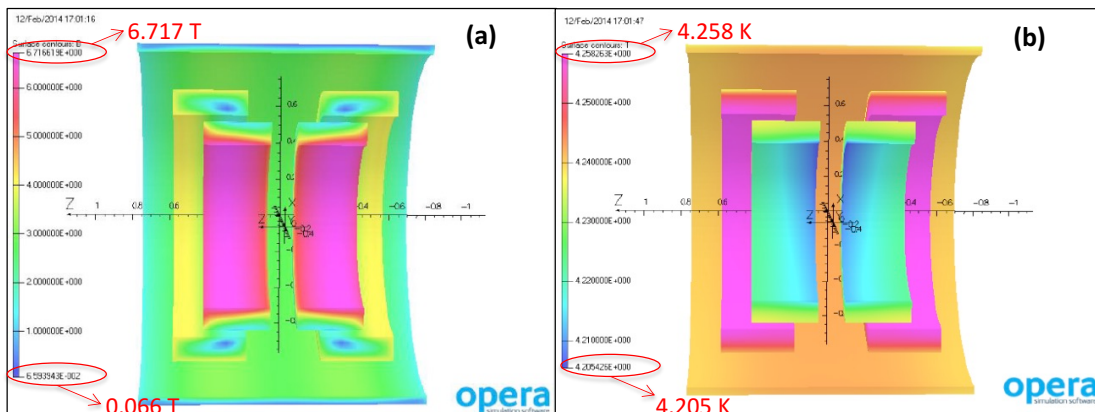


Fig. 13 (a) Magnetic field distribution on the solenoid coil surfaces, (b) Temperature distribution in the coils at end of ramp up to full field.

TABLE XII
SOLENOID – FIELD AND TEMPERATURE MARGINS FOR COILS

JLAB Thermal report							
Coil Number	T _{coil} (K)	B _{max} (T)	I _C (A)	SSP (%)	T _C (K)	T _{CS} (K)	ΔT (K)
1 and 2	4.68	6.56	6548	36.90	6.451	5.797	1.117
3 and 4	4.81	4.21	11022	21.92	7.578	6.971	2.161
5	5.62	3.05	10202	23.68	8.093	7.507	1.887

T_{coil}= Coil temperature, B_{max}= Maximum field in the coil, I_C= Critical current at B_{max} and T_{coil}, SSP= Short sample percentage, T_C= Critical temperature at B_{max}, T_{CS}= Current sharing temperature, ΔT= Temperature margin

Figure 14 illustrates the general protection scheme for the solenoid that was used as the basis for the quench and fault scenarios analyzed.

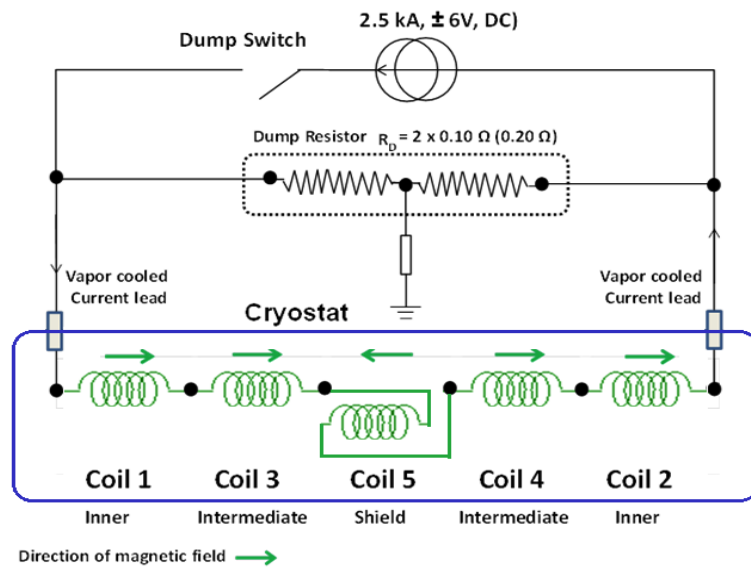


Fig. 14 Solenoid magnet protection circuit.

Table XIII summarizes all the analyzed quench and normal operating scenarios together with observed results and any appropriate mitigation.

TABLE XIII
SOLENOID - ANALYZED QUENCH AND NORMAL OPERATING SCENARIOS

	Quench Scenario	Results from Analysis	Mitigation
1	Quench initiating in C1, assuming presence of AC losses and electromagnetic coupling between coils	Peak temperature = 91 K, Peak voltage across coil = 102 V	No special mitigation was necessary as the coils are self-protecting and the coils are insulated for 1000 V to Ground.
2	Quench initiating in C3, assuming presence of AC losses and electromagnetic coupling between coils	Peak temperature = 87 K, Peak voltage across coil = 108 V	No special mitigation was necessary as the coils are self-protecting and the coils are insulated for 1000 V to Ground.
3	Quench initiating in C5, assuming presence of AC losses and electromagnetic coupling between coils	Peak temperature = 79 K, Peak voltage across coil = 156 V	No special mitigation was necessary as the coils are self-protecting and the coils are insulated for 1000 V to Ground.
4	Quench initiating in C1, assuming all the stored energy is dissipated in only one coil – i.e. no electromagnetic coupling with other coils	Peak temperature = 108 K, Peak voltage across coil = 96 V	No special mitigation was necessary as the coils are self-protecting and the coils are insulated for 1000 V to Ground.
5	Quench initiating in C3, assuming all the stored energy is dissipated in only one coil – i.e. no electromagnetic coupling with other coils	Peak temperature = 99 K, Peak voltage across coil = 101 V	No special mitigation was necessary as the coils are self-protecting and the coils are insulated for 1000 V to Ground.
6	Quench initiating in C5, assuming all the stored energy is dissipated in only one coil – i.e. no electromagnetic coupling with other coils	Peak temperature = 99 K, Peak voltage across coil = 156 V	No special mitigation was necessary as the coils are self-protecting and the coils are insulated for 1000 V to Ground.
7	Quench initiation in C5 with all coil leads and	Peak temperature = 41 K	No special mitigation was necessary as

	splices between coils included		the coils are self-protecting with quenches propagating faster due to the physical connections (splices) between coils
8	Quench initiation in a coil splice	Peak temperature = 42 K	No special mitigation was necessary as the coils are self-protecting with quenches propagating faster due to the physical connections (splices) between coils
9	Eddy current effects in the thermal shield due to a fast discharge of the magnet, the fastest rate being about 281 A/s	High forces experienced by the Al-1100 thermal shield.	The shield was designed with multiple slots which significantly reduced eddy current formation and thus forces.
10	Training of the solenoid coils to full field	Preliminary analysis of the shield coil indicated that the potted conductor and epoxy were in tension and that this could potentially be a cause for multiple training steps to full field.	The shield coils (as well as Coils 3 and 4) were manufactured with slip planes between the coils and their formers (bobbins). Coil 5 (the shield coil) was also over-bound with multiple layers of glass cloth during the manufacturing process. As a result, there was minimal training of these coils to full field during commissioning. There were a total of 5 training quenches (C3: 937 A, C4:1014 A, C4:1035 A, C3:1059 A and C3:1066 A)
11	Torus-Solenoid electromagnetic interactions [16]. The following scenarios were analyzed: <ul style="list-style-type: none"> ▪ Solenoid alone under normal operating conditions ▪ Solenoid and torus under normal operating conditions ▪ Solenoid under fault conditions ▪ Solenoid under fault conditions with various operating conditions of the torus 	<p>i. The long straight sections of the torus coils experience a force in the presence of the solenoid coils. The force on the straight coil sections closer to the solenoid is almost 3 times the forces on the far straight sections and varies from 1 kN to 6 kN. This force is balanced by other coils (so the net force is zero). These forces are in the X and Y directions, there is no axial force on the torus coils. The forces and the X and Y directions explain the slight buckling of the torus coils. The direction of the buckling depends on the relative directions of currents in both the magnets. This buckling phenomenon can be observed from the load cell data‡.</p> <p>ii. Under certain fault conditions, the torus can exert very small torques on the solenoid magnet.</p> <p>iii. The worst but very improbable case (maximum torque) is for the torus with one of torus coils at 90% of full operating current (Fault #1) and no active shield in the solenoid, as a mitigation action solenoid was tested independent of torus magnet.</p> <p>iv. During subsequent post-commissioning runs, it was discovered that there is some low-level coupling between the torus magnet coils and the shield coil (Coil 5) of the solenoid. The mutual inductance has been estimated as being approximately 0.2 H. So if the torus quenches or undergoes a fast dump, it is likely that the voltage across Coil 5 of the solenoid will rise and exceed the threshold for quench protection, thereby causing the solenoid to undergo a fast dump also. This has happened at least once without any ill-effects for either magnet – apart from all the helium being lost from the reservoirs of both magnets.</p>	Overall these values are well within the design limits for coil buckling. The set limits on the load cell are well above this observed behavior.

‡ Initial electromagnetic studies between the two magnets show almost no interaction. However in this initial analysis each torus coil was modelled as one conductor and only the net force on that conductor was taken into account. A more detailed analysis was then performed modelling the torus coils as 8 sections: 2 long straight sections, 2 short straight sections and 4 corner sections. The results from this subsequent analysis match closely to that observed during normal operation of these magnets.

Additional analyses included assessment of forces on the coils due to the proximity of ferromagnetic components – for example the structural space-frame within the hall, the walkway that spans the left and right halves of the space-frame, and the Central Time-of-Flight (CTOF) detector [Ref?] located close to the bore of the magnet with its multiple iron-shielded photomultiplier tubes. Eddy current analyses were also performed to verify and mitigate forces on electrically conductive components located within the bore of the solenoid – for example the copper heat exchanger for the Silicon Vertex Tracker (SVT) [Ref?]. The results from the analyses were used to either confirm that there was minimal or no risk of damage to the magnet or the components in question, or to facilitate a re-

design of the components to reduce the risk of damage. The CTOF shields exert a net force of about 5 kN. The magnet vendor (ETI) was provided with the detail of the CTOF shields and designed the z-restraints for a 4.9 kN force. The Central Neutron Detector (CND) shields exert a net force of about 400 N [Ref?]. The other components are the steel hall space-frame structure (which provides staff with multi-level access within the hall, to the magnets and electronics) and iron shields for the photomultiplier tubes in the Micromegas Vertex Tracker (MVT) and Silicon Vertex Tracker (SVT) [Ref?]. The forces on the coils due to the hall structure depends on the magnet position; in the normal operational position the coil forces are about 500 N. Most of the material in the MVT and SVT inserts is non-magnetic. To counteract the 4.9 kN force from the CTOF detector shielding, an iron compensating ring was been installed on the downstream end of the solenoid – bolted to the vacuum jacket's end closure plate. This compensating ring reduces the forces on the coils from the CTOF detector by about 3.6 kN. The total forces on the coils in the presence of all the components are summarized in [Table XIV](#), indicating a resultant axial force on the coils (in the beamline direction) of about 2.4 kN with the compensating ring installed.

TABLE XIV
SOLENOID – FORCES ON COILS DUE TO PROXIMITY OF FERROMAGNETIC OBJECTS

Components close to the Solenoid Magnet	Fz (N)
Torus magnet	0
CTOF	4884
CTOF + compensating ring	1239
CND	414
HTCC	-35
Hall structure	499
SVT mounting tube (stainless steel)	196
SVT mounting tube (aluminum) during quench	22
SVT region 4 mounting tube (aluminum) during quench	76
Total without compensating ring	6056
Total with compensating ring	2411

Solenoid and Torus Interactions

A fast dump of the torus produces a voltage rise across the shield coil of the solenoid that can trigger the solenoid's quench protection system, thus causing the solenoid to undergo a fast dump itself. While the electromagnetic analysis predicts the sum of the overall forces on each torus coil to be zero, locally the load cells of the out-of-plane supports (OOPS) of the torus coils do experience a force. These OOPS, which are located in the center of the race track coil, show large changes in force when the torus is at field and the solenoid is energized. Electromagnetic analysis shows that the OOPS near the upstream leg of the torus coil will see a force change in the opposite direction of the one near the downstream leg. The OOPS are instrumented to read up to 8.9 kN of force, their failure load is 44.5 kN. Load changes of up to 4 kN were recorded. These changes in load are repeatable and nicely match those predicted by the analysis in magnitude and direction. All the OOPS are operating well below the maximum read-back value. [Figure 15](#) illustrates the combined stray field maps of the torus and solenoid for various operating conditions.

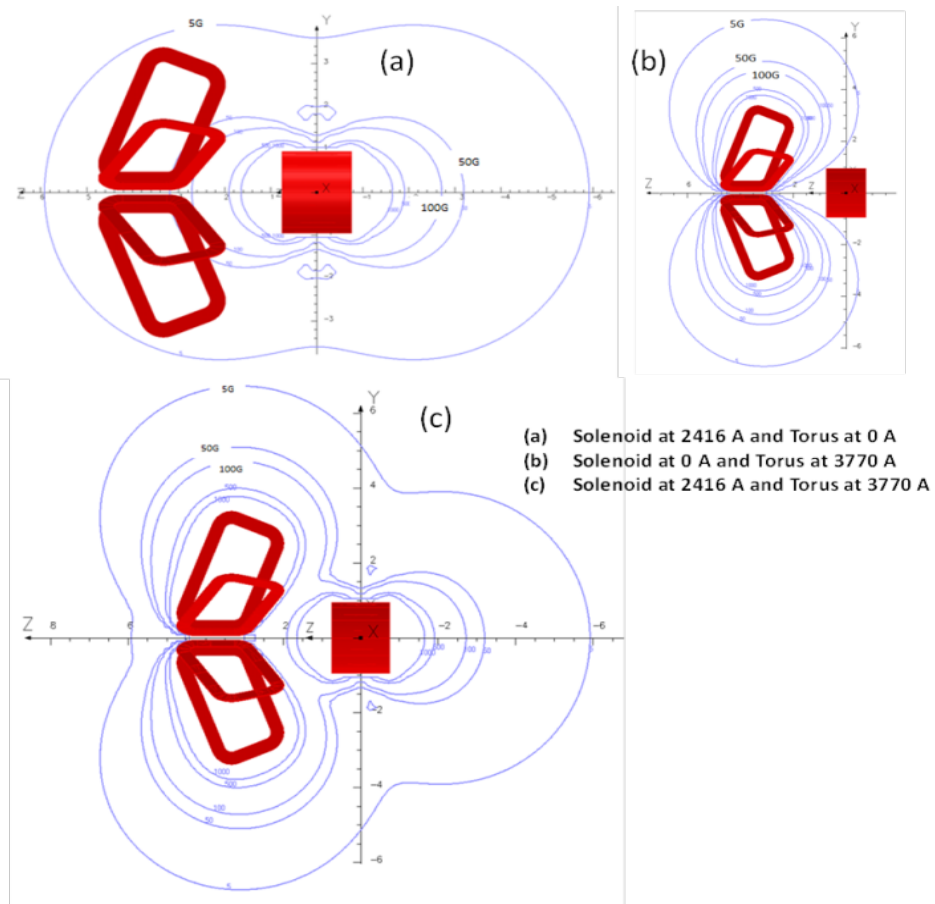


Fig. 15 Solenoid and torus stray field maps under different operating conditions.

The common supply and return lines from the refrigerator supplies both magnets and a liquid-helium dewar that is used to fill cryogenic targets. These lines could produce coupling between the torus, solenoid, buffer dewar, and target, in particular the warm return piping. Passive and active control elements have been put in place to minimize the potential for damaging the magnets due to these cryogenic coupling phenomena – for example check valves on the vapor-cooled leads prevent reverse flow, automated vent valves allow flow to continue in the event of a pressure rise to prevent leads from warming and remain open until a magnet completes a controlled ramp down. There are also check valves in the torus and solenoid supply and return U-tubes to prevent back flow of hot gas from either magnet going into the other. These check valves also delay the instantaneous pressure rise that back flow would cause. Operational experience has shown that either magnet can be fast dumped and the system design allows the other not to be effected cryogenically.

IV. POWER SUPPLY, CONTROLS AND INSTRUMENTATION

Superconducting Magnet DC Power Supply

Each magnet is energized using identical superconducting magnet power supplies (MPS). This was a bespoke design from Danfysik based on their model 8500/T854 power supply [19]. The MPS DC output is low voltage, high current, designed for near

zero resistance loads; however, the impedance seen at the magnet/power supply output terminals can go from purely inductive to an almost purely resistive state during a quench. Due to the requirements for high stability and low drift on a static magnetic field, a linear series-pass regulation topology was selected. The MPS output utilizes two-quadrant operation, allowing for smooth and continuous ramping of the current into the magnet [18]. The power supply is programmed to sweep magnet currents at predetermined rates at different current levels without user intervention. The MPS incorporates features designed to mitigate or prevent failure modes during magnet operation. These features include: controlled current ramping (up or down), a fast-opening dump switch and dump resistor (124 mΩ and 200 mΩ for the torus and the solenoid, respectively) to rapidly de-energize (fast dump) the magnet, a slow dump capability that utilizes the last-used ramp rate to run the magnet down, an integrated polarity reversal switch, and redundant DC current transducers for current-based interlocks. Additionally, a separate rack-mounted, PLC-based controller allows the programming of current ramp rates and the monitoring of interlocks and the overall health of the magnet. Salient MPS and energy dump specifications are given in [Table XV](#).

TABLE XV
TORUS - DC POWER SUPPLY AND FAST ENERGY DUMP SPECIFICATIONS

Description	Specification					
Output current/voltage	± 4000 A / ± 6 VDC					
Ramp rate	Variable: ±0.2 to ±3.0 A/s					
Supply voltage	480 V/3-Φ/60 Hz.					
Ambient temperature	15-35 °C					
Cooling water (flow, temperature)	60 l/m, 15-35°C					
Pressure	300 psig					
Ground isolation	>1.0 MΩ					
Quench protection	Fast DC output breaker					
Absolute accuracy	-0/+100 ppm					
Stability (30 min)	< ± 5 ppm					
Stability (8 hours)	< ± 10 ppm					
Magnet	I _{OP} (A)	L _{TOT} (H)	E _{ST} (MJ)	V _{DUMP} (V)	R _{DUMP} (Ω)	T _{MAX} (°C)
Torus	±3770	2.0	14.21	< 500	0.124	<350
Solenoid	±2416	6.0	17.50	< 500	0.200	<350

The power supply is designed to react to a quench, which is detected by a set of hard-wired quench detector electronic units, and automatically switch power off to the magnet [17]. The hard-wired quench detection sub-system acts directly on the dump switch as part of the primary protection system. The quench protection system is capable of detecting quench-induced voltages at multiple points on the magnet, namely magnet coils, bus-bars, and splices within the cryostat. The quench fault thresholds are set to the expected quench voltages derived from simulations. The voltage thresholds and the inductance of the magnet set upper limits on the MPS current ramp rate in order to avoid false trips.

The power supplies' default factory settings meant that there was a total time delay of about 750 ms between when the set quench threshold voltage was exceeded to the time when the dump switch was fully opened during a fault condition. Although this delay

time would likely have been adequate for the torus and solenoid, operational experience with similar designs of power supply within the laboratory suggested that reducing this time delay would provide a larger safety margin in terms of minimizing peak hot spot temperatures within the coils. The overall time delay consists of three time components - (a) T_q is the time between quench initiation within the superconductor and when the quench voltage threshold is exceeded, (b) T_{qi} is the time between when the quench voltage threshold is exceeded and the quench-interlock relay contact opens, which is a constant attributed to the associated electronics, and (c) T_{dsw} is the subsequent time for the dump switch to fully open. The control circuit for the dump switch was modified following consultations and instructions from the power supply vendor and the resulting total time delay has now been reduced to about 120 ms.

Magnet Current Leads and Ice-Management System

Water-cooled leads (WCLs) are used to connect each magnet power supply to the respective magnet's vapor-cooled leads (VCLs). Air-cooled multi-stranded (flexible) copper jumpers are used to transition between the hard *connection* points at the power supply end as well as at the magnet end (see [Figure 16](#)). The [Tables XVI,XVII, and XVIII](#) summarize the main features of these current transfer components.

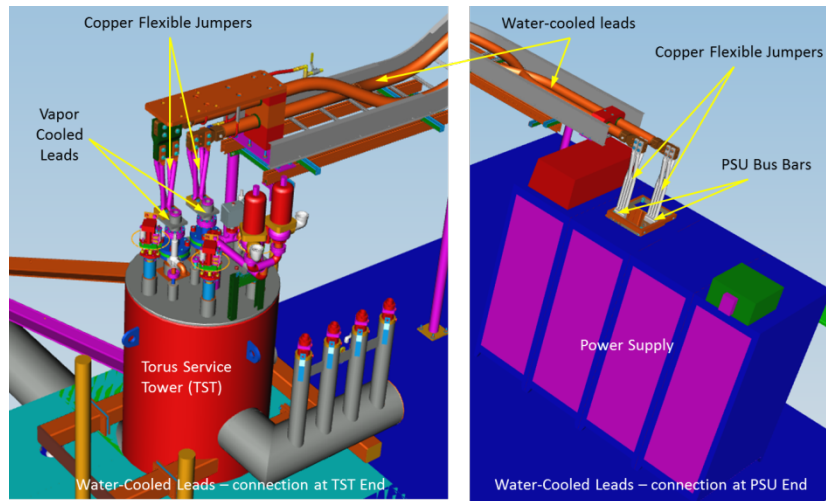


[Fig. 16](#) Torus – water-cooled leads, flexible jumpers, and vapor-cooled leads. The set-up for the solenoid is similar.

TABLE XVI
WATER-COOLED LEADS SPECIFICATIONS

Description	Torus	Solenoid
Operating current	4000 A	3000 A
Cable cross sectional area	2000 MCM	2000 MCM
Voltage drop per lead pair @ 4000 A (torus) @ 3000 A (solenoid)	1.1 V @ 50°C	1.3 V@50°C
D.C. resistance for both leads connected in	$274 \mu\Omega$	$475 \mu\Omega$
Input water temperature	40°C	40°C
Output water temperature	50°C	50°C
Max. operating pressure rating	300 psig	300 psig
Test pressure	400 psig	350 psig
Insulation to ground voltage rating	2 kV	3 kV
Minimum allowable water flow @ 4000A (Torus) @ 3000A (Solenoid)	1.2 gpm	3.2 gpm

1 MCM (1 thousand circular mils) = 0.5067 mm^2

TABLE XVII
AIR-COOLED JUMPER SPECIFICATIONS

Description	Torus	Solenoid
Maximum design current	4000 A	3000 A
Jumper cross sectional area	3000 MCM	3150 MCM
Voltage drop for jumpers per lead @ 4000 A (torus) @ 3000 A (solenoid)	One jumper pair = 0.06 V @ 70°C	One jumper = 0.014 V @ 70°C
D.C. resistance for jumpers per lead @ 70°C	One jumper pair = 15 $\mu\Omega$	One jumper = 4.7 $\mu\Omega$

1 MCM (1 thousand circular mils) = 0.5067 mm²

TABLE XVIII
VAPOR-COOLED LEADS SPECIFICATIONS

Description	Torus	Solenoid
Rated operating current	5000 A	2500 A
Operating helium consumption @ 5000 A	20 liters/hr. per pair	7 liters/hr. per pair
Standby helium consumption	15 liters/hr. per pair	6 liters/hr. per pair
Minimum recommended lead gas flow per lead @ 5000 A / 4000 A (torus), @ 2500 A (solenoid)	118 SLPM /112 SLPM	42 SLPM
Maximum allowable voltage drop per lead @ 5000 A (torus) and @ 2500 A (solenoid)	100 mV	100 mV
Allowable operating time with no gas flow	150 sec	150 sec

SLPM = Standard Liters per Minute

Band and cartridge heaters are installed at the top of the vapor-cooled leads where they exit the magnet service towers to keep ice-formation to a minimum (see [Table XIX](#)).

TABLE XIX
LEAD HEATER SPECIFICATIONS

Description	Torus Specification (per lead)	Solenoid Specification (per lead)
Upper heater set – No. of heaters / power / voltage	1/ 400 W per heater / 120 VAC (Mica band heater 3" ID, 1.5" width)	2/ 150 W per heater / 115 VAC (cartridge heaters)
Central heater set – No. of heaters / power / voltage	2 / 300 W, 600W / 115 VAC (heater tapes) - <i>proposed</i>	1 / 600W / 115 VAC (Mica band heater)
Lower heater set – No. of heaters / power / voltage	1 / 600W / 115 VAC (heater tapes) - <i>proposed</i>	2 / 300 W, 600W / 115 VAC (Mica band heaters)

In case of heater failure, an ambient vaporizer is installed between the VCL and the warm return piping. The piping between the VCL and the vaporizer is vacuum jacketed. These features keep water from dripping onto the detectors.

Controls and Instrumentation

Depending on where instrumentation was mounted on the magnet, all selected sensors had to be compatible with cryogenic temperatures and magnetic fields with regards to reliability and reproducibility of read-outs with all detectors in their final locations.

The cycling of large currents in the superconducting magnets during ramp-up and ramp-down operations results in heat loads caused by eddy current effects. This phenomenon, together with the level of ambient noise within the experimental hall, guided some

of the instrument choices. The risk analysis also identified the various forces that arise during operation of the torus and solenoid magnets, viz. eddy current forces, Lorentz forces, thermal loading, and also the electromagnetic and cryogenic interaction between the torus and solenoid magnets. Therefore, for safe magnet operation, it is necessary to monitor and control all of the following parameters - temperatures, pressures, pressure drops, liquid levels, mass flows, vacuum levels, voltages, strains, loads (see [Table XX](#)) [\[4\]](#), [\[20,21\]](#). Extensive instrumentation was used to verify the design under various operating conditions during commissioning and to allow flexible, reliable, and safe control of all sub-systems by non-expert personnel post-commissioning.

Instrumentation is monitored using the following key electronic sub-systems:

- a. JLab-designed multi-sensor excitation low voltage chassis (MSELV or LV chassis) + National Instruments Compact Real-Time Input Output controller or cRIO (slow DAQ refers to slow data acquisition) - Magnet temperatures and strains
- b. National Instruments cRIO (fast DAQ refers to fast data acquisition) – Magnet-related voltages
- c. Cryo-Con readout units – Cryogenic system temperatures (Cryo-Con refers to Cryogenics Control Systems Inc.)
- d. Programmable Logic Controller (PLC) – Cryogenic system pressures, vacuum levels

Monitoring and control of the entire system (including valves and flow indicators) were performed by Allan Bradley PLCs. The design of the sensor read back [LV](#) chassis was based on the requirements of the torus and solenoid instrumentation in terms of quantity and types. Commercially available read out boxes for sensors are usually limited to a certain number of channels and the multi-functional capability of these devices usually means that these devices are expensive. The motivation to accommodate all the sensor types (temperature, pressures, strains, loads, magnetic field – termed ‘slow data’) that would be used on both magnets together with a reduced set of functions, to only meet the required control system needs of the magnets and no more, led to a JLab-designed and developed FPGA-based [LV](#) chassis that sets the excitation current or voltage for a sensor and also provides read back [\[4, 22\]](#). The data read back would then be routed to a NI-cRIO (the slow DAQ system) that would pass data to the PLC for control of the various sub-systems and interlocks. The majority of instruments are powered and read out via the LV chassis:

1. The MSELV sends the unscaled raw readouts to the NI-cRIO via individual RS232 ports. Each port is selectively assigned based on instrument type, temperature, strain, etc. The NI-cRIO takes the raw data for each instrument and converts it to engineering units from specified calibration tables. This ‘slow’ data is sampled at 1 Hz.
2. The cRIO device puts scaled sensor readouts into arrays, based on instrument type, and sends these arrays to the PLC via Ethernet.
3. The PLC interrogates these data sets and then uses prescribed routines (cool down, power up, etc.) to force action on valves, heaters, power supplies, etc. The PLC also transfers this data to an EPICs IOC (input-output controller) to allow for archiving

and site-wide system control (e.g. the cryo compressor in the End Station Refrigerator can use one of our cryogen liquid levels to help determine cryogenic heat load).

- In parallel another cRIO (fast DAQ) uses its 24-bit ADCs (Analog to Digital Converters) to monitor the voltage taps. This cRIO directly sends 10 kHz data to the EPICs IOC for off-line analysis. In parallel, it also sends the voltage tap data to the PLC at a rate of 5Hz for the redundant (secondary) protection system.

TABLE XX
TORUS AND SOLENOID MAGNET SYSTEM SENSORS AND VOLTAGE TAPS

(A) TORUS Magnet System

Measurement	Voltage		Temperature (4 K)		Temperature (77K)		Strain		Load cell		Hall sensor		
Sensor/wiring type	8 mil Kapton insulated-multi-strand copper wire (pair)		Cernox™(1070) – 4 wire		Calibrated PT100 – 4 wire (Omega F2020-100-B)		Cryogenic series 350 Ω (CFLA-6-350) 4-wired/3-wired for measurement		LOAD CELL - FUTEK FSH02239 (2000 LBS), 4 wire, 300 K		Cryogenics hall generator (axial), HGCA-3020, 4 wire		
Sensor location / No. of sensors	Magnet	23	Magnet	54	Thermal shield	60	Coil Cold Mass (CCM)	24	OOPS	26	Vacuum Vessel		
	Zero-Flux Current Transducer	2	Cooling Tube	12	Current - Leads	2+2	Axial sup	6	FMEA result	3 (Hub)			
	FMEA Result	1 (Power supply- One bus bar)	Splices	6+2	Axial sup	3	Vert sup	8					
	Line-GND/Dump Resistor	1	VCL in Cryostat	2+2	Vert sup	4	FMEA result	24 (Hex)					
Connection wiring	Copper		Constantan multi-core harness		Constantan multi-core harness		Constantan multi-core harness		Copper		Copper		
Wire gauge	24 AWG		36 AWG		36 AWG		36 AWG		28/32 AWG		28/32 AWG		
Signal amplitude	Magnet	300 V pk	3 mV (300K) to 50 mV (4.2K)	0.1 V (77K) to 0.5 V (300K), actual excitation Current = 2.5 mA	0-5 V for resistance measurement the variation is 0-0.5 Ω or 10 μV – 1 mV (CFLA-6-350)	~ 2.0 mV/V	~ 1.00 mV/kG (at 298 K)						
	Dump R	250/500 Vpk											
	ZFCT	50 mV											
	PSU	6V											
Sampling rate	> 2 kHz		100 Hz		100 Hz		100 Hz		100 Hz		100 Hz		
Excitation current or voltage	n/a		0.20-20 μA		1-5 mA		0-10 V (2.5 V in operation as chosen)		0-10V (2.5 V in operation as chosen)		100 mA		
No. of channels	24		71		61		38		26		12		
Multiplexed	NO		YES		YES		YES		YES		YES		
Control	Primary-Hard wired to quench detection/Secondary - PLC		PLC		PLC		PLC		PLC		PLC		
Fast DAQ	FPGA		FPGA		FPGA		FPGA		FPGA		FPGA		

(B) SOLENOID magnet System

Measurement	Voltage		Temperature (4 K)		Temperature (77K)		Load cell		Hall sensor			
Sensor/wiring type	8 mil Kapton insulated-multi-strand copper wire (pair)		Cernox™ – 4 wire (4.2 – 325K)		Calibrated PT100 – 4 wire		LOAD CELL, 4 wire, 300 K (Force)		Cryogenics hall generator (axial), HGCA-3020, 4 wire			
Sensor location / No. of sensors	Magnet	21	Magnet	26	Thermal shield	18	8 (LCM307) 0-10 kN (axial)		Vacuum Vessel	3		
	Zero-Flux Current Transducer, Power supply Bus	4					8 (KMR300kN) 0-165 kN (radial)					
Connection wiring	Constantan/Manganin/Copper		Constantan harness		Constantan harness		Copper		Copper			
Signal amplitude	Magnet	718 V pk	3 mV (300K) to 50 mV (4.2K)	0.1 V (77K) to 0.5 V (300K), actual excitation Current = 2.5 mA	~ 2.0 mV/V	~ 1.00 mV/kG (at 298 K)						
	Dump R	250/500 Vpk										
	ZFCT	50 mV										
	PSU	6V										
Sampling rate	> 2 kHz		100 Hz		100 Hz		100 Hz		100 Hz			
Excitation current or voltage	n/a		0.20-20 μA		1-5 mA		0-10V (2.5 V in operation as chosen)		100 mA			
Control	Primary-Hard wired to quench detection/Secondary - PLC		PLC		PLC		PLC		PLC			
Fast DAQ	FPGA		FPGA		FPGA		FPGA		FPGA			

Analog data collection from other devices not listed above are: Pressure transducers, EV electric valves, PV pneumatic valves, RV pressure relief valves, VCL lead heaters, VCL lead flow indicators, vacuum pump control (gauges and gate valve), bus-bar water flow switches, magnet power supply water flow, and temperature monitors.

The magnet Quench Protection System (QPS) was developed for both magnets based on the analysis of several quench scenarios and is comprised by primary and secondary sub-systems [17]. Parallel path voltage taps from multiple locations throughout the magnet (magnet coils, splices, bus-bars, leads, etc.) feed both these sub-systems. The voltage taps feeding the primary protection sub-system are hardwired directly from the magnet to the Danfysik Quench Detector units – i.e. with no electronics or any software manipulation in between.

The secondary quench protection sub-system is also fed from the same voltage tap locations but this time the information is acquired by a fast data acquisition system (Fast DAQ), using a National Instruments cRIO device, and then routed to a PLC that performs summations and subtractions of various voltages to provide back-up for the hard-wired primary sub-system. A quench-induced voltage that exceeds pre-set voltage thresholds will trigger the primary system closely followed by the secondary system.

Each hardwired Quench Detection (QD) module consists of four differential input channels, i.e. an upper and lower channel. The voltage signals are fed into the lower and upper channels and are then subtracted from each other. The resultant voltage is compared with the pre-set voltage threshold (i.e. set by the operator). If the resultant voltage is higher than this threshold and remains above this threshold for a pre-set time period, then the QD will trip and fast dump the magnet—i.e. the dump switch will open to isolate the magnet from its power supply and the magnet will run down through the external dump resistor. Between 43-63% of the stored energy within the magnet is extracted and dissipated in the external dump resistor. The remainder of the energy is dissipated within the magnet coils and cryogenic system itself. [Figure 17](#) illustrates a set of typical voltage taps for the solenoid magnet, feeding both the primary QPS (i.e. to the quench detector units, QD-U) and also to the secondary QPS (DAQ).

The secondary QD system routes voltage tap data from the magnet via Knick isolation amplifiers (iso-amps) [23,24] to a second dedicated NI-cRIO having eight four-channel N9239 24-bit analog input modules. The voltage tap data are then manipulated by the PLC to produce summed and subtracted voltages that are then routed to the various interlocks.

Two sets of thresholds are employed here - one set to initiate a controlled ramp down and a second set that is deployed as a backup for the hardwired QD and also acts directly on the fast dump contactor.

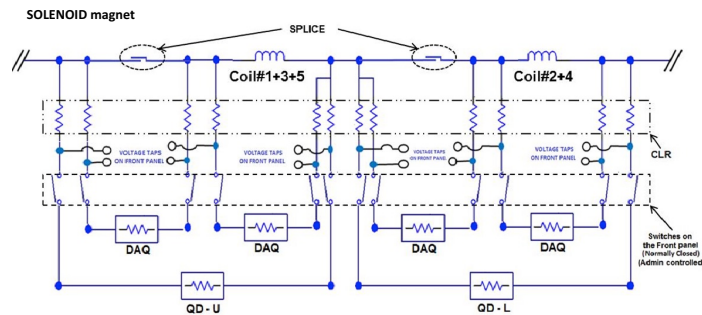


[Figure 17](#) Schematic arrangement of a typical section of the solenoid magnet for impedance-matching simulations – Current Limiting Resistor (CLR), Op-Amp, QD board.

The design of the quench protection and voltage tap sub-systems was driven by the anticipated levels of voltages developed during a magnet quench. The quench protection provides valuable data during a quench event via data capture of the voltage and temperature waveforms. The magnets are continuously monitored during ramp up, steady state operation, and also ramp down—i.e. the QPS is always active—so inductive voltages across coils during ramp up and down operations are also captured and have been used during the commissioning process to ensure the correct balancing of voltages between the various coils and thus QD channels.

The same cRIO also feeds VT waveform data to EPICS at 10 kHz for online review via parallel Ethernet communications. The primary and secondary voltage thresholds for the torus and solenoid are summarized in [Table XXI](#), which also provides the full list of interlocks that are managed by the control system.

TABLE XXI
TORUS AND SOLENOID MAGNET HARDWARE AND SOFTWARE INTERLOCK THRESHOLDS

TORUS Magnet system			
	Acceptable operating Range	Actual Trip Limit	Expected Threshold
Hardwire Interlocks (FAST DUMP)			
Liquid Helium Level (SC probe)	21-110%	<20%	<20%
Liquid Helium Level (Diff Press)	21-110%	<20%	
Vapor Cooled Lead Temp	4.5-15 K	>15 K	>10 K
Danfysik QD's	>200mV, 100mV(VCL), >2250 mV		Varies across sections identified
PLC Interlock - I (Fast Dump)			
Current Limit (Hard coded)	Not to exceed ± 3880 A	3850 A	± 3880 A
Software Quench, 2nd Threshold	Coil voltages are compared>350mV, VCL >125 mV		Coil voltages are compared>350mV, VCL >125 mV
PLC Interlock - II (Controlled Ramp Down)			
CCM Load Cell	Top 600lbs, bottom 1300lbs	Top 600lbs, bottom 1300lbs	Top 600lbs, bottom 1300lbs
Vertical Support	-9500lb		-9500lb
Coil Compartment 1st Threshold	Coil voltages are compared>250mV		Coil voltages are compared>250mV
Vacuum	>5x10^-5 ATM		>5x10^-5 ATM
Pressure Helium Tank	PT8120<2.3 ATM		PT8120<2.3ATM
Supercritical Helium Pressure	2.4-3.0 ATM	<2.3 ATM	
Pressure Nitrogen Tank	<2.0ATM		<2.0ATM
LL Helium Tank	<90%		<90%
LL Nitrogen Tank	<90%		<90%
VCL Flow	± 15 SLPM of SP		± 15 SLPM of SP
VCL Temp	>10 K		>10 K
VCL Voltage	80 mV		80 mV

SOLENOID Magnet system			
	Acceptable operating Range	Actual Trip Limit	Expected Threshold
Hardwire Interlocks (FAST DUMP)			
Liquid Helium Level (SC probe)	21-110%	<20%	<20%
Liquid Helium Level (Diff Press)	21-110%	<20%	
Vapor Cooled Lead Temp	4.5-20K	>20 K	<15 K
Danfysik QD's	>200mV, 100mV(VCL), >1500 mV		Varies across sections identified
PLC Interlock - I (Fast Dump)			
Current Limit (Hard coded)	Not to exceed ± 2500 A	2500 A	± 2500 A
Software Quench, 2nd Threshold	Coil voltages are compared>350mV, VCL >125 mV		Coil voltages are compared>350mV, VCL >125 mV
PLC Interlock - II (Controlled Ramp Down)			
Axial Support	0-8000 Lbs		
Radial Support	0-18000 Lbs		
Coil Compartment 1st Threshold	Coil voltages are compared>250mV		Coil voltages are compared>250mV
Vacuum	>5x10^-5 ATM		>5x10^-5 ATM
Pressure Helium Tank	PT8120<2.3 ATM		PT8120<2.3ATM
Supercritical Helium Pressure	2.4-3.0 ATM	<2.3 ATM	
LL Helium Tank	<90%		<90%
VCL Flow	± 15 SLPM of SP		± 15 SLPM of SP
VCL Temp	4.5 - 15 K		>17 K
VCL Voltage	80 mV		80 mV

V. FABRICATION AND ASSEMBLY

Torus

The six coils make up a hexagonal assembly where the hex beams carry the elements to make the hydraulic and electrical connections between coils; they also contain re-coolers that are tube-in-shell heat exchangers (see [Figure 18a](#)). The re-coolers re-cool the helium that exits each coil before it enters the next and also provide cooling for the inter-coil splices (see [Figure 18b](#)). The design is a coiled tube in a shell and works equally well both during cool down and at steady state at 4K. During cool down variable

temperature gas is transferred into the shell side. At steady state the shell side is filled with liquid helium by a thermosiphon from the reservoir in the Torus Service Tower (TST). All coils, hex beams and the service tower share a single vacuum space that is pumped on by two 8 in turbomolecular pumps.

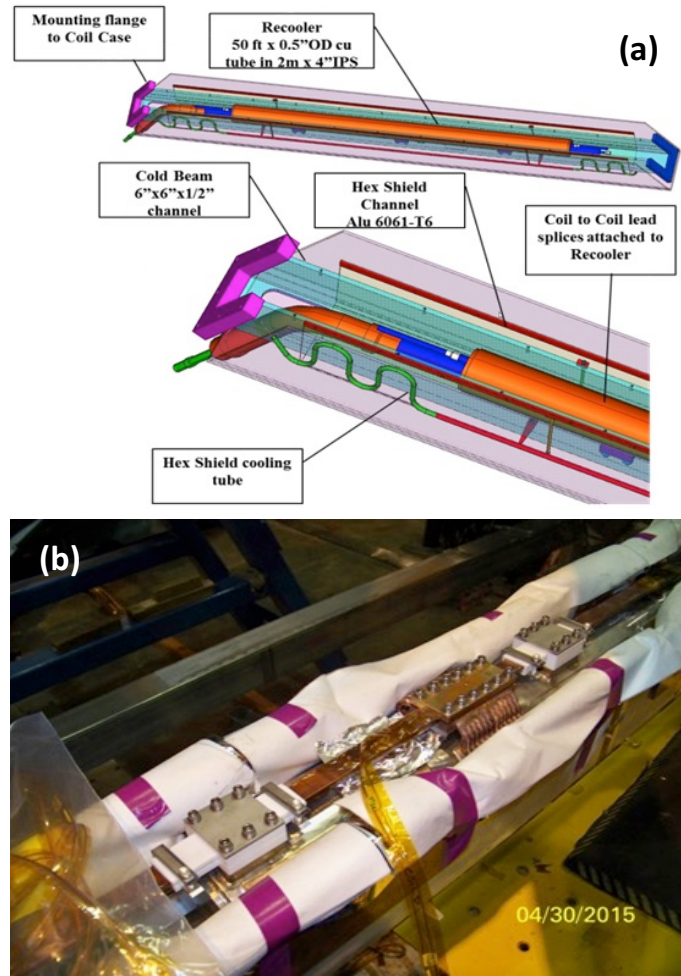


Fig. 18 (a) Typical Hex beam detail, (b) Coil splice (soldered joint) attached to re-coolers.

The individual coils are housed in an aluminum case that is approximately $2 \times 4 \times 0.05$ m, [25]. The conductor is insulated with fiberglass tape and each of the coils is wound as a double pancake. Each coil is conductively cooled by supercritical helium at 4.6 K that flows in cooling tubes located on the inner diameter of the coil. Two layers of copper sheet are soldered to the cooling tubes on each side of the double pancake and completely encase the coil, providing the main path for conduction-cooling. To allow for visual inspection of the coil potting quality the coils were first potted without the copper sheets. Ground plane insulation was then added followed by the installation of the copper sheets. The coil was then positioned and potted for a second time within its aluminum case (see Figure 19).

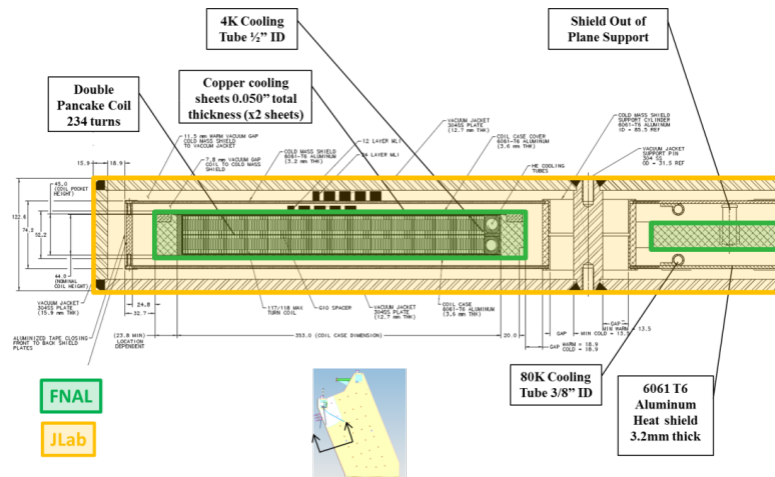


Fig.19 Coil and cryostat design (FNAL – components fabricated by Fermi Lab, JLab – components fabricated by JLab)

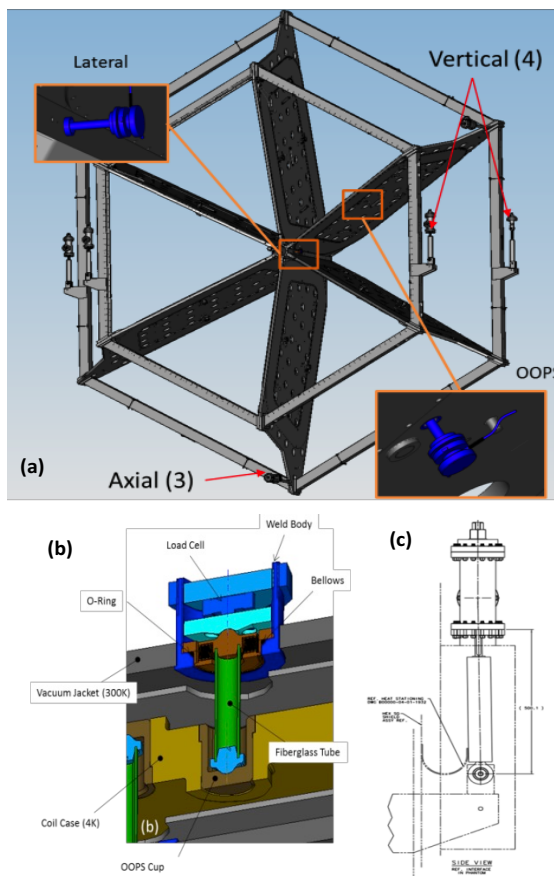


Fig.20 (a) Cold mass support system, (b) Out-of-Plane support, (c) Vertical support.

The coil case is shielded from the vacuum jacket by a 3 mm thick 80 K thermal shield. The shield is cooled by thermo-siphon-driven liquid nitrogen circulating through tubes welded to the shield. The shield is supported from the coil case by low thermal conductivity bumpers and thin-walled support arms. The shield is constructed of Al-6061 with Al-1100 strips epoxied to the shield at maximum temperature regions on the shield. The Al-6061 provides mechanical strength to the shield, while the high thermal conductivity Al-1100 strips reduce the peak temperatures. The shield has been segmented to reduce the effects of eddy currents generated during a rapid discharge of the magnet coils as described earlier.

The entire torus cold mass is supported by 3 axial supports (i.e. in the beam direction), 4 vertical supports, 2 lateral out-of-plane supports (OOPS), and 24 coil OOPS supports (see [Figure 20](#)). The coil OOPS eliminate the sag in the coils due to gravity and react to any out-of-plane forces due to misalignments and forces that arise from energization of the solenoid. The OOPS design consists of a fiberglass tube epoxied to spherical bearings. The bellows at the vacuum case maintain vacuum, allow adjustment in the out of plane direction and allow force-leveling between upstream and downstream OOPS. The bellows also allow movement of the coil during cool-down. The assembly includes a room temperature load cell connected to the data acquisition system so that the out-of-plane force seen by each coil is always known. The axial and vertical supports are stainless steel links with strain gauges mounted near the warm end. Each end has a spherical bearing rod-end and they connect the cold mass to the vacuum jacket. The vertical supports take the entire gravity load for the 25 Ton cold mass, while the axial supports react to any loads in the beam direction to adjust the magnet in the pitch and yaw directions and to handle the seismic loads.

A top-level summary of the key manufacturing steps of torus magnet construction is given in [Table XXIII](#) followed by detailed descriptions of the various steps.

TABLE XXIII
A SUMMARY OF THE KEY MANUFACTURING STEPS - TORUS

Manufacturing Step	Location
1 Superconducting Rutherford cable soldered into C-shaped copper channel	Advanced Engineering Systems (AES) LLC, PA, USA
2 Clean and inspect conductor (supplied by JLab)	
3 Wind cooling tube and apply ground insulation	
4 Insulate conductor	
5 Wind first pancake layer, set coil dimensions	
6 Turn to turn short tests	
7 Install ground insulation on coil OD	
8 Install layer-to-layer insulation	
9 Wind second layer, set dimensions, repeat tests	
10 Install ground insulation, and molding hardware	
11 Push into potting mold and flip assembly	
12 Install ground insulation on first pancake	
13 Form leads	Fermi National Accelerator Laboratory (FNAL)
14 Close and seal the mold	
15 Vacuum impregnate the coil, cure the epoxy.	
16 Remove from the mold – full coil electrical test	
17 Survey conductor location on both sides	
18 Solder copper cooling sheets on each side of coil	
19 Position coil in aluminum Case	
20 Vacuum epoxy impregnate and cure	
21 Final electrical test	
22 Ship to JLab	
23 Apply multi-layer insulation (MLI) to coil case	
24 Fit thermal shield and insulate with MLI	
25 Fit vacuum jacket and transport to hall	
26 Install torus	JLab
27 Fabricate and distribution box	
28 Fabricate torus service tower (TST)	
29 Install distribution box	
30 Install TST	
31 Commission torus	

Conductor Manufacture

Jefferson Lab contracted with AES to solder the Rutherford cable into a copper channel for the two magnets. Soldering required bonding the cable to the channel and also bonding the two layers of the key-stoned cable. Bonding between the strands adjacent to the channel was nearly perfect, but the bonding between the layers was more difficult. The main reason for the difficulty of the inter-layer bonding was the age and cleanliness of the cable. Many trials of soldering were done and much of the iteration had to do with cleaning methods. With a Minimum Quench Energy (MQE) of 47 mJ for the torus magnet the following limits were set as requirements based on a factor of safety of 10 or 4.7 mJ. An acceptable void area was determined to be about 82 mm² which implied a 9 mm diameter or approximately 4x20² mm void. Similarly, the solenoid MQE is 20 mJ and an acceptable void area is 30 mm², which translates to a 6.2 mm diameter or 5.5 mm x 5.5 mm void. A continuous automatic void monitoring system was attempted with limited success and thus improved process control was the only solution. Control of overall dimensions was also extremely important, so wiping the exterior surfaces free of solder was a key step in the fabrication process. Another key element of the process was to make each production length of conductor as a single run thus minimizing any deterioration of quality associated with the line starting and stopping. This required multiple shifts to keep the line running around the clock. To check the quality of the soldering process, cables were peeled from the channel and then strands removed from one layer to expose the center solder joint. Once the process was optimized, each soldered length of conductor had several meters removed, about 50 m in from its beginning and end, and inspected to ensure that good quality soldering was being achieved. The flux used was SUPERIOR #75 warmed to 38°C together with 60/40 tin/lead solder. After soldering, the surface solder layer was removed from the copper using buffering wheels on 4 sides to improve epoxy bonding and then the completed conductor was shipped to the Fermi National Accelerator Facility (FNAL) to start the coil winding process.

Coil Winding and Impregnation

The Magnet Department at FNAL was contracted to wind, insulate, and impregnate the torus coils before shipping them to JLab already installed in their individual aluminum coil cases. Because of the large size of the coils, FNAL had to develop new tooling and processes to support coil production operations [3,25]. At FNAL the conductor was de-spooled and cleaned once again before being wound onto a specially prepared spool (see Figure 21). These spools were also electrically insulated so that the conductor could be hi-pot tested during insulation application. The conductor was then insulated with an automated machine that applied ½ lap 0.08 mm fiberglass tape insulation around the conductor immediately prior to the start of winding. Coils were wound by first winding the 2 turns of cooling tube around the winding mandrel, followed by winding of the coil. The coil was wound as a double pancake by winding 117 turns of the first layer with the cable for the second layer supported on an insulated spool above the

coil winding table. A 0.38 mm thick sheet of G10 was placed upon the first pancake so it would be in-between the coil pancakes, then winding the second layer for a total length per coil of ~2000 m (see [Figure 22](#)). The ground insulation between the conductor and copper cooling tubes or copper sheets varies in thickness but has a minimum of 4 layers of 0.18 mm glass cloth. After each coil layer was wound, G10 shims were installed between the cooling tube and the first turn at the hub and the first 0.7 m of the upstream and downstream straight sections; shims were not applied along the radii at the corners near the hub. The primary purpose was to ensure coil to coil uniformity in the high field area (close to the hub region) and to push the extra material caused by dog-boning to the outer portions of the coil where it would have little effect on the field or physics of the CLAS12 detector system. After potting, the coils were removed from the potting mold and the FNAL survey team used photogrammetry to provide JLab with actual locations of the conductors around the perimeter of each coil (discussed later).



[Fig. 21 \(a\)](#) The conductor being cleaned from right to left. The aluminum spool with conductor from the soldering company is positioned on the winding table at right. The cleaning station (inset), is located between the two wooden spools. The tensioner with the FNAL aluminum spool is on the left, (b) Partial view of the coil fabrication shop at FNAL showing a coil being wound; the second spool is seen above the winding table.

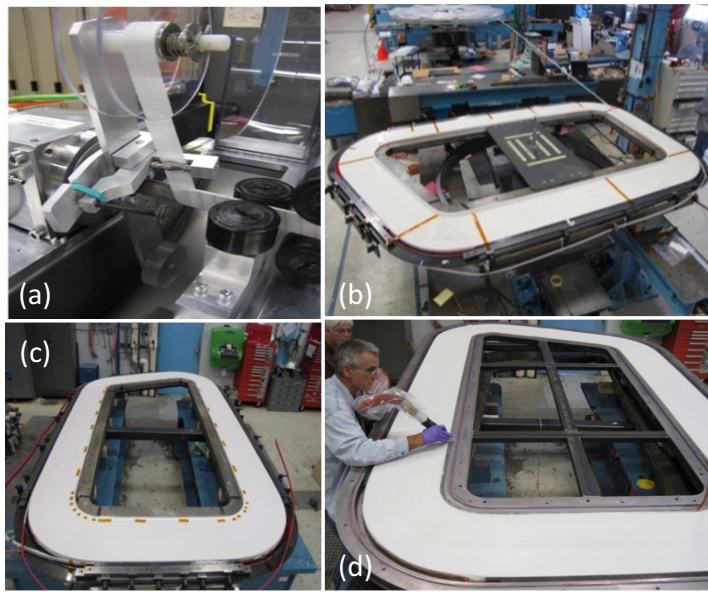


Fig 22 (a) Conductor being insulated, (b) The start of the 2nd pancake winding, (c) After 2nd pancake winding, (d) Coil in the potting mold.

During winding, the coil was also subjected to a turn-to-turn short test measurement capable of detecting both ‘hard’ and ‘soft’ (of about $1\ \Omega$) shorts between adjacent turns. Additional copper stabilizer was added to the leads before an initial Vacuum Pressure Impregnation (VPI) in a sealed mold with CTD-101K epoxy. The impregnation procedure was designed, and qualified, for proper degassing, and to prevent outgassing of the epoxy during impregnation. The temperature of the coil and of the mold was driven and maintained via resistive heating of the coil itself. Temperature uniformity was monitored and controlled via sensors mounted along the mold. The coil was then allowed to soak for 24 hr at 58°C before the cure cycle began. The cure cycle took place over 3 days with gel, cure, and post-cure stages. A layer of polypropylene mesh was incorporated between the mold and a peel-ply adjacent to the coil to allow a uniform epoxy flow over the surface of the coil, as well as to provide a route for trapped and evolved gasses to escape to one of the 3 main vacuum pump-out ports (see Figure 23).

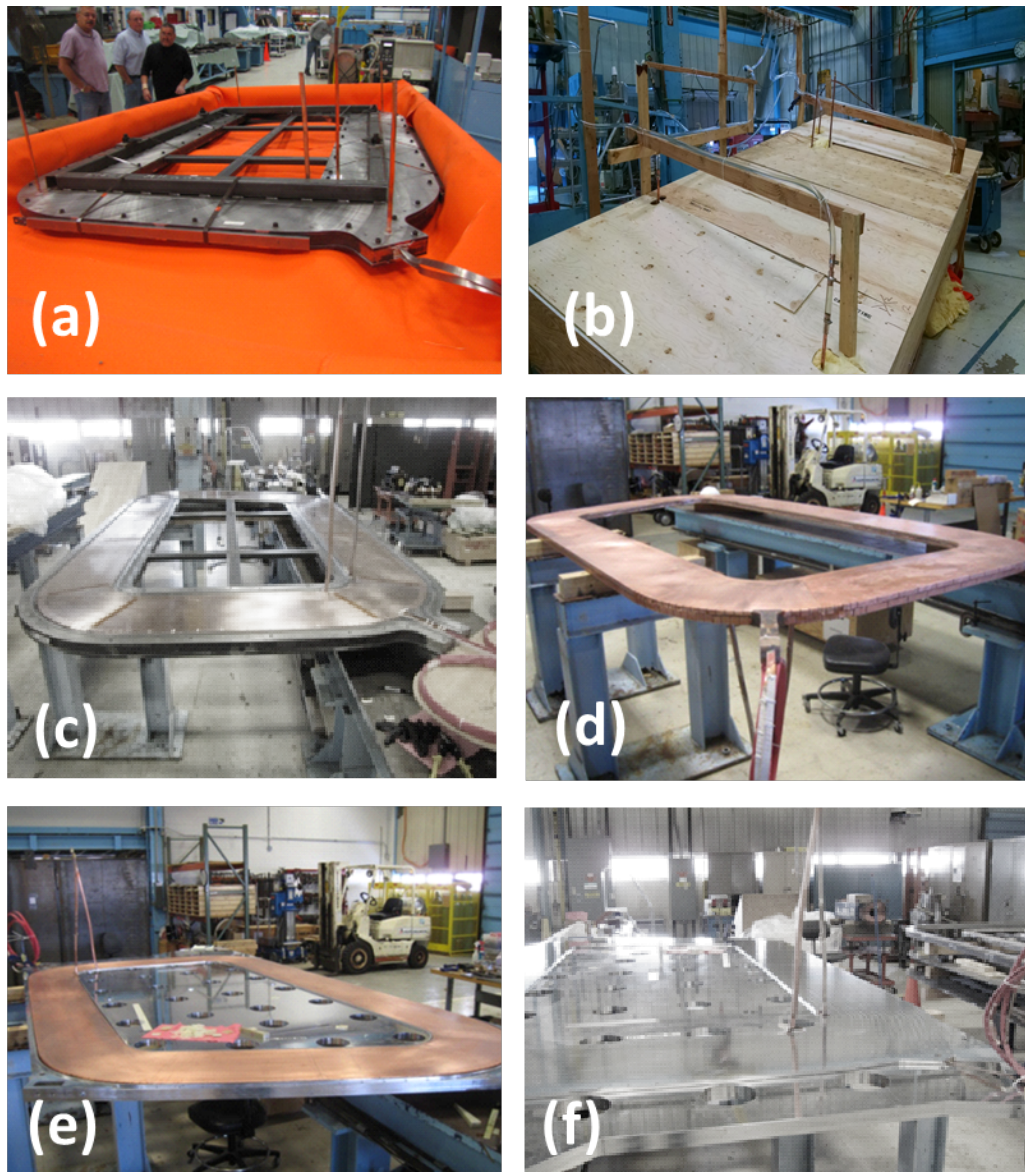
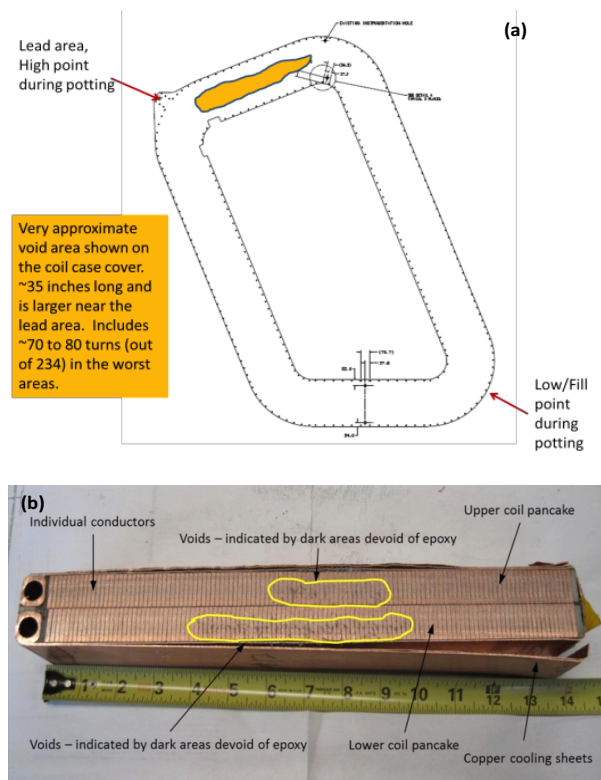


Fig 23 (a) Potting mold closed up ready for potting, (b) Hot box with potting mold installed, magnet leads, and fill/vent tubes penetrating. Box is sloped for bottom fill
(c) Top cover removed from potting mold after coil potting, (d) Coil removed from mold and flipped for mold flash cleaned up and ready for cooling sheet attachment,
(e) Coil aligned in coil case, (f) Coil case cover installed over the coil.

Upon removal from the mold, a thorough visual inspection was carried out of both sides of the potted coil to check potting quality. After initial potting, two sheets of 0.635 mm annealed OFE copper were soldered to the cooling tubes on each side of the coil and then folded over the outside of the coil. Two layers of .006 in Kapton were installed on the inner layer of copper for ground insulation and an additional layer of glass was installed between the Kapton and coil to aid in epoxy flow between the two during the second coil potting. The coil was then placed into its Al6061-T6 aluminum coil case and a second impregnation step was carried out using the same basic procedures as developed for the first potting (see Figure 23f). The difference in thermal expansion between aluminum and copper ensured an adequate preload on the coils after cool down. After the second potting, the coil case modules had

their cooling tubes formed, received their final round of quality control tests, and were then shipped to JLab for installation into their individual vacuum jackets and ultimate assembly in Hall B.

As part of the Quality Assurance plan a practice coil was fabricated by FNAL and delivered to JLab. Following the 80 K test on the practice coil and a subsequent dissection, the coil was discovered to have several “dry” areas where the epoxy had not penetrated fully (see [Figure 24](#)). A team was formed to investigate and address this problem and included experts from the USA and overseas organizations. Over a four month period, this team reviewed the impregnation process and carried out multiple trial runs on coil samples. An improved impregnation process was developed and implemented. This resulted in the successful production of six coils and two spares. The improvements to the impregnation process were also shared with the vendor for the solenoid magnet.



[Fig 24](#) (a) Voids identified on practice coil, (b) sectioned coil indicating problem areas.

Key changes in the fabrication for the torus coils included:

1. Changing of the sequence assembly by attaching the copper cooling sheets after first potting thus allowing complete visual inspection
2. Adding material (polypropylene mesh and peel ply) in the coil potting mold to take up the space left by the copper and ground plane and to allow resin distribution and removal of the spacer
3. Fine tuning of resin degassing and infusion process

80 K Cold Test and Cryostating

A “Cryostat Factory”, set up at JLab, facilitated the assembly of each coil as it arrived from FNAL. Upon arrival, each coil was inspected, instrumented with temperature sensors and strain gauges, and underwent a cool down test to 80 K (see [Figure 25](#)) to assess the robustness of the coil’s electrical insulation and its structural integrity, as well as to test the efficacy of the employed conduction cooling method [\[26\]](#). Table XXII summarizes the results obtained from the 80 K test, data extrapolation to 4 K, and comparison with the results obtained from the finite element analysis. The results indicated that the conduction-cooling system was indeed functioning as designed with more than adequate safety margin.

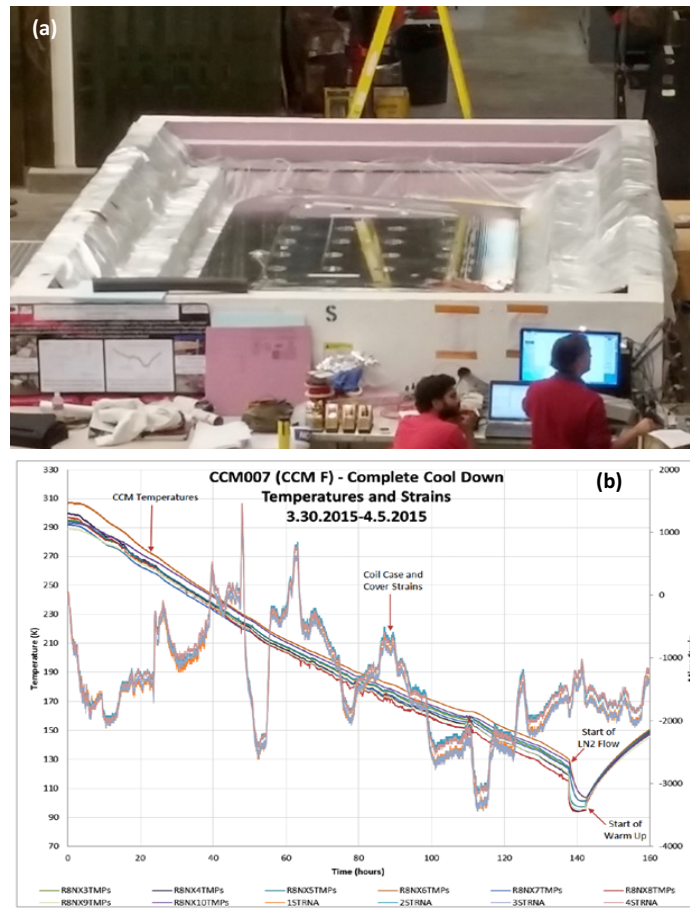


[Fig.25](#) (a) Coil placed in large ‘foam’ box being prepared for the 80 K test, (b) Cool down curve during 80 K test.

TABLE XXII
80 K DATA CORRELATION TO CALCULATED RESULTS

LOCATION	80 K Test	80 K Test	4 K Scaled	4 K Scaled	4 K
	Result Front	Result Back	Result Front	Result Back	ANSYS FEA
Temperature difference at Hub (bore) K	4.00	3.10	0.12	0.09	0.251
Temperature difference at Downstream HEX K	7.20	4.80	0.22	0.15	0.834

Consistent with the program risk mitigation approach of practicing every quality or schedule-critical procedure, the Cryostat Factory practiced cryostating a full-scale empty coil case, which was later disassembled and returned to FNAL for use on a production CCM. This early practice allowed refinement of the assembly procedures and construction time estimates.

After warm-up from the 80 K cold test, the CCM was then wrapped in multi-layer insulation (MLI), fitted with its MLI-covered nitrogen-cooled thermal shield (see [Figure 26](#)), and vacuum jacketed before being moved to the experimental hall for final system assembly (see [Figure 27](#)).

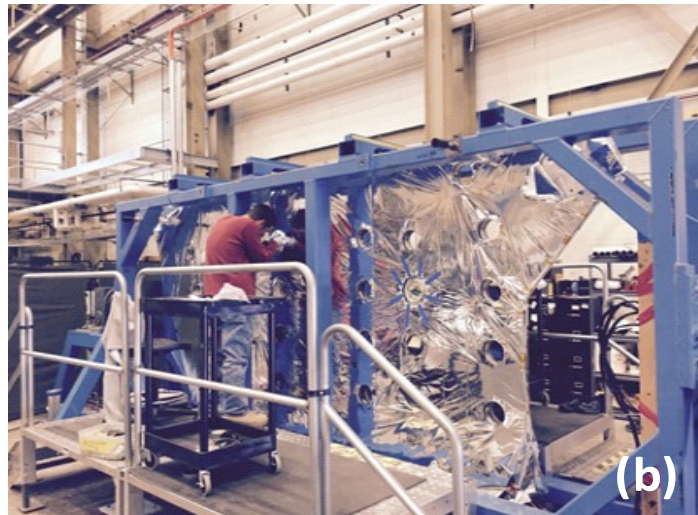




Fig. 26 (a) First production coil in its case received from FNAL, (b) Applying Multi-Layer Insulation (MLI) to coil case, (c) coil with thermal shield installed and in rotatable jig (to allow fitting of instrumentation on the other side).

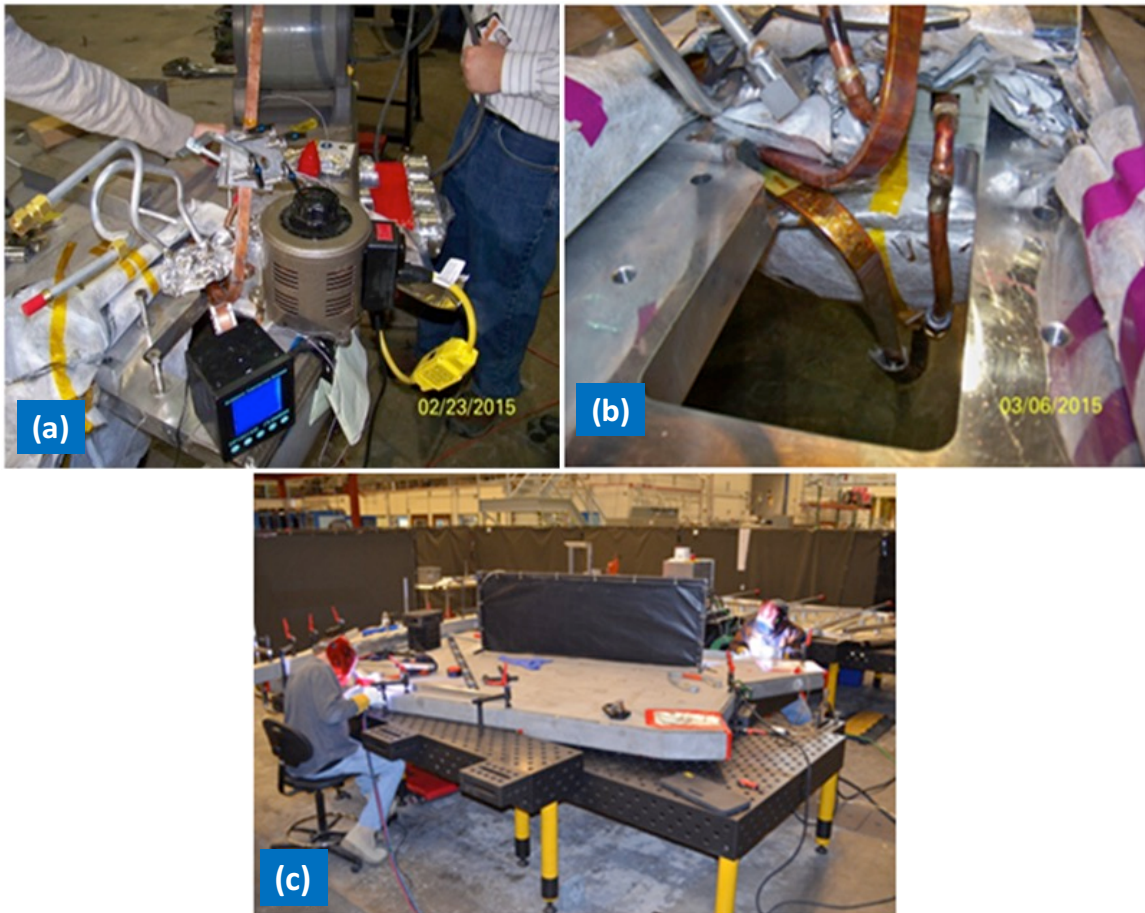




Fig 27 (a) Soldering additional copper stabilizer to the leads as they exit from the vacuum jacket, (b) Stabilized leads bent to required shape and insulated – ready for transport to the hall, (c) Welding shut the vacuum jacket, (d) Final coil to be delivered to the hall from the JLab Cryostat Factory.

Solenoid

The superconducting Rutherford cable for the solenoid was soldered into its copper channel by Advanced Engineering Systems LLC and transported to Everson-Tesla Inc. in Nazareth, PA, where it was de-spooled, inspected, cleaned, and re-spooled prior to the start of winding. The solenoid magnet was fabricated at Everson-Tesla and the whole process was overseen by JLab engineers.

A top-level pictorial view of the manufacturing and build sequences with a summary (see [Table XXIV](#)) of the overall magnet construction at the solenoid vendor (ETI) follows (see [Figures 28-33](#)):

TABLE XXIV
A SUMMARY OF THE KEY MANUFACTURING STEPS - SOLENOID

Manufacturing Step	Location
1 Superconducting Rutherford cable soldered into C-shaped copper channel	Advanced Engineering Systems LLC, PA, USA
2 Conductor inspected and cleaned	
3 Conductor insulated with glass-cloth and wound onto bobbin (coil former)	
4 Leak check and pressure test of C1-4 bobbin cooling channels and pipe work	
5 Wind Coil 1 (inner coil) and epoxy pot	
6 Wind Coil 2 (inner coil) and epoxy pot	
7 Wind Coils 3 and 4 (intermediate coils) on common C1-4 bobbin and epoxy pot	
8 Wind Coil 5 (shield coil) and epoxy pot	
9 Cool down Coils 1 and 2 (using LN ₂ boil-off) and shrink-fit into C1-4 bobbin	Everson-Tesla Inc (ETI), PA, USA
10 Assemble Coil 5 over C1-4 bobbin using 4 cross-member beams	
11 Rivet and solder thermal ‘copper fingers’ between all coils	
12 Assemble thermal shield and C1-4 bobbin into vacuum jacket	
13 Fit suspension links	
14 Leak check and pressure test of internal circuits	
15 Weld shut vacuum jacket	
16 Leak check	
17 Ship to JLab	
18 Fabrication of solenoid service tower (SST)	JLab
19 Installation of SST and solenoid	
20 Commissioning of solenoid	



Fig. 28 Left to right: (a) central cooling channel with Helium ‘buttons’ installed – the copper cooling sheet fingers were later soldered to these buttons, (b) inset picture showing a helium button before welding into channel (the ‘fins’ on the button are located inside the channel), (c) one of the two inner coils being wound, (d) One of the two inner coils after epoxy potting was completed (the slotted copper cooling sheet can be seen on the inner surface of the coil, potted with the coil).



Fig. 29 Left to right: (a) Coil 3 being wound into its pocket on the Coil 3-4 bobbin, (b) Coil 4 (lower coil in the picture) having its potting mold being fitted around it in preparation for epoxy potting, (c) the Coil 3-4 bobbin being lowered over one of the two inner coils for the shrink fit operation (the copper cooling sheet with fingers can be seen potted in with coils 3 and 4 on their outer surfaces), (d) Coils 1 and 2 assembled within the Coil 3-4 bobbin and Coils 3 and 4 being instrumented with CERNOX temperature sensors.

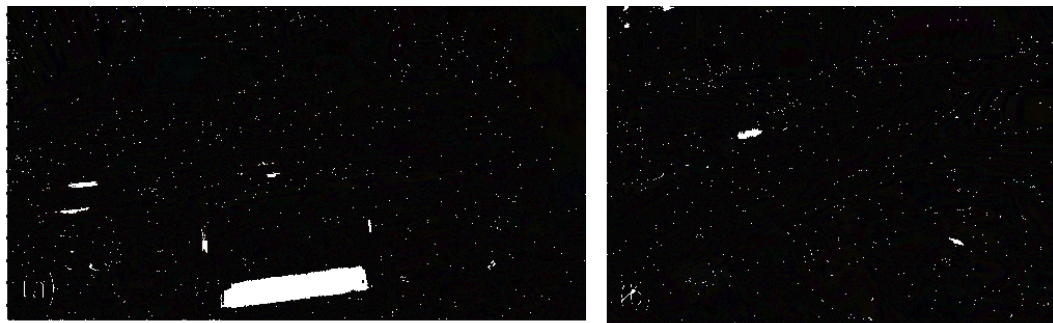


Fig. 30 (a) Coil leads being routed on the outside of Coils 3 and 4, (b) Additional copper stabilizer being soldered to leads.



Fig. 31 Left to right: (a) Stycast being painted onto the outer diameter of Coil 5 after epoxy potting before being overwrapped with additional glass fiber cloth tape,
(b) Inserting Coils 1-4 into the Coil 5 bobbin, (c) All five coils assembled together.



Fig. 32 (a) Copper cooling ‘fingers’ being riveted and soldered across all coils – these fingers provides the conduction cooling path from the central helium annular channel to each individual coil, (b) Fingers being taped over with aluminum tape.

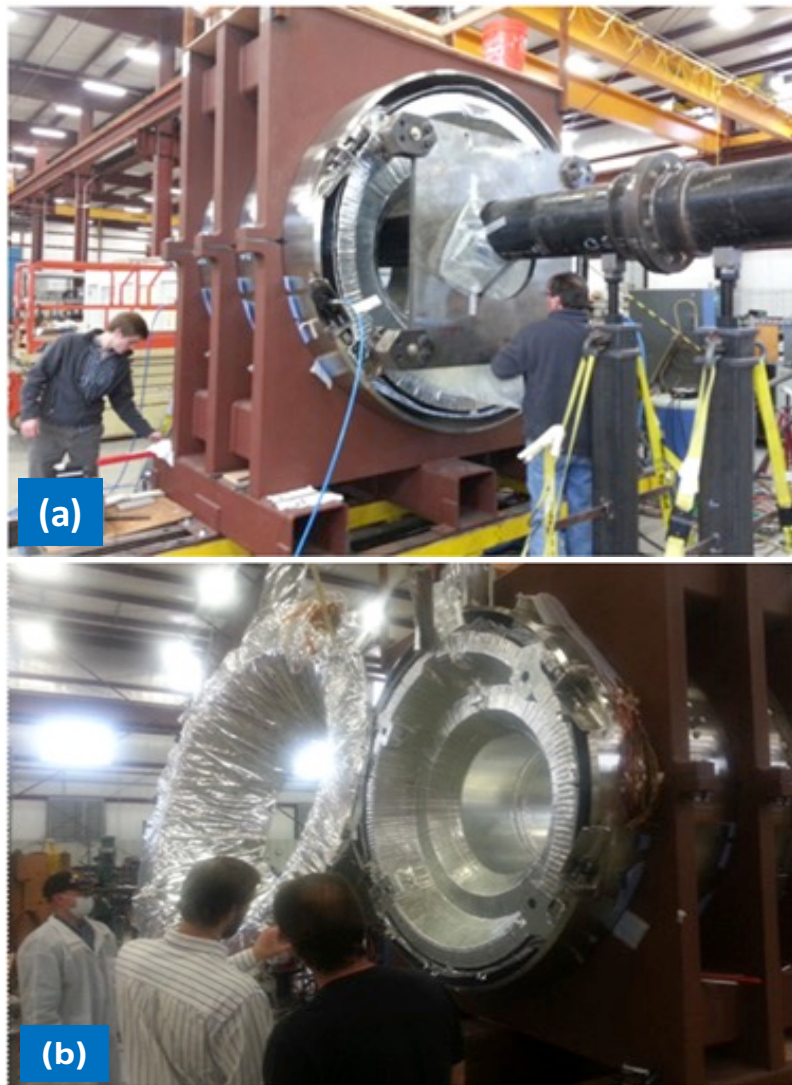




Fig. 33 Left to right: (a) Cold mass inserted into vacuum jacket, (b) Thermal radiation shield end cap being installed, (c) Solenoid in shipping cradle and transport fixture being loaded onto air-ride low-loader truck bed at vendor's site.

VI. INSTALLATION IN EXPERIMENTAL HALL

Torus

Installation in the hall used the “rotating spit” method (see Figure 34a). Individual coils assembled in their individual vacuum cases, (with a portion of the vacuum case open to enable attachment to the central hub, see Figure 34b), were transported into the experimental hall. After the first coil was attached to the hub, two adjacent hex beams were attached and the whole sub-assembly was rotated before the next coil was brought in and connected to the hex beams and so on until all 6 coils were assembled (see Figure 35). This whole sub-assembly was freely rotatable around the central axis to allow critical operations (like splicing or welding) to be performed at a convenient and safe location and orientation.

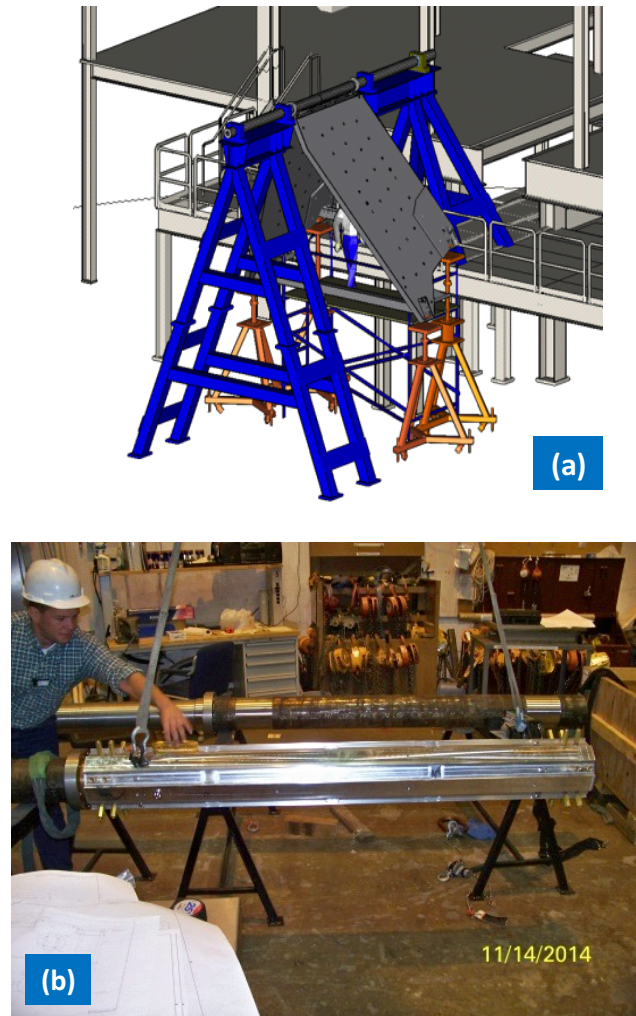
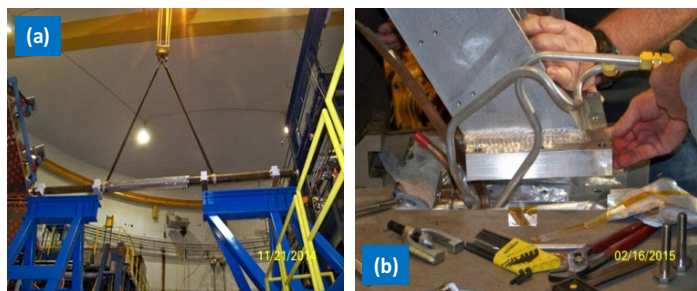


Fig. 34 (a) Installation philosophy used the “rotating spit” method, (b) Inspecting the hub before lifting into place on the ‘spit’.

Given the complexity of assembling the torus magnet within the hall (see Figures 36-42), it was important to pay special attention to the in-process Quality Assurance (QA) checks. Although not an exhaustive list, the QA checks fell into three major categories: a) electrical checks, b) leak and pressure checks, and c) survey checks. Each time a coil-to-coil splice was made in the hall, a room-temperature resistance measurement was taken across the splice and between the start and end leads for the entire coil). At that point, the inductance was measured using an inductance (LCR) meter, with extrapolation to the DC value. Finally, a hi-pot to ground test was carried out to verify the splice insulation. Likewise instrumentation checks were carried out routinely at the completion of each hex beam fitting, and each time the coils were rotated.



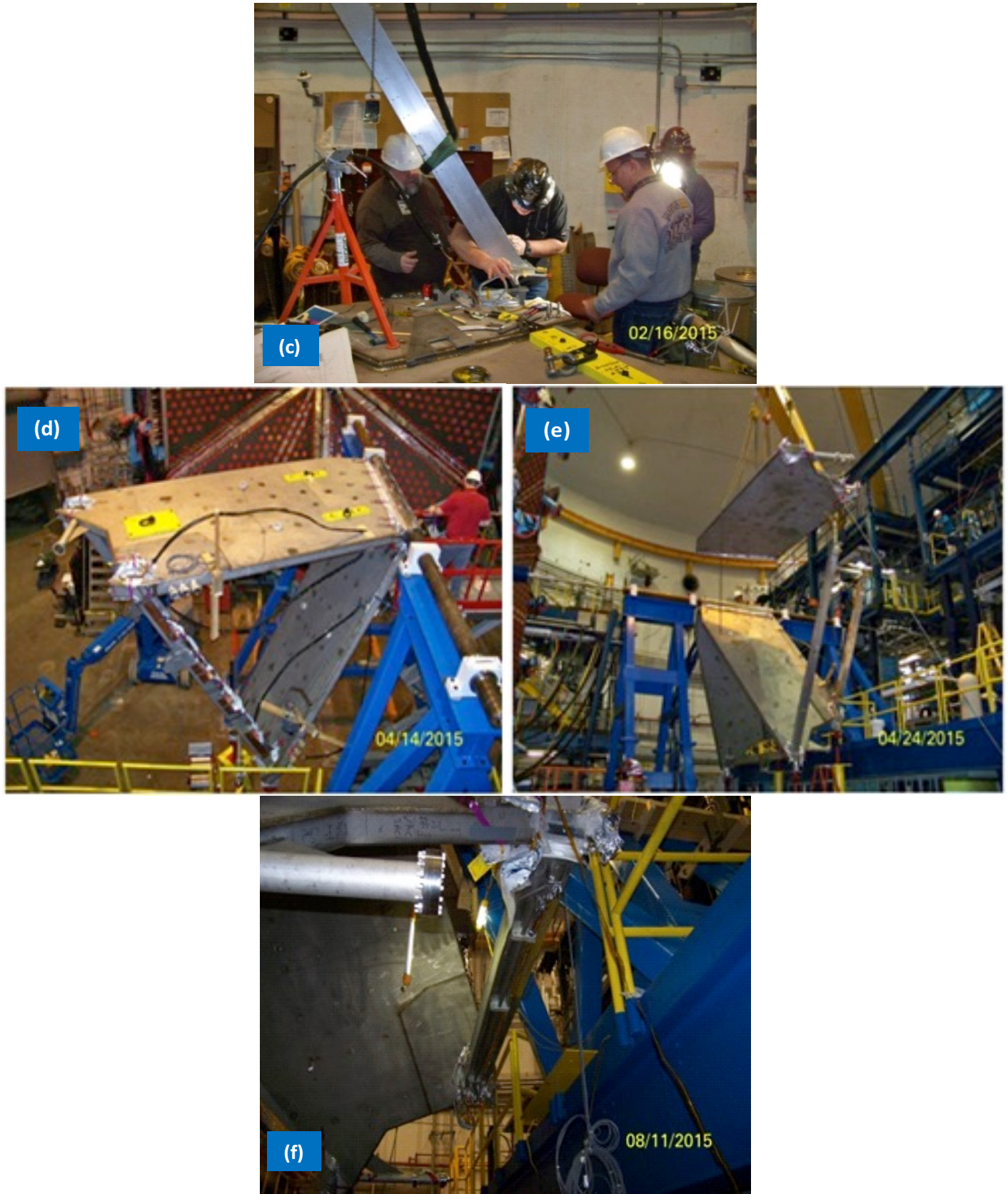
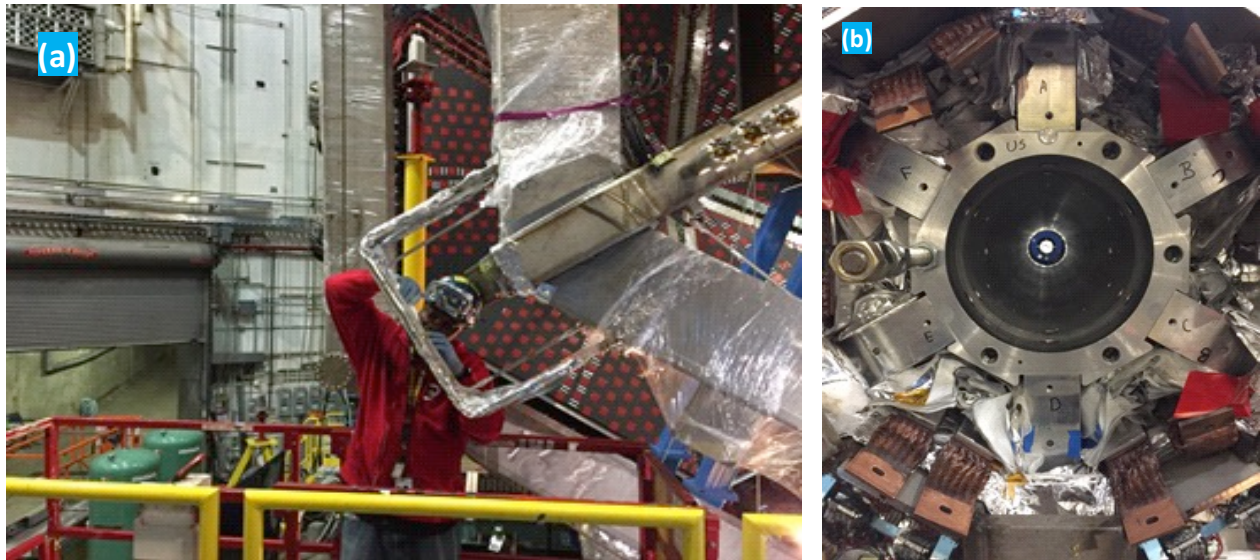


Fig. 35 (a) Installing the hub, (b) and (c) Trial fit of a hex beam to a coil (d) hex beams fitted between the coils (e) Third coil on the crane with torus rotated and hex beams installed to accept it, and (f) upstream hex beam in horizontal position to allow for convenient and safe working.



Fig. 36 (a) Splice soldering using purpose-built temperature-controlled heating rig, (b) Applying MLI to the splice joints, (c) Load testing an axial support.



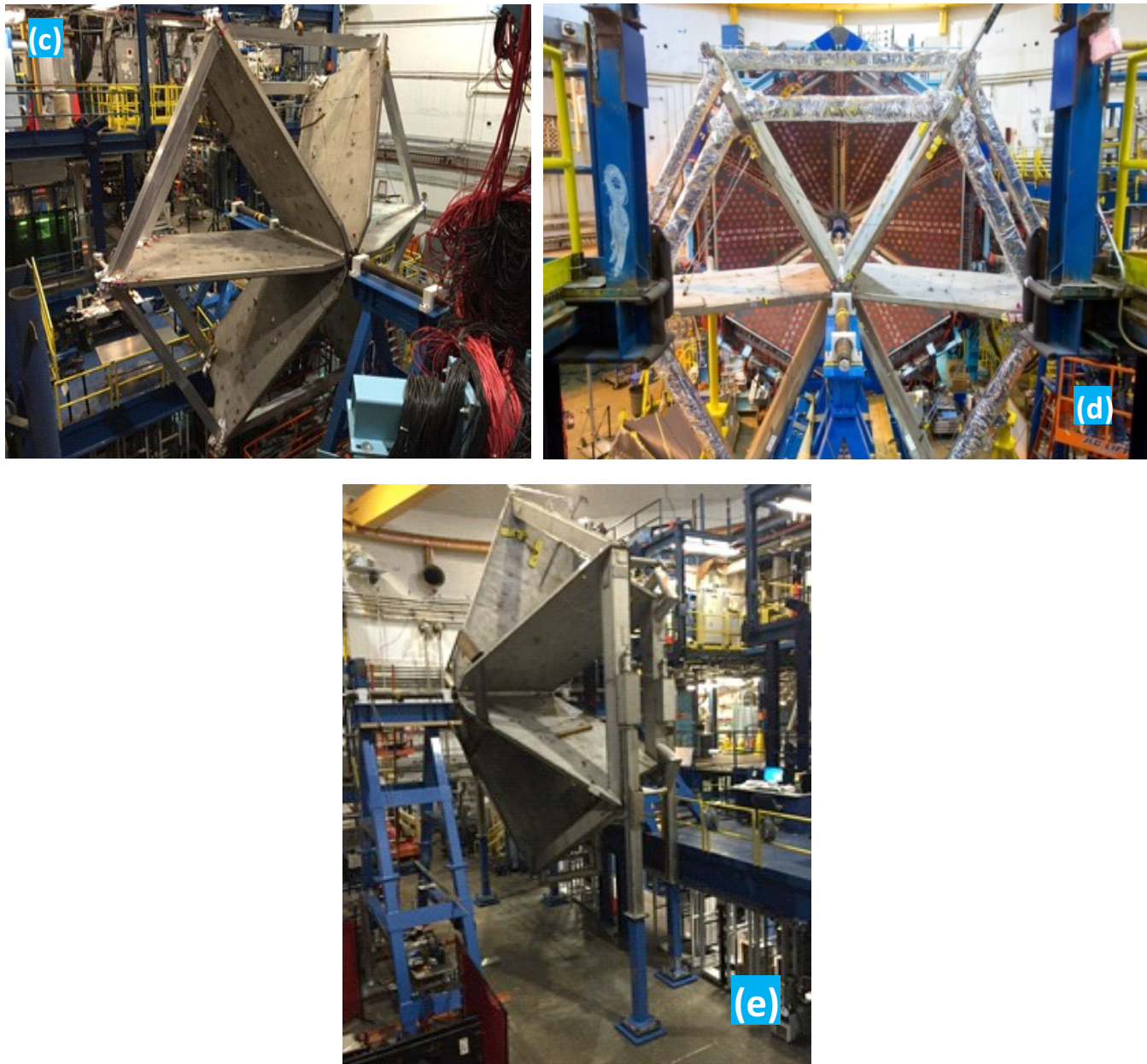


Fig. 37 (a) Insulating a cryogenic ‘jumper’ between hex beams, (b) Aligning and shimming the coils on the hub – the ends of the six coils (A,B,C,D,E,F) can be seen located on the hub, (c) All torus coils and hex beams installed, (d) hex beams wrapped in MLI, (e) torus rotated to final position with legs installed.

All connections of each cooling circuit between coils within the vacuum jacket were made by either welding or brazing. Aluminum welds and copper brazes received a liquid nitrogen cold shock but stainless steel welds were exempt. Once each circuit that joined the 6 coils was completed it was pressure and leak tested prior to burying it in MLI. Surveys for alignment were also carried out after attaching each coil to the hub, and a global survey was done at the completion of the hexagon. Torus leak testing did not find any internal leaks, even after the pressure testing. For the external leak testing we employed two leak detectors, one at the TST and one at coil D (6 o’clock position). This arrangement was sufficiently accurate in finding external leaks and upon completion of testing, there was no sign of any leaks even on the most sensitive scale of the leak detectors.

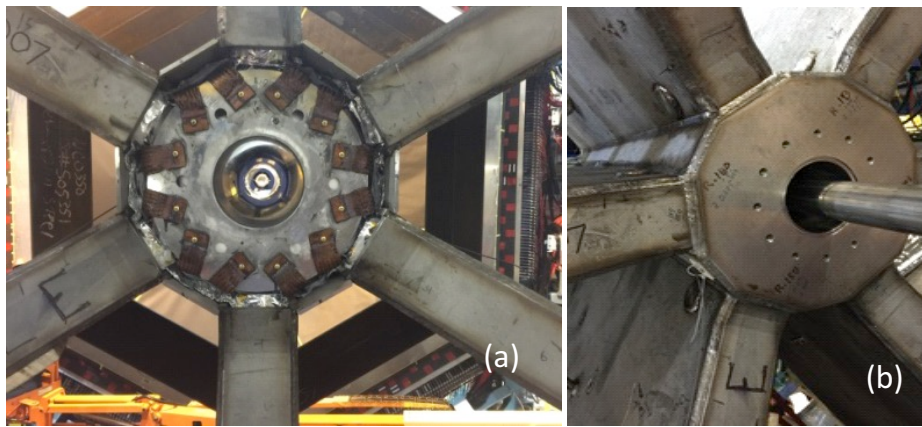


Fig. 38 (a) Aluminum thermal shield inside the bore installed with copper thermal straps, (b) Hub vacuum jacket ready to be welded shut.

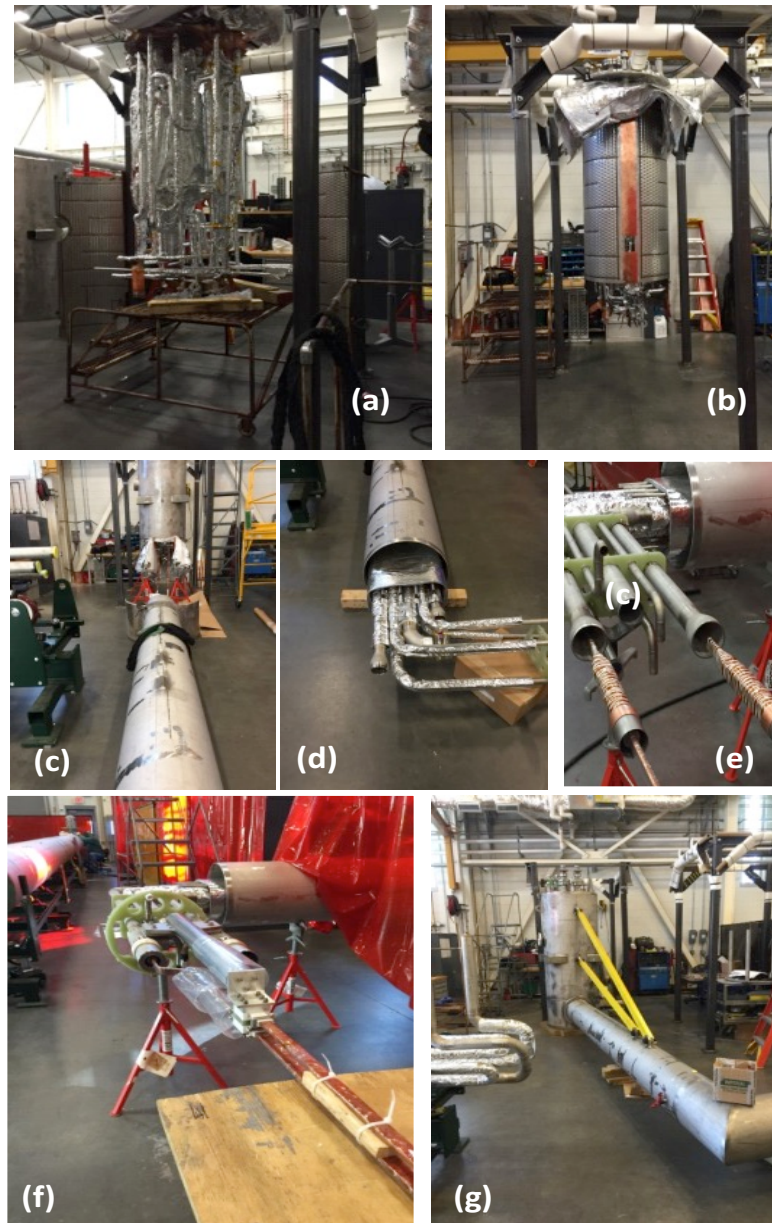


Fig. 39 (a) Torus Service Tower (TST) internals insulated with MLI, (b) Thermal shield fitted, (c) Preparing the cryo-duct for attachment to the TST, (d) Cryo-duct pipework insulated with MLI, (e) Superconductor splice joints and leads at the helium-vacuum interface, (f) Insulated leads, (g) Cryo-duct welded to TST body.

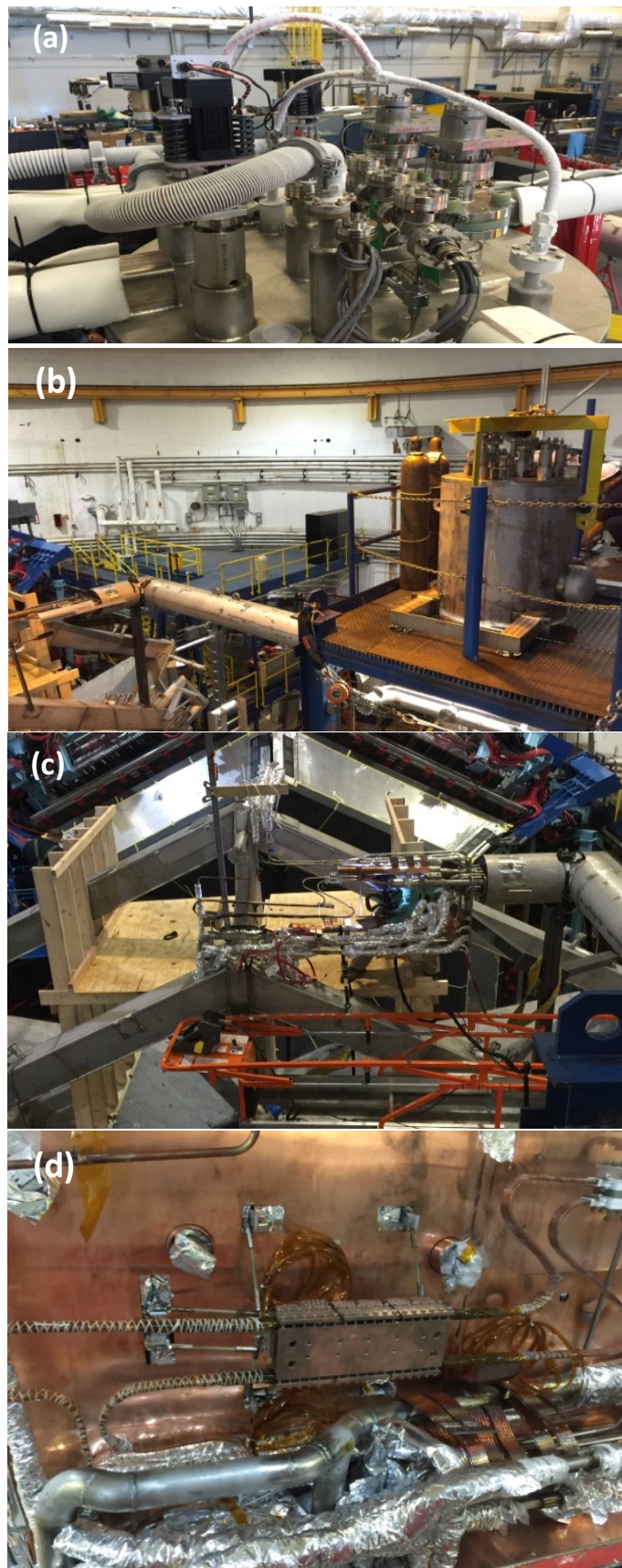


Fig. 40 (a) Cold testing TST pipework, (b) TST in place on the space-frame, (c) Cryo-lines connected between the TST and the torus, S-shaped conductor splices completed, (d) Conductor splices in the torus 'chimney'.

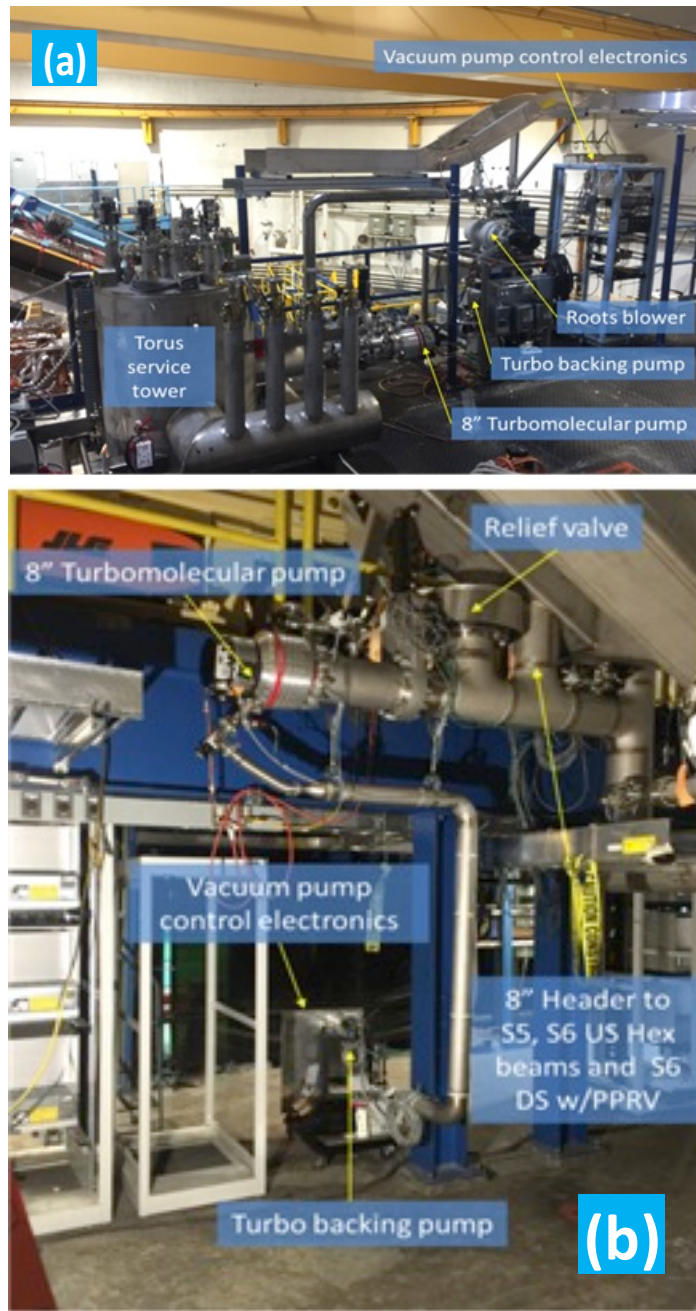
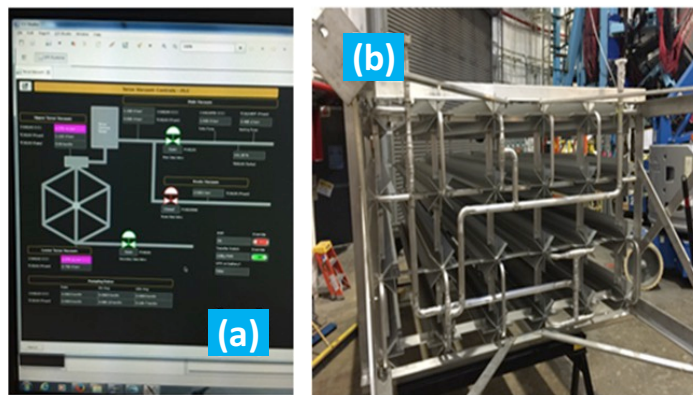


Fig. 41 (a) Primary pumping system mounted on service tower, (b) Supplemental pumping system mounted on hex beam at the lower end of the torus.



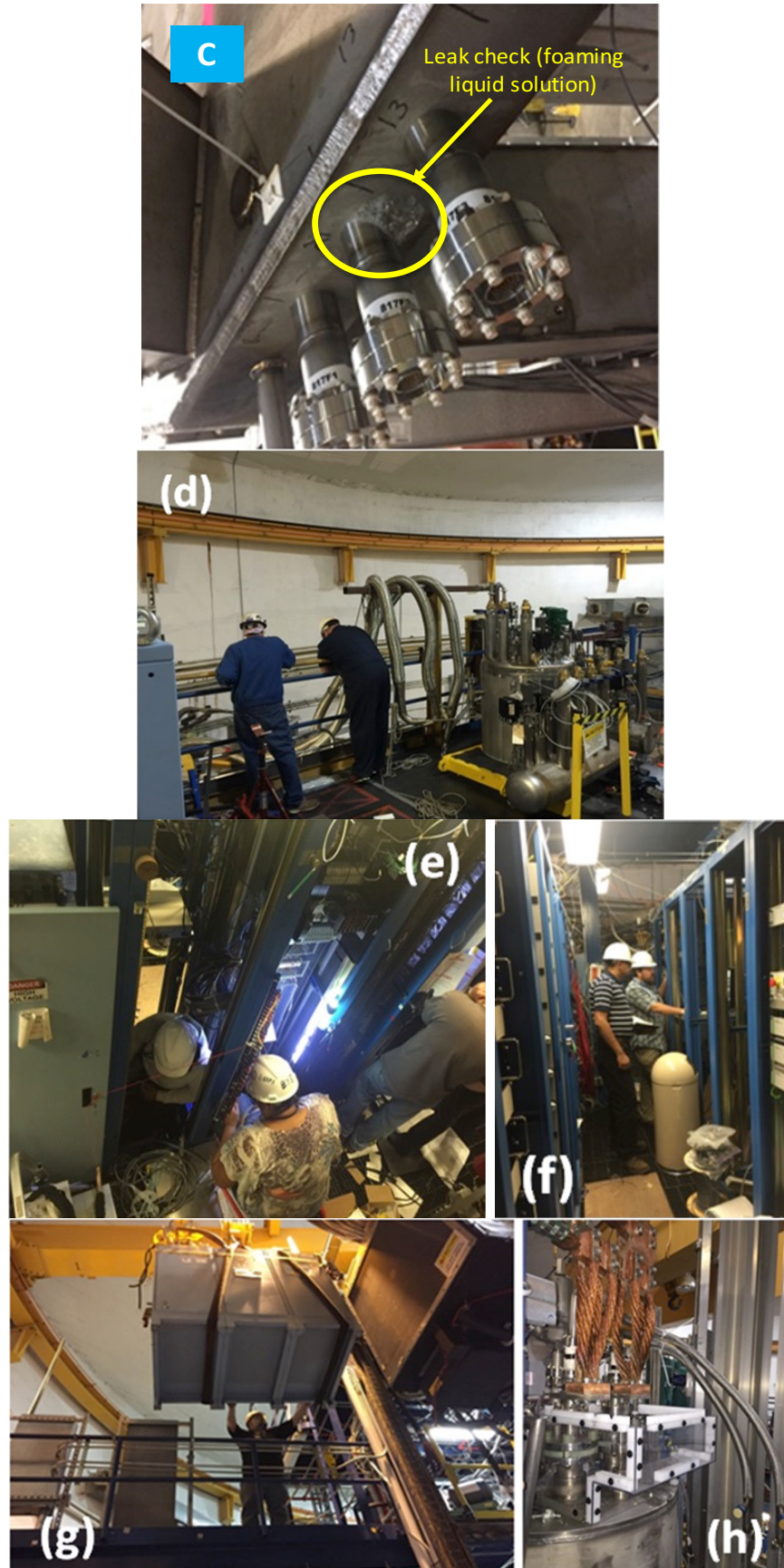
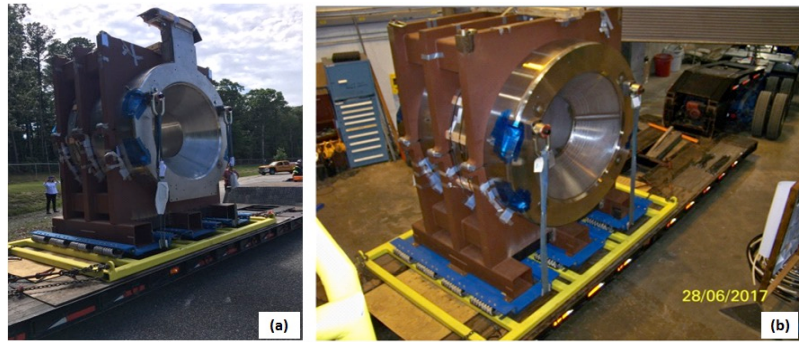


Fig 42 (a) Vacuum control screen for the torus, (b) Modifications to an ambient vaporizer from the previous CLAS6 system to reduce pressure drop, (c) Leak checking with foaming liquid solution, (d) Distribution can in place in Hall B, (e) Wiring up instrumentation racks, (f) Carrying out checks on the instrumentation, (g) Lifting a magnet power supply into position (h) Flexible copper jumpers connecting the torus water-cooled leads to the magnet vapor-cooled leads.

Solenoid

The magnet was built by Everson-Tesla Inc. (ETI) and transported by road to JLab using a purpose-built shipping cradle and vibration isolation transport fixture (see [Figure 43](#)). To assure safe transport, several dummy runs between ETI and JLab were carried out and data on the acceleration loads were collected. These data were used for analysis of the magnet structure with temporary shipping supports.



[Fig. 43](#) (a) Solenoid in shipping cradle and transport fixture arrival at JLab, (b) solenoid arrival in Hall B at JLab.

Upon arrival at JLab, a visual inspection was completed along with testing of the internal sensors and their wiring. The magnet was then lifted onto its installation cart on the beamline in Hall B. It was rough-aligned by the JLab survey and alignment team and the temporary shipping braces were replaced with the final supports and load cells. The solenoid service tower (SST) built by JLab was ready several months before the solenoid arrival, and was already in Hall B and roughly positioned upon the space frame above the beamline (see [Figure 44](#)). With the solenoid on the beamline, the SST was then aligned to the solenoid. The two splices that connect the SST to the magnet were completed and instrumented with voltage taps and temperature sensors before the internal welding commenced. Pressure and leak tests followed, similar to the torus. Finally the multi-layer insulation blankets were applied and the vacuum jacket was welded shut (see [Figure 45](#)).

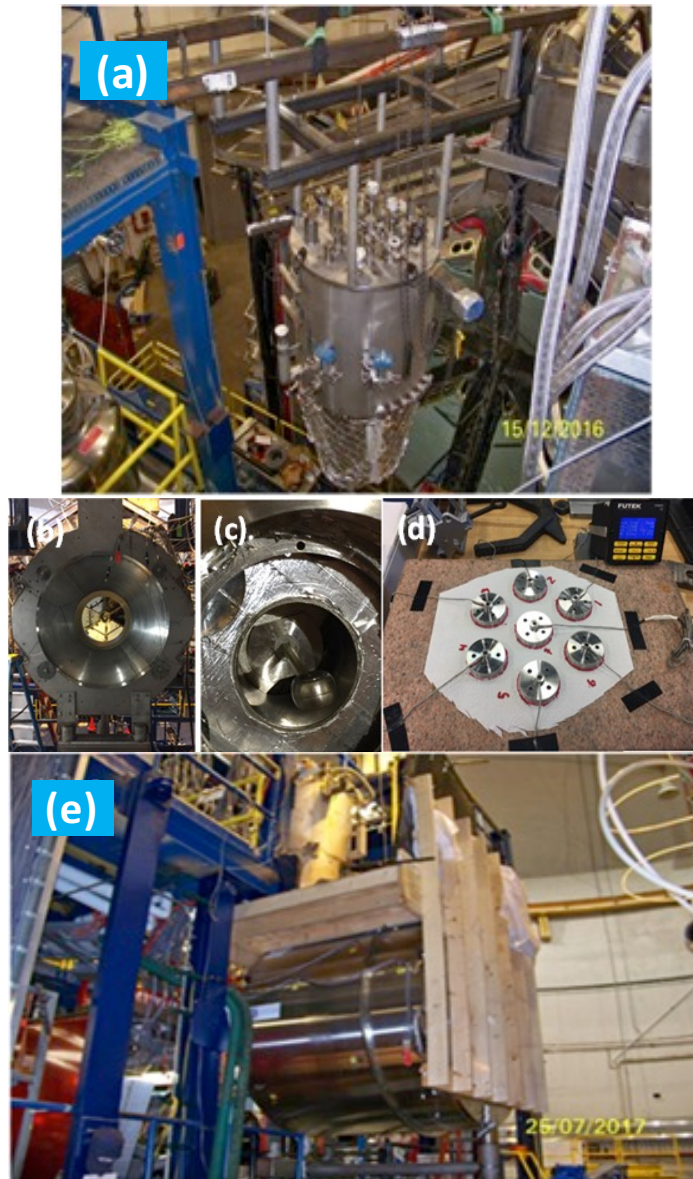


Fig 44 (a) The Solenoid Service Tower being lifted into place on the space-frame within the hall to await the arrival of the magnet, (b) Solenoid on its cart awaiting removal of axial support shipping fixtures and installation of axial support rods, (c) one of eight axial support rods being fitted within a pocket which will then be connected to a load cell, (d) Axial support load cell readings being checked for consistency prior to installation, (e) Solenoid in position on its 'cart' with a temporary wooden platform installed to allow welding of the service tower to the magnet.

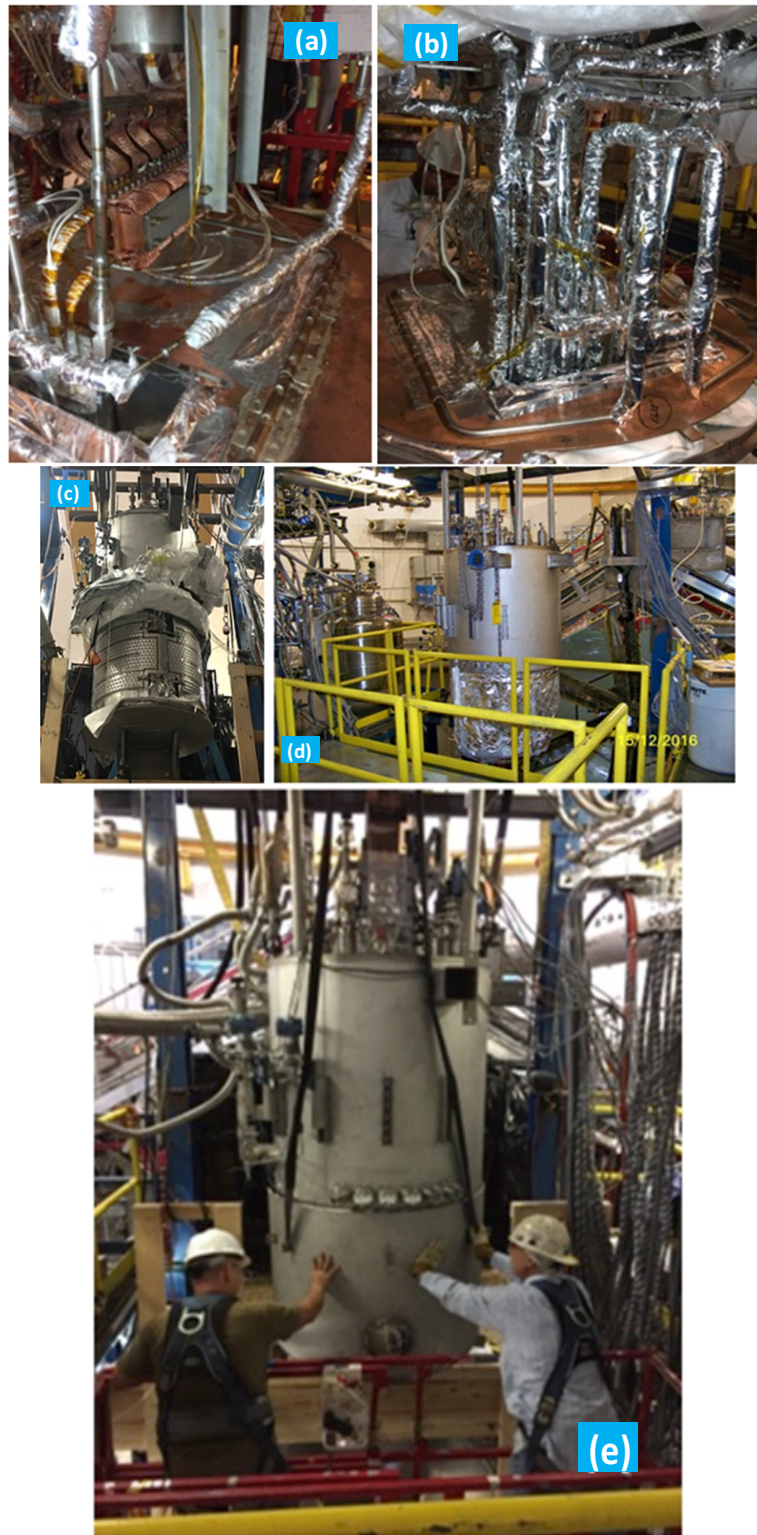


Fig 45 (a) Splices joining the magnet start and end leads to the vapor-cooled leads in the SST, (b) Splice block and cryogenic pipework wrapped in MLI, (c) Service tower thermal shield welding completed, (d) Service tower – ready to have its vacuum jacket closed up, (e) Fitting the SST vacuum jacket prior to final welding.

The magnet arrived from the vendors at the end of June 2017 and was fully installed by early August 2017. The whole installation process took less than 2 months using multiple teams working around the clock. The final installed magnet is shown in [Figure 46](#).

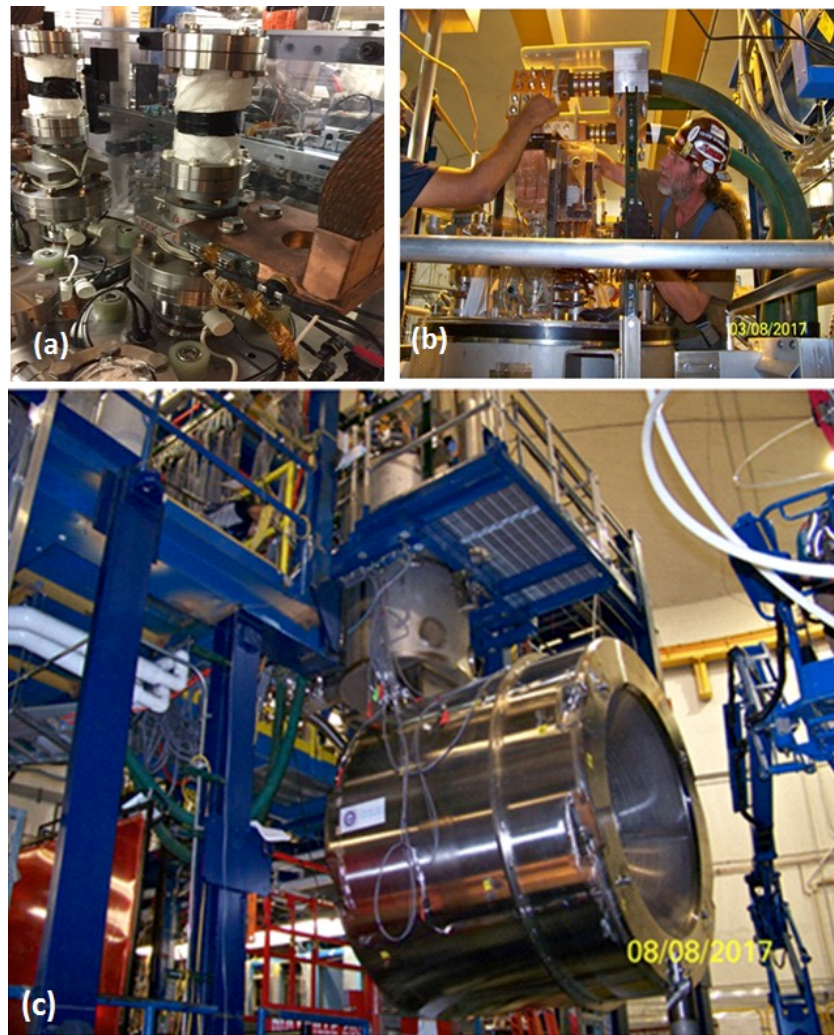


Fig.46 (a) Ceramic break fitted to the top of vapor -cooled leads – temporarily wrapped in paper, (b) Connecting the water-cooled leads to the vapor-cooled leads at the top of the SST, (c) Solenoid magnet installation complete with ‘crow’s nest’ service platform installed around the SST.

VII. COMMISSIONING AND TEST RESULTS

The vacuum spaces of both magnets were pumped down before being cooled to operating temperature. Then tests were carried out at predefined excitation currents to confirm that the overall system response was as designed. All electromagnetic and cryogenic parameters were monitored during the tests to validate the cryogenic circuit design. Additionally, each magnet was ramped to low currents to minimize its stored energy before a controlled fast discharge was initiated. This allowed the JLab team to check that all system protection mechanisms were operating as designed, thereby mitigating any further risk when the magnets were run at their full operating currents. The torus magnet reached its full operating current of 3770 A without any quenches in November 2016 while the solenoid reached its full operating current of 2416 A in September 2017 with 5 quenches in Coils 3 and 4 attributed to training quenches. The solenoid retained all its quench training.

Each magnet has its own cryogenic service tower, which is fed from a common cryogenic distribution box. The monitoring, control, protection, power, vacuum, and cooling sub-systems are similar but independent for each magnet. Although the systems are separate, a cryogenic ‘event’ in one magnet can affect the other and vice versa since both magnets share the same distribution box

[4].

Torus

Pump Down - Before the final vacuum pump down proceeded, all the OOPS were properly set to allow for vacuum jacket deflection. The pump down started gradually at about 2 psig/hr for the first 7 hours to alleviate any coil-case ‘ballooning’ effects and to minimize any movement of the MLI. A roots blower followed by turbo-molecular pumps were used to reduce the pressure to about 10^{-4} Torr before initial cool down and several backfills with gaseous nitrogen were used to assist with the removal of water within the system. The pressure in the system reached about 5×10^{-5} Torr after cool down started.

Purification -A process piping purification process using gaseous nitrogen (GN_2) and gaseous helium (GHe) was used to clean the nitrogen and helium circuits. The nitrogen circuit only needed to be free of water and flow purged with warm GN_2 . The helium circuits needed to be free of water as well as all other contaminate gases.

The initial purification of the torus included purification of the entire Hall B cryogenic system. This included all the warm gas piping, ambient vaporizers, cryogenic transfer lines, distribution box (DBX), U-tubes that interconnect the DBX to the 500 liter helium buffer dewar, U-tubes that interconnect the DBX to the torus, the Buffer Dewar and the torus. There are 3 cold connections at the End Station Refrigerator (ESR) that are used, 4K helium supply, 4K helium return, and LN_2 supply. There are two warm gas connections to the ESR, 300 K 4 atm helium and 1 atm 300 K return helium.

Cold-connection U-tubes at the ESR were not installed and warm connection valves were closed. Where possible each circuit was purged with room temperature boil off nitrogen gas for several days to drive off moisture. The warm helium supply line could not be purged this way because there is no vent on the ESR end. It is also noted that care was taken not to pressurize the helium circuits above 1 atm with nitrogen, to keep from contaminating the operating ESR. The nitrogen circuits were then pumped between 0.5 atm and 0.1 Torr three times and backfilled with nitrogen. At this point the N_2 circuits were considered clean.

The helium circuits were pumped and backfilled through the same pressure range five times. Pumping and backfilling allowed access to the small dead end ranges of the circuits such as pressure transducer lines and relief valve lines. After pumping and backfilling the helium circuits, purging through the system was done using clean helium from the ESR and sending it back to the refrigerator helium recovery system. This recovery system has nitrogen contamination monitors to verify the level of contamination in the return gas. After the pump and backfills, the return gas to the recovery system indicated that little to no contamination was returned, thus our N_2 purge and helium pump and backfills were deemed to have been successful and complete. A similar process but on a much smaller scale was performed for the solenoid.

Cool Down – The unique nature of the torus structure with a cold hub and cold beams made it especially critical to minimize temperature differences between the beams and the coils. Detailed FEA calculations were done and showed that a maximum DT

(temperature gradient) of 50 K between them could be tolerated during the cooling process at temperatures between 300 and 100 K for the 4 K mass. The independent nature of the LN₂ shields did not have this physical requirement. The piping of the supercritical circuit is nearly 200 m long with most of it split equally between tubes in the coils and re-coolers. Due to this long length, limited flow at room temperature can be pushed through this circuit with the 4 atm helium supplied to the hall at room temperature. To achieve the required cool down time of 3 weeks, the re-coolers were also designed to be used during the cool down process and performed well.

The cool down of the torus was carried out using variable temperature helium gas provided by the distribution box. Inside the distribution box are two heat exchangers that cool one stream of helium to 80 K. This 80 K helium was mixed with room temperature helium to allow variable temperature gas to be fed to the supercritical circuit and also the shell side of the re-coolers. This then allowed the even cooling of all the coils and the hex beams. During the cool down the maximum difference between the average coil temperature and the average Upstream Hex beam temperature was 12 K and it averaged about 10 K. For the downstream beams vs. the coils, the maximum difference was 25 K at the beginning, but once the flows were balanced, it averaged about 2 K. With these achieved values we were very safe compared to our allowable difference of 50 K. For safety we had the PLC programmed to shut off all cool down flow if the differences ever exceeded the allowable maximum.

To gently cool the heat shield we took 80 K boil off from the LN₂ pot in the distribution box and with an electrical heater in the U-tube between it and the TST, heated the gas to provide a controlled temperature gas to the shield. Again this was interlocked to turn off the heater and the flow if the maximum difference between any of the six coil shield outlets and the shield supply reached 60 K.

From room temperature to about 100 K the cool down rate of the torus was 0.5-0.7 K/hr. The cool down time from 300 K to about 4 K for the torus was calculated to be about 14 days assuming a maximum temperature differential across the cold mass of 30 K and helium flow rate of 7 g/s. In reality, the cool down took longer and was carried out in several steps. During the cool down process (at about an average CCM temperature of 209 K), it was noted (via observation of strain gauge readings on the supports) that the four torus vertical supports were apparently bending. This necessitated a slow-down in the cooling process (to about 170 K) and finally a temporary halt while measurements and strain gauge calibrations were checked. It was discovered that although some of the strain gauges were not being adequately temperature-compensated, the vertical supports were indeed experiencing some level of bending. A risk review was convened to plan the path forward and four options were considered – which included a ‘worst’ case option that required a warm-up to room temperature to repair the vertical supports by cutting into the vacuum jacket. A spare vertical support was tested at liquid nitrogen temperature and was demonstrated to have a more than adequate strength safety factor under bending (see [Figure 47](#)). It was thus determined that it was safe to continue with the torus cool down, which was then resumed and the torus achieved its helium operating temperature of 4.5 K without any further issues.

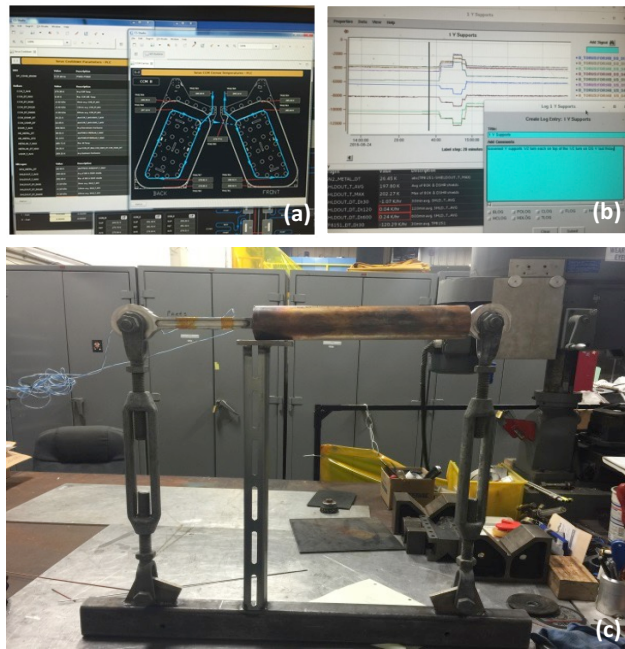


Fig 47 (a) Monitoring coil temperatures during cool down, (b) Investigating strange bending behavior of vertical supports - monitoring forces on supports, (c) Bend testing a spare vertical support.

Steady State Cooling - The US (upstream) cold hex beams contain the cryogenic and electrical connections (splices) between coils, as well as the re-cooler heat exchangers. The re-coolers contain liquid helium and are connected by large tubes to the helium reservoir at 1.3 atm. located within the Torus Service Tower (TST). Two small tubes originate at the bottom of the TST and run through the three re-coolers, exiting at the bottom of the re-cooler outer shell. Since the liquid in the small tube is denser than the heated fluid in the re-cooler's outer shell, a thermosiphon is used to exchange the cooler reservoir liquid with the shell side fluid. The 1.3 atm. liquid helium cools the 3.0 atm helium before entering each coil.

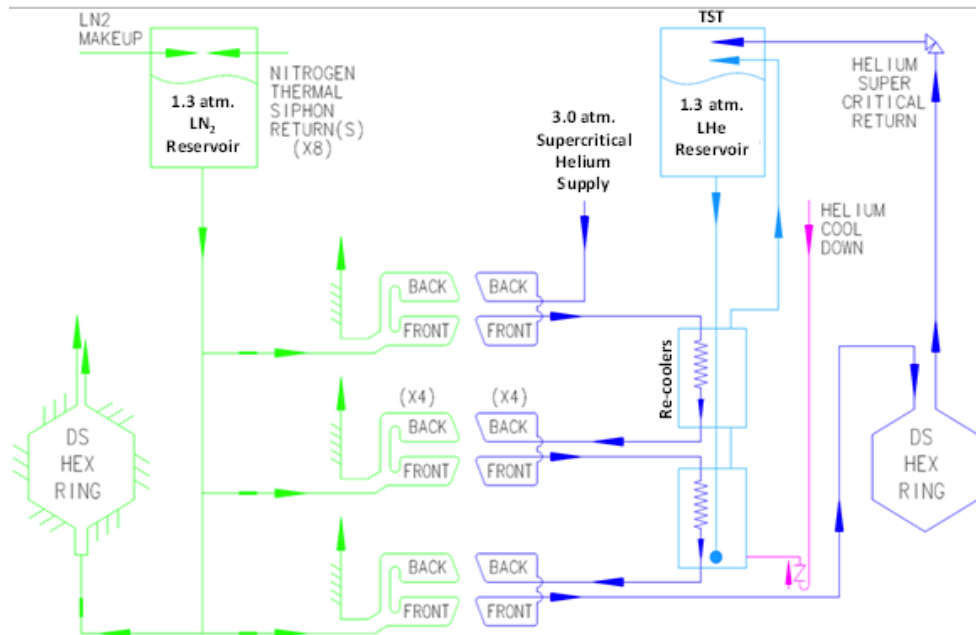
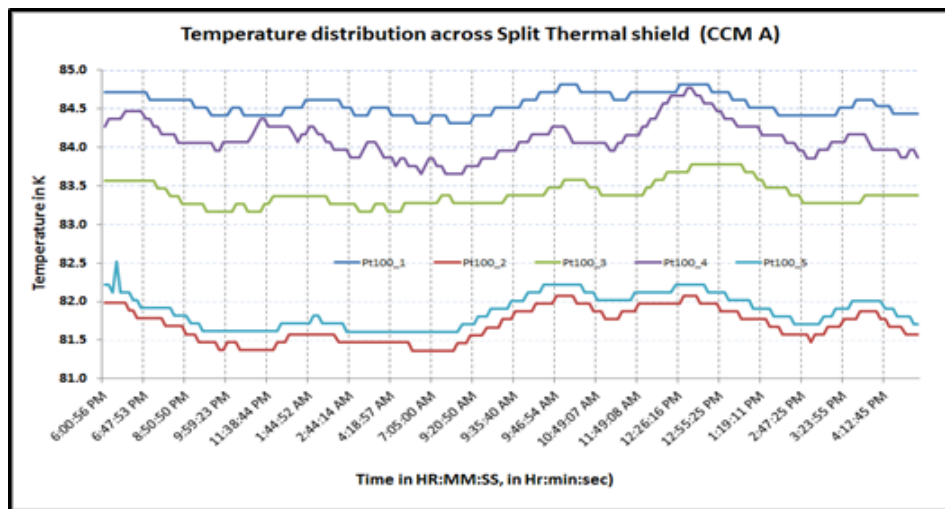


Fig. 48 Simplified flow diagram of the CLAS12 torus helium and nitrogen cooling circuits.

The cooling scheme (see [Figure 48](#)) consists of three separate flow circuits as follows:

- 1.3 atm helium circuit* - helium fills the LHe reservoir (light blue) within the TST, it then flows down through the re-coolers to the blue dot. Thermal siphon flow returns back up through the re-cooler outer shells and the upstream hex beams.
- Supercritical helium at 3.0 atm* - (dark blue) passes through a re-cooler coil in the TST helium reservoir, then through six coil/re-cooler sets, through tubes cooling the downstream cold hex beams, and through a final heat exchanger coil in the TST helium reservoir prior to flowing through the Joule-Thompson valve that fills the TST reservoir.
- The 1.3 atm LN₂ circuit* – (green) also utilizes a thermosiphon flow with one main feed separating into 8-parallel branches that keeps each shield at ~80 K to reduce thermal radiation to the coils and cold hex beams (see [Figure 49](#)). Out of 8 total branches, 2 feed into the downstream hex beam shields and 6 feed into coil shields.



[Fig 49](#) Steady state temperature distribution across one of the thermal shields.

Solenoid

Pump down and Purification

The pump down of the solenoid was much faster and easier because the magnet has much less surface area, an overall smaller size and better conductance between the turbo pump and the magnet. Purification was done similarly to the torus using a GN2 purge for several days, followed by 5 pump and backfills then flowing to the purifiers while monitoring the contamination level.

Solenoid Cooling

This five-coil magnet is also conduction cooled by 4.5 K helium, but unlike the torus coils, the heat is directly transferred to liquid instead of supercritical gas. The cool down system for the solenoid is the same one as for the torus and was used while the torus was at 4.5 K. Similar interlocks and controls were used to assure safe cool down. The magnet's liquid helium cooling channel is located between the two main inner coils and runs around the inner diameter of the bobbin. The thermal shields are cooled using the boil-off from the magnet LHe reservoir. The magnet is held at its operating temperature by conduction cooling via a thermosiphon helium

circuit from the magnet reservoir (see [Figure 50](#)). Adequate instrumentation with redundancy is provided to monitor and control the magnet cool down and steady state operation.

Pre-commissioning checks on all sub-systems, controls, and instrumentation were carried out for each magnet prior to starting the commissioning process. The torus and solenoid were cooled in 2-steps. Variable temperature gas was used to cool from 300 K-100 K, followed by LHe to 4.5 K.

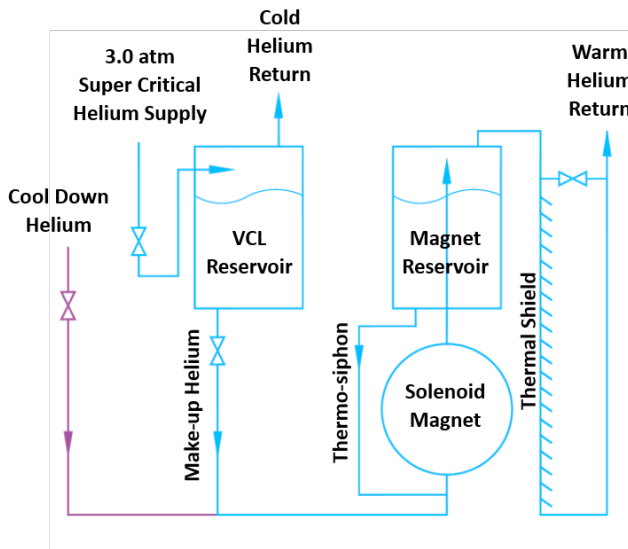


[Fig 50](#) Simplified cooling circuit schematic for the solenoid.

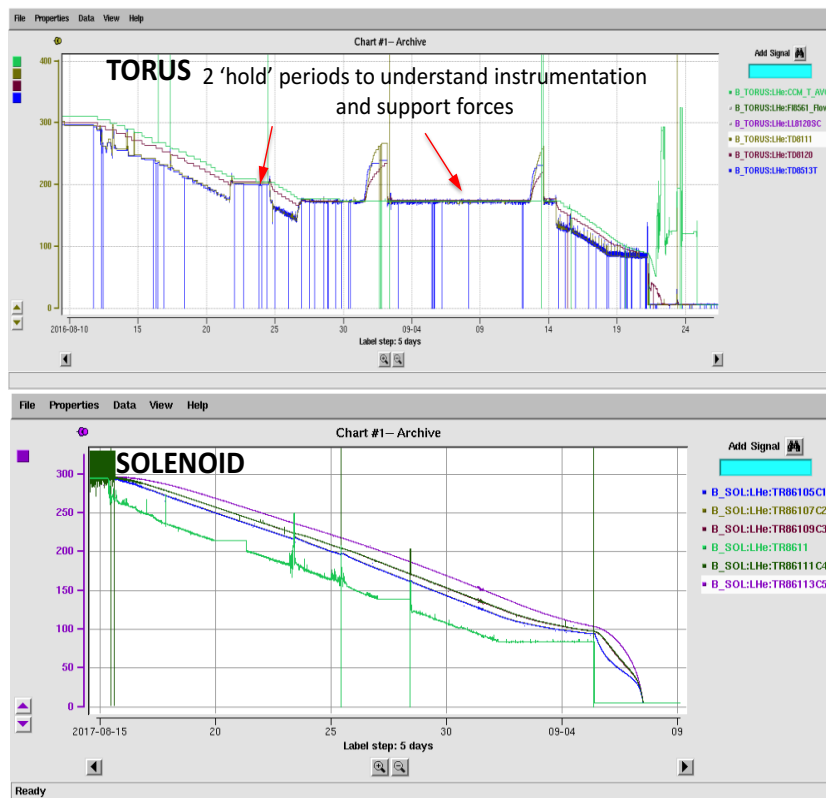


[Fig. 51](#) Torus and solenoid cool down (torus cool down: Start-August 12, 2016; Complete-September 22, 2016 and solenoid cool down: Start-August 5, 2017; Complete-September 7, 2017).

Inlet temperature to the coils, average coil, and outlet temperature were monitored. The maximum cooling rate was limited to 2 K/hr (see [Figure 51](#)).

- Total time = 43 days (torus), 23 days (solenoid)
- Cooling time = 19 days (torus), 23 days (solenoid)
- Helium temperature controlled at 45 K below the maximum metal temperature for the torus and between 35 K and 60 K below maximum metal temp for the solenoid
- Maximum allowed metal temperature differences for the torus was limited to 50 K, while for the solenoid it was 46 K. In practice the maximum temperature differences were controlled to about 25 K for the torus and about 40 K for the solenoid.
- Cool down helium flow rate for the torus was 6-7 g/s and 5-6 g/s for the solenoid

At steady state the solenoid magnet itself requires only 0.4 g/s of liquid helium for its cooling. This flow was measured directly using a room temperature flow meter. This flow rate does not include the amount of flow needed for the [VCLs](#), the lead reservoir, or the primary supply and return U-tubes.

Torus process safety

The operational protocol developed for the cryogenic process was guided by results of a study carried out by Ghoshal *et al* [27], which considered the worst-case scenario of having a loss of vacuum (LOV) and a simultaneous magnet quench.

During an LOV, quench, or fast dump the piping systems are protected from over pressure by over-pressure relief valves. There are five relief valves placed along the 3.0 atm cooling circuit. Three valves, set to vent at 5.3 atm, are placed strategically along the path of the CCM's and re-coolers and are located on the Hex Ring Vacuum Jackets, while two valves are set to vent at 4.6 atm and are located on the TST. In the event of a fast dump, a check valve in the supply U-tube prevents any back pressure into the Distribution Box. The 1.3 atm circuit is protected by a 2.7 atm relief valve located on the TST.

During a LOV and magnet quench, the highest system pressure for this circuit will occur at the farthest point from the relief valve in the re-cooler piping. The majority of the energy imparted to the 1.3 atm circuit comes from the LOV. The energy imparted [by](#) the magnet quench is much lower as it is indirectly transferred to the 1.3 atm system; (a) first to the 3.0 atm helium flow and (b) then into the 1.3 atm system through the re-coolers.

However, in the 3.0 atm circuit during a relief event the highest system pressure is realized at a point in the circuit between relief valves, buried within the coils and re-coolers where flow may go both ways. Using a simple model to estimate the system pressure rise (assuming all energy generated is transferred to the helium), the estimated pressure rise (during a fast dump) is shown in Figure 52. It is apparent that if all the energy from the 3000 A fast dump was transferred to the helium, the design pressure of 20.0 atm of the system would be exceeded. However, using calculations from a more detailed model, it was demonstrated that the 20.0

atm pressure rating of the pipes would not be exceeded in the torus circuit due to the distribution of energy throughout the entire system. Our commissioning tests have since validated the findings of this analysis.

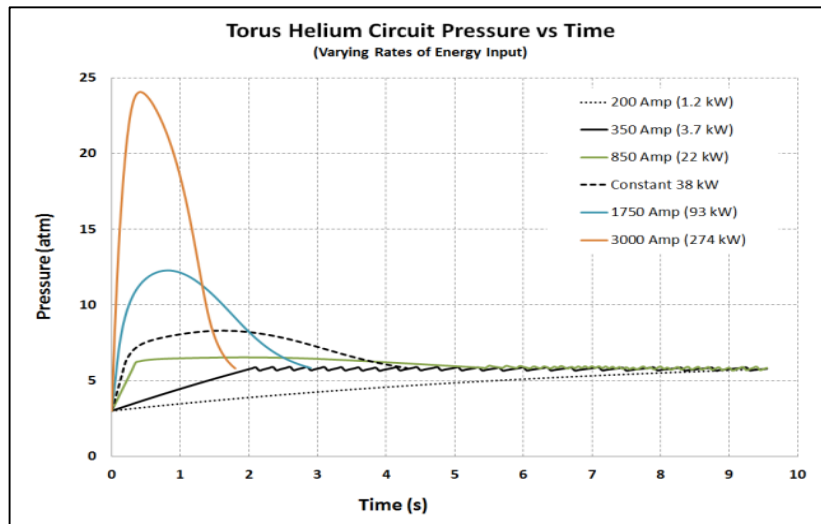


Fig. 52 Estimate of torus helium circuit pressure with time at increasing operating currents based on the simple model.

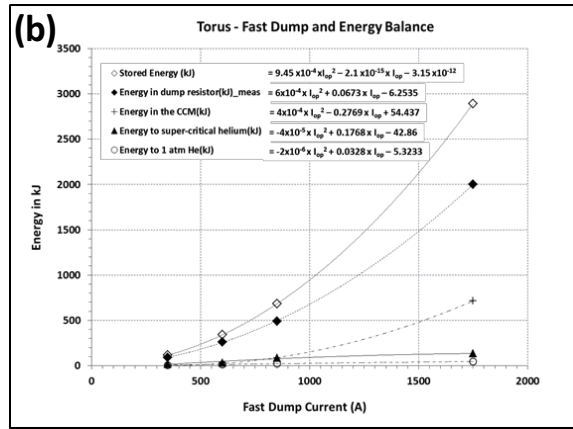
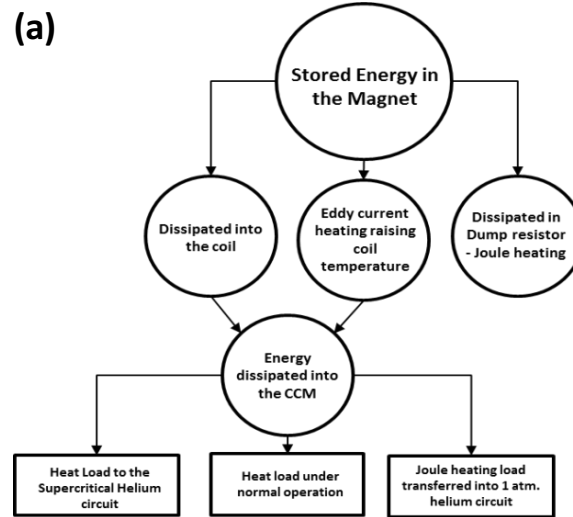


Fig. 53 (a) Flow diagram representing the extraction of stored energy in the magnet during a fast dump or in the event of a quench, (b) Plots for the energy calculated based on measured data during fast dump events at various operating currents up to 1750 A (approximated with a polynomial fit to the measured data points).

System Energy Balance Modelling - The system heat loads were estimated for each of the energization states planned as part of the

commissioning process. The heat loads were calculated using a Detailed Predictive Model (DPM), which is based on the Wilson model [28]. The DPM assumes a fast dump releasing all the magnet-stored energy (see Figure 53). The DPM predicts that the torus was safe to operate for all energization states and fault scenarios up to the nominal operating current of 3770 A.

After initial testing at low currents, the magnet was ramped up to 3000 A and parked. During this period, an unexpected fast dump was triggered by the PLC comparator controls. Taking advantage of the captured data, the team reviewed the 3000 A fast dump data and the results indicated that the magnet was safe to fast dump from 3770 A.

A maximum temperature (average for all the CCM's) was recorded as <40 K during the 3000 A fast dump. The commissioning tests and analysis as carried out thus validated the pressure relief design and design assumptions for the torus cryogenic system confirming that the system was indeed safe.

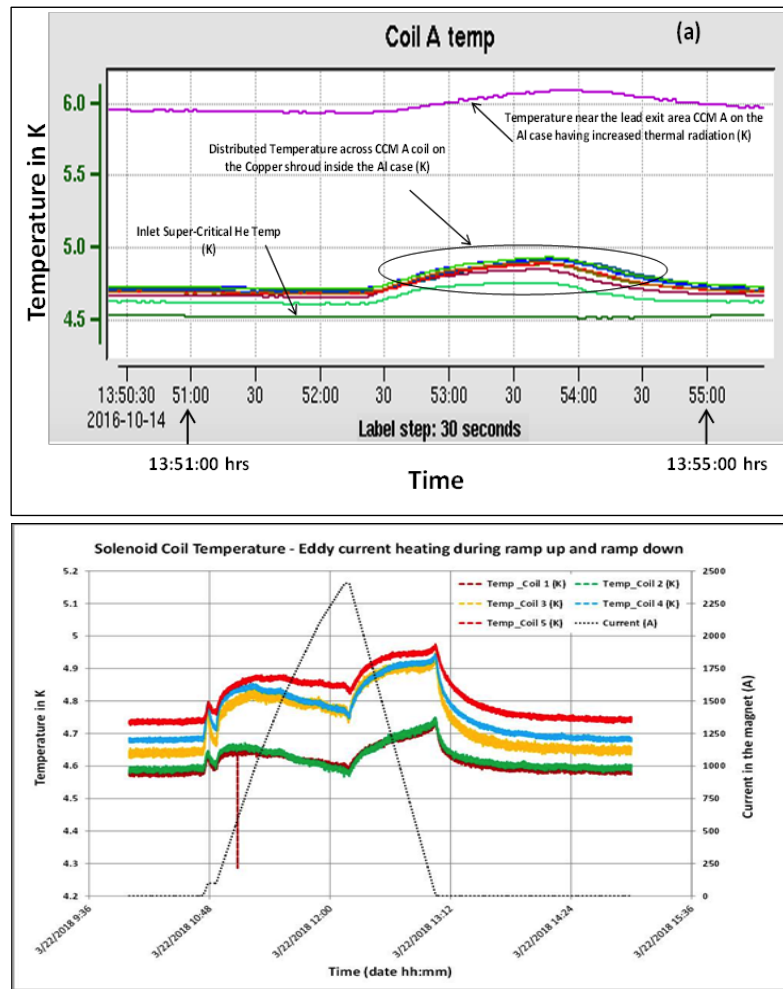


Fig. 54 (a) Torus CCM B temperature rise during a ramp to 150 A at 2 A/s due to eddy current heating, (b) A typical plot of temperature rise in the solenoid coils during normal ramp-up and down.

During commissioning, both the torus and solenoid were energized in steps to full operating current. Predetermined fast dumps were also carried out to check on the instrumentation and proper functioning of the magnet protection. Typical temperature rises of the torus and solenoid magnet coils during ramp up and down to and from full operating current are shown in Figure 54 and are as a

result of eddy current heating within the coils themselves. The temperature rises were modest (no higher than about 0.3 K) and well within the calculated 1.2 to 1.5 K temperature margin of the coils, but were nonetheless used to modify the ramp rates for both magnets to minimize eddy current heating.

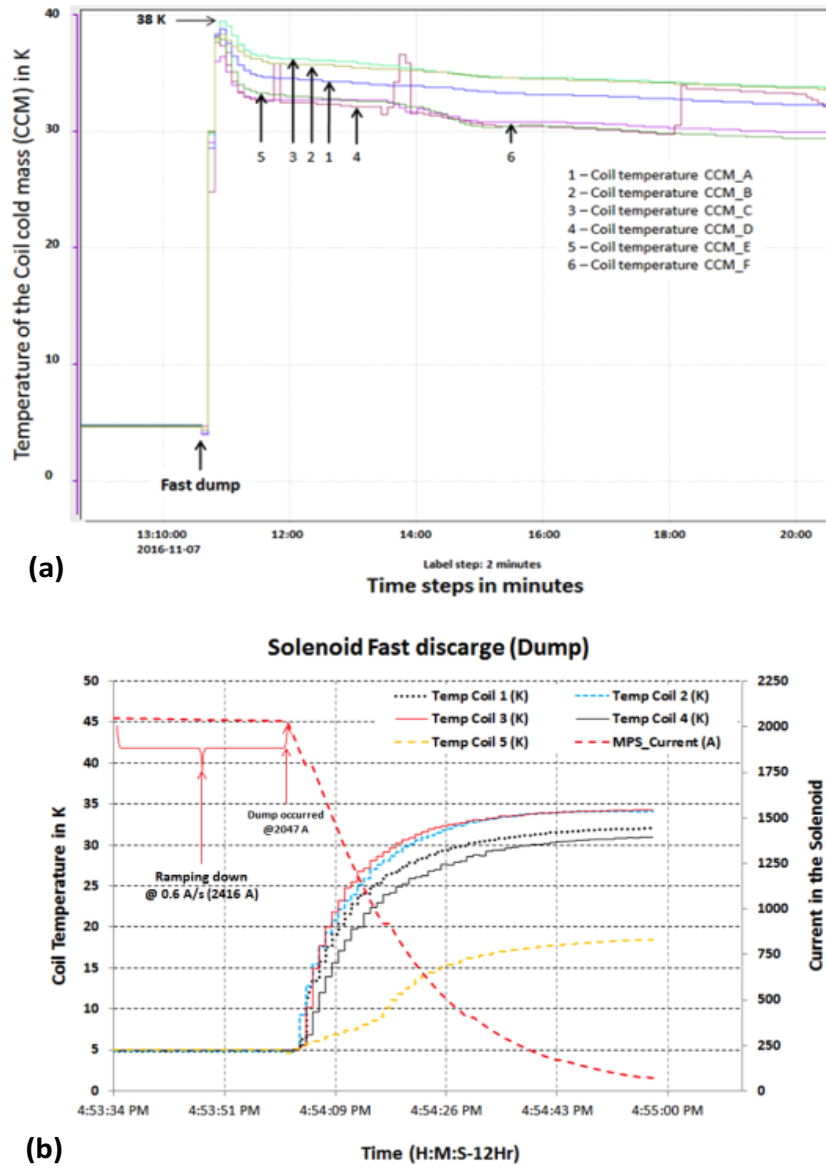


Fig. 55 Coil temperature rise - during a fast dump (a) Torus (b) Solenoid.

As part of the commissioning process, several fast dumps were carried out at low stored energies in the magnet and were found to match well with the predictive models. All tests carried out indicated that both magnets had more than adequate safety margins with regards to pressure relief of sub-systems and coil temperature rise. The coil temperatures recorded during a fast dump event, 3000 A (torus) and 2047 A (solenoid) are shown in Figure 55.

There is a level of electromagnetic coupling between the torus and solenoid coils [29]. As the torus is ramped to full field (3770 A) Figure 56 a shows the change in the OOPS load cell readings for the torus CCM-A. This change in force is small and due to slight

mechanical asymmetry in the spacing between the 6 coils. The solenoid radial and axial load cell readings also change during a ramp up of the solenoid to its full operating current of 2416 A, followed by a controlled ramp down to zero amps (see Figure 56 b). Based on the defined load cell limits, the force experienced by the torus coil within its vacuum jacket during energization is not high enough to initiate a controlled ramp down of the magnet. This behavior is demonstrated by all the 6 torus coils with only minor variations depending on the location of the coil on the magnet due to gravity-loading. This behavior was also noted to be extremely repeatable following many cycles of magnet energization and de-energization. For the solenoid, it is encouraging to note that all the forces revert back to almost the original values after de-energization, illustrating linear response of the coil support structures and it has also been shown from subsequent runs that this process is very repeatable.

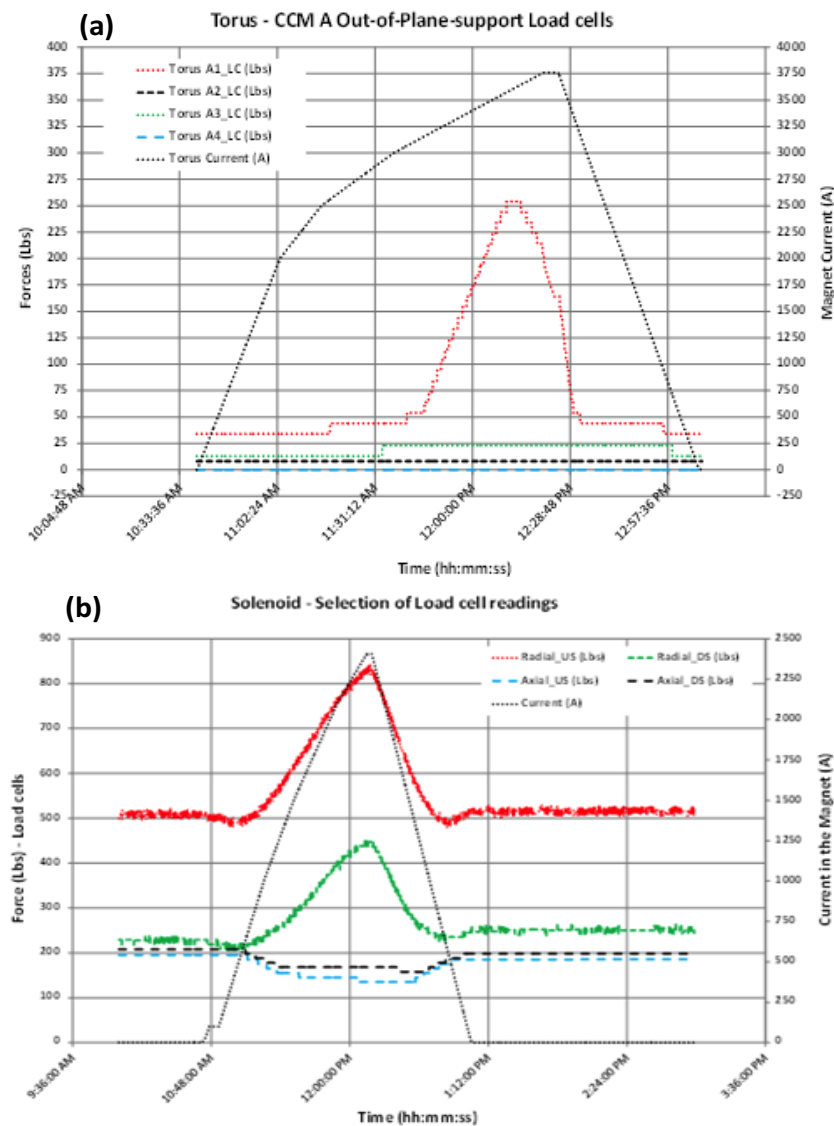


Figure 56 (a) Torus – Change in the Torus CCM-A OOPS load cells during ramp up to the full operating current of 3770 A, followed by a controlled ramp down to zero amps, (b) Solenoid - Change in the radial and axial load cells on the solenoid during a ramp up to the full operating current of 2416 A followed by a controlled ramp down to zero amps.

A. Field Mapping – Torus [30,31]

Forward tracks of charged particles (angles between 5° and 40°) are momentum analyzed by passing through the magnetic field of

the torus. The magnet provides a $\int \mathbf{B} \cdot d\mathbf{l}$ of almost 3 T-m at 5° falling to about 1.0 T-m at 40° . The design requirements are listed in **Table XXV**. Such forward tracks will first traverse the High-Threshold Cerenkov Counter (HTCC) [Ref?] and then enter the first Drift Chamber [Ref?] at a distance of 2.1 m from the target. The track continues through the magnetic field region and its trajectory is measured in two more drift chambers located at 3.3 m and 4.5 m from the target, respectively. The three regions of drift chambers are expected to have spatial resolutions of about 300 μm per layer, which should allow determination of the momentum to better than 0.5% accuracy. This sets the requirement that we know the $\int \mathbf{B} \cdot d\mathbf{l}$ to an accuracy of better than 0.3% at small angles.

The field was mapped at four locations within each coil sector (i.e. between coils) – one measurement at a radius of 30 cm and three measurements at a radius of 46.5 cm but at different Φ angles, as well as within the bore. Multiple measurements were made at each of these locations along the z-axis – i.e. in the direction of the beamline. The mapping equipment consisted of a digital voltmeter, 2 in diameter carbon tube referenced to survey points, three single axis calibrated Hall probes (one for each of the x, y and z axes) positioned in a cylindrical block of Delrin® spaced 5 cm apart in the z-direction, and a control system (for motion, data-recording, and interlocks). A commercially available Group 3 MPT-141 series transverse Hall probes with DTM-151 Tesla-meter was used for the field measurement. The measurement accuracy of the probes and meter at 25°C with a shielded cable length of 300 mm x ø6.5 mm is $\pm 0.01\%$ of reading + 0.006% of full-scale maximum. The Hall probes are temperature compensated and were also surveyed to a positional accuracy of 0.040 mm within the Hall probe holder. Precisely machined plates were attached to the upstream and downstream ends of the torus with matching through holes used to locate long lengths of carbon fiber tubes. The Hall probe holder was moved along the z-axis inside the carbon fiber tubes using a linear slide and stepper motor while magnetic field data was recorded at each measurement point.

The magnetic field measurement fixtures with locations are represented in **Figure 57**.

TABLE XXV
TORUS MAPPER SPECIFICATIONS SUMMARY

Field & Position	Accuracy
B_o	0.1 %
B_r	1 %
B_z	1 %
Radial	$\pm 0.1 \text{ mm}$
Azimuthal	$\pm 0.1 \text{ mm}$
Z-position	$\pm 0.5 \text{ mm}$

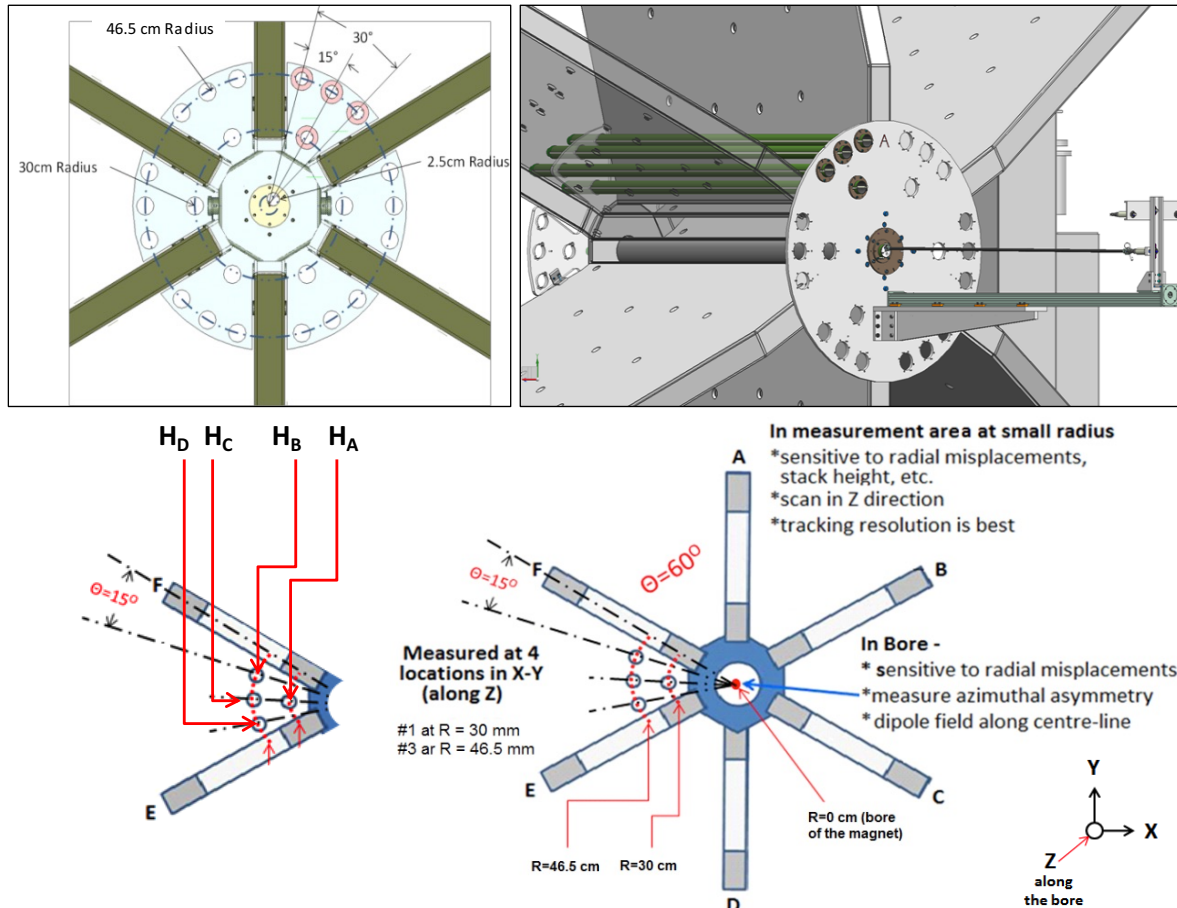
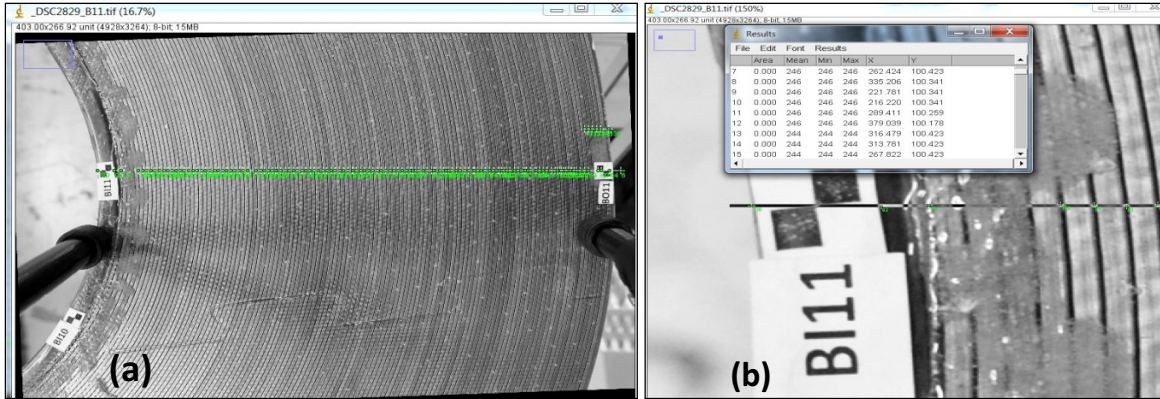


Fig 57 Magnetic field measurement locations – 4 locations in each sector and 7 locations in the bore (1 in the center and 6 spaced 60° apart at a radius of 2.5 cm) – field measured at 5 cm increments in z (along the beam axis) along with the torus magnetic field measurement locations (H_A , H_B , H_C , and H_D are within each sector, i.e. between coils).

The original electromagnetic model was used to generate a field map. This model included thermal contraction but was based on the nominal coil design that did not include the real effects of “dog-boning”, the shimming, or compaction in the areas of tight bend radii. The “dog-boning” of a winding of conductor is the phenomenon that occurs when multiple layers of insulated wire are wound around mandrels that have straight and circular sections such as a rectangle with rounded corners. As additional layers are added, the inner layers are compacted against the winding mandrel at the corners. This compaction tends to decrease the tension in the conductor of the inner turns. If enough compaction occurs then the conductor in the straight sections can go into compression, thus causing it to bow and create space between the turns. In order to avoid producing spaces between turns, pressure along the straight sections can in some cases re-establish the desired conductor location and spacing, the extra material then moves to the corners and this can create a shape that for long narrow coils resembles a dog-bone. As a result, this creates an uneven spacing of conductors with decreased packing density in some portions of the winding. Another cause of dog-boning is that during winding some portions of the conductor can be bent enough to yield into a permanent bend, and unless it is over-bent it will still have portions of it that are not yielded and the conductor will try to spring back into a straighter geometry. This effect produces different levels of radial stress around the winding and thus varies the compaction of the coil, which can affect the packing density.

As stated earlier in the coil fabrication discussion, spacers were added prior to the first potting to allow more accurate and consistent conductor positioning especially closer to the hub. Data from the optical surveys allowed better knowledge of the actual positioning of conductors within the coil (see [Figure 58](#)). This was then used to create a new electromagnetic model of the coil. That model was compared with data from the field map.



[Fig 58](#) A close-up view of a coil near one bend after 1st impregnation (a) Data capture-coil close-up mapping of the location of each turn in the coil (b) Resulting coil co-ordinates from the mapped photos in (a).

Torus Design Model and Analysis: The torus model coil design was carried out using commercial software OPERA-TOSCA from Cobham and field maps were produced as the baseline for magnet field measurement (see [Figure 59](#)). All design models were analyzed utilizing cold (contracted) dimensions with the magnet at its full operating current of 3770 A. The mapping of the field was carried out at 3000 A and the model data was scaled from 3770 A to 3000 A. The measured results obtained were significantly different from the original model data. The results were analyzed to calculate the “distortion field” – i.e. the difference between measured and calculated field values using a chi-squared function (χ^2) that compared the measured data deviation from the nominal modeled field data [32].

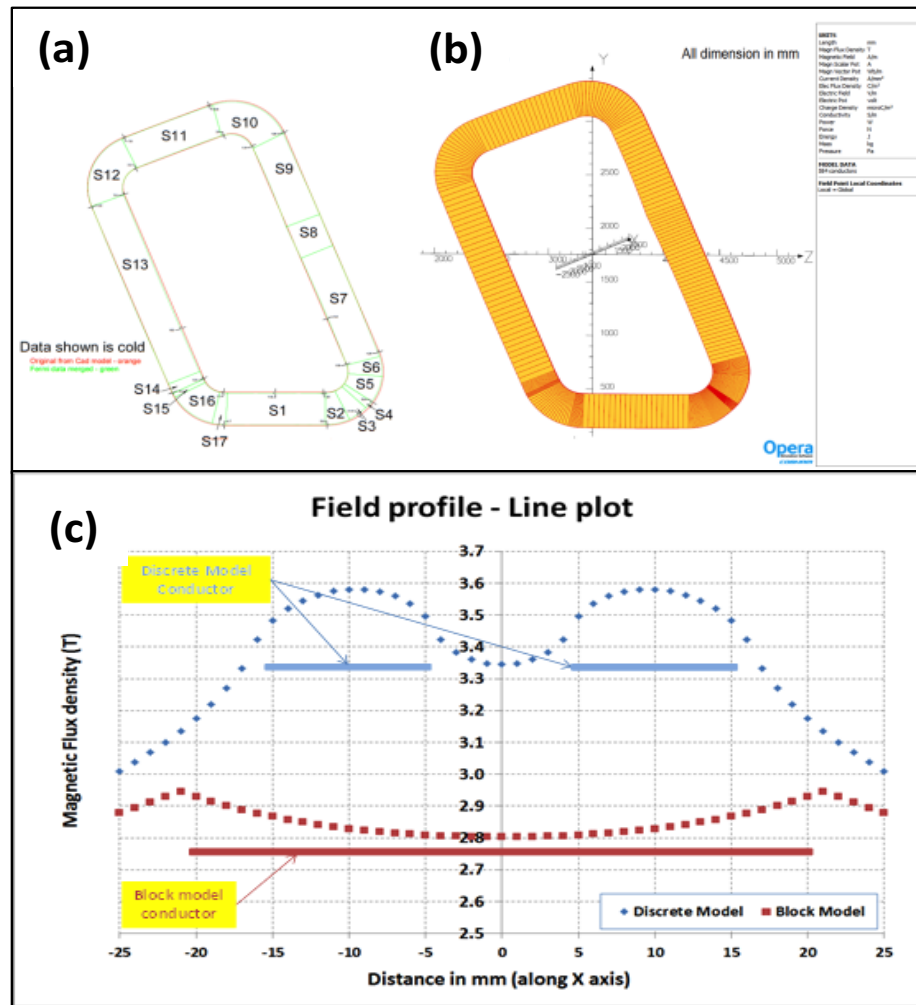


Fig 59 Single pancake of one torus coil (a) Coil survey points from 17 sections in the coil, (b) The design model prepared in Opera® with 17 sections and further discrete subsections, (c) Magnetic flux density variation near and though the coil case of the torus for a simplified version of the conductor (assuming one large contiguous conductor block) and a refined discrete model where the two coil pancakes are modeled individually with current flow only within the superconducting Rutherford cable.

The magnetic field modeling was improved via a 4-stage process:

- **Stage I: Symmetric “Block Model”** - Symmetric ideal coil model (nominal with cold coil dimension, 2 pancake coils simply modeled as one large contiguous block);
- **Stage II: Asymmetric Block Model**- Block model combined with relocated coil position;
- **Stage III: Symmetric “Discrete Model”** - Symmetric coil model with surveyed conductor location (with cold coil dimension), with 2-individual pancakes; Current in individual pancakes considered.
- **Stage IV: Asymmetric Discrete Model** – coil model with surveyed conductor locations combined with relocated coil positions.

The absolute field data plot is presented in [Figure 60](#). The plots show that the variation in the magnetic field distribution is about +4.96 % for the block model and about -0.9 % for the discrete model in a sector, when compared to the measurements.

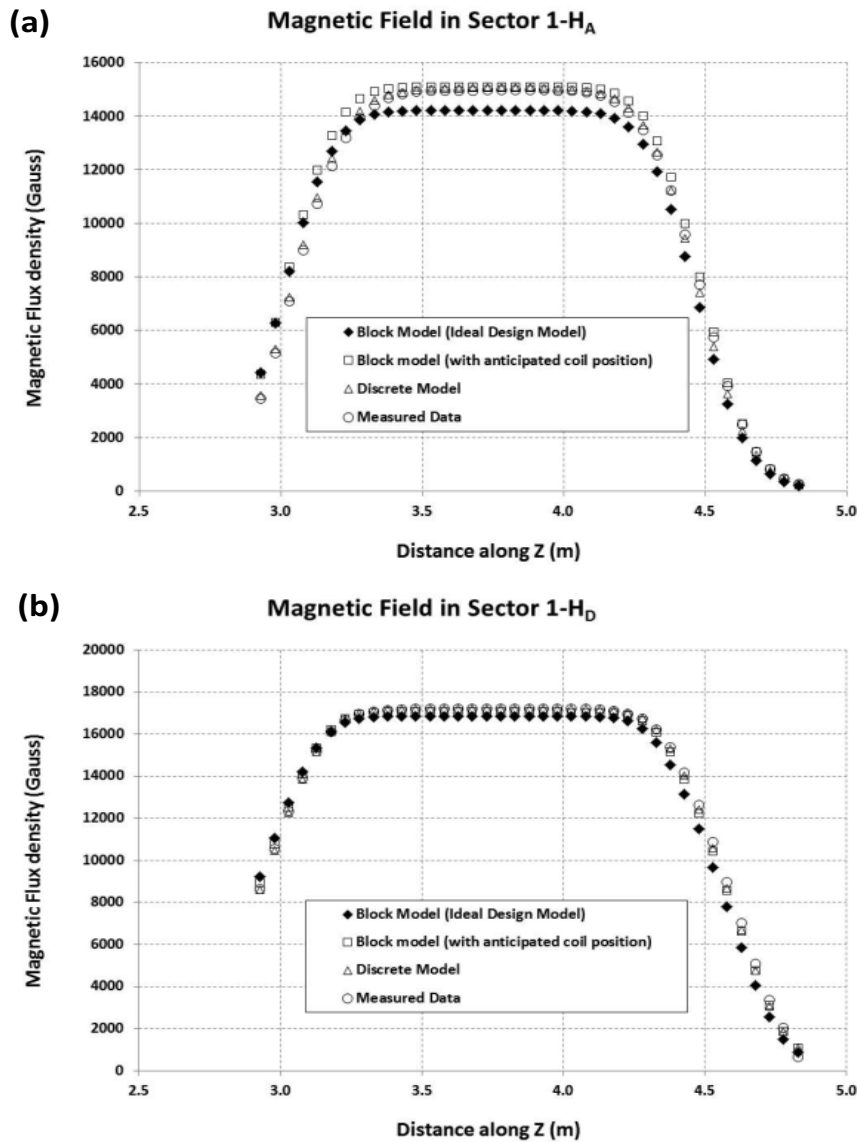


Fig 60 Magnetic flux density distribution (a) sector 1 - H_A (b) sector 1 - H_D, between block model – symmetric, asymmetric and “discrete model” compared with measured data.

Summary of findings - At distances far from the Hub and Coils, all models accurately represent the field, but since the detector needs a model that accurately represents the field at small angles (near the hub), as well as over a large azimuthal angle in Φ (from one coil to the next), only the discrete model should be used.

- The percentage variations cited are for one-to-one comparisons using two-dimensional percentage analysis (*block model and discrete model*) and the averages were calculated separately based on χ^2 .
- Average inner (30 cm radial position) measurements indicate a 0.5% deviation from the measured data.
- Average outer (46.5 cm radial position) measurements indicate a 0.05% deviation from the measured data.
- Fluctuations in the inner measurement deviations are consistent and attributed to the effect of a 1.5 mm change to the outer radius of the coil shape.

Solenoid field mapping - Measurements were carried out to establish the following:

- a. To quantify the magnetic length of the solenoid.
- b. To verify the high homogeneity region (over a 25 mm diameter x 40 mm length cylinder) at the center of the magnet.
- c. To measure the magnetic fringe fields at the specified detector locations.

The torus mapper was adapted for the field mapping of the solenoid magnet [33]. The external fixture holds the 2 in diameter carbon fiber tubes at precise x-y positions and uses a linear stage drive to move the probes in the z-direction.

ection. The Hall probe holder was placed within the carbon-tube in order to zero the z-position of the linear slide before the start of the z-map for the particular location in question. The z-map consisted of driving the Hall probe holder in 5 cm steps along z and pausing for 5 s for the Hall probes to settle before recording the probe data for each of the 3-sensors. Figure 61 shows the typical arrangement for the solenoid magnet field measurement along the bore and off-center locations.

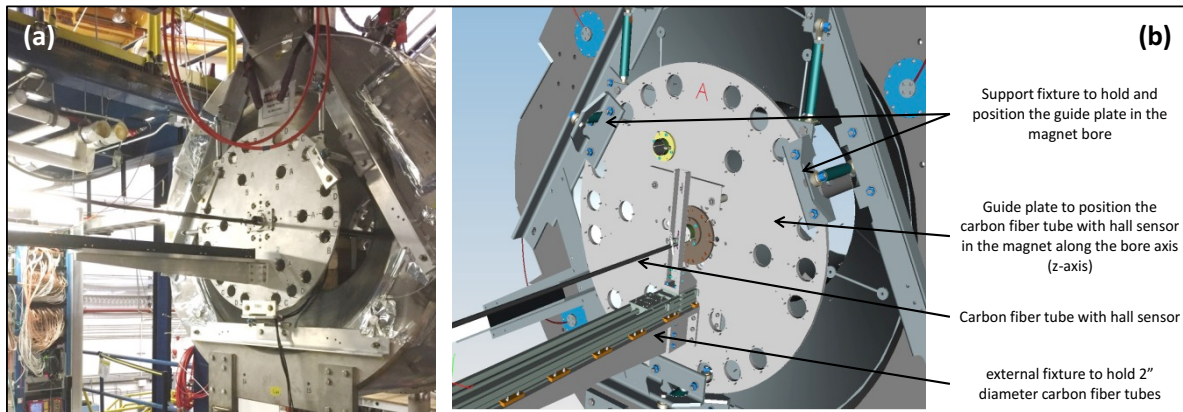


Fig 61 Typical arrangement for solenoid magnet field measurement along the bore and off-center locations

During commissioning of the solenoid magnet, the field mapping was carried out at different operating currents in order to confirm the design specifications. Field mapping was performed along the z direction at 9 locations; one at the geometrical center of the magnet and at 8° to 45° positions at a radius of 12.5 mm. The magnetic field was also measured along the z-axis at a 30 cm radius at a 60° angle from horizontal. To verify the field homogeneity of the magnet, measurements were taken at the center of the magnet at 10 mm intervals along the z-axis.

The magnet length, L, defined as $B_0^{-1} \int B \cdot dl$ was measured to be 1.41 m. The measured homogeneity, $\Delta B/B_0$ over a 40 mm long x φ25 mm cylinder was better than 300 ppm and satisfied present physics experimental requirements. To achieve the desired 100 ppm for planned future polarized target experiments, the JLab Target Group is intending to design and install small superconducting corrector coils that will be positioned directly over the target. Fringe field measurements at the detector locations were carried out using a hand-held field probe and a template board to help position the probe.

The central field of the solenoid is 5 T, but the Hall sensors were calibrated only to 3 T. Therefore, field mapping was limited to 3 T (corresponding to an operating current of 1450 A). The central field at higher currents was verified using an NMR probe.

Another limitation of this mapper was the extent to which it could map in the z-direction, as the linear stage was limited to about 1.9 m. The measured field over this length was compared with the model data to find the effective length of the magnet. Field mapping results are summarized in [Table XXVI](#).

TABLE XXVI
SOLENOID – REQUIRED AND MEASURED PERFORMANCE PARAMETERS

Performance parameter	Broad specification	Actual measured
B_0	5T	5.0 T
$L = B_0^{-1} \int B \cdot dl$ (B_0 field at the center (0,0,0) of solenoid)	$L = 1$ to 1.4 m	1.41 m
Field uniformity in target area	$\Delta B/B_0 < 10^{-4}$ in cylinder 0.04 mm length x 0.025 mm (100 ppm)	318 ppm <i>(to be improved using superconducting corrector coils around the target)</i>
Field at HTCC PMTs location	$B < 35$ G - for the four HTCC PMT locations	$B = 6-22$ G
Field at CTOF PMT locations	$B < 1200$ G - for the two CTOF PMT locations	$B = 43-1041$ G

The mapped data was compared with the as-wound cold-contracted (4.5 K) coil model data. There is still a slight discrepancy between the two data sets for the central field and the field at a radius of 30 cm. The model uses 208 block conductors, as follows - each layer for the inner and intermediate coils is assumed to be one block conductor, while each layer for the shield coil has been split into 2 block conductors:

- 2*42 layers for inner coils (84 block conductors)
- 2* 46 layers for intermediate coils (92 block conductors)
- The shield coil has 16 layers, but each layer was divided into 2 block conductors (32 block conductors)

The discrepancy between the model and measured data could be attributed to coil positioning errors or coil movement during energization. The theoretical model is being improved to better match the mapped data. One of these improvements involves moving the inner and intermediate coils radially or axially - these results are shown in [Figures 62, 63, 64, and 65](#). [Figure 62 \(a\)](#) shows the field in the central region while [Figure 62 \(b\)](#) shows the off-axis field data. It is clear from [Figure 62](#) that inner coil axial movement alone is not sufficient to reproduce the mapped data. [Figure 63](#) shows the same data with radial movement of the inner coils and again the mapped data and data modeled with this radial change do not match. [Figures 64 and 65](#) show similar data with the middle (intermediate) coil moved axially and radially. It is clear from the manipulation of the modeled data that a single coil movement alone cannot fully explain the variation between the modeled and mapped data. A combination of inner and middle coil movement together with a movement variation in the shield coil might result in a better match between model and mapped data. This work is still in progress.

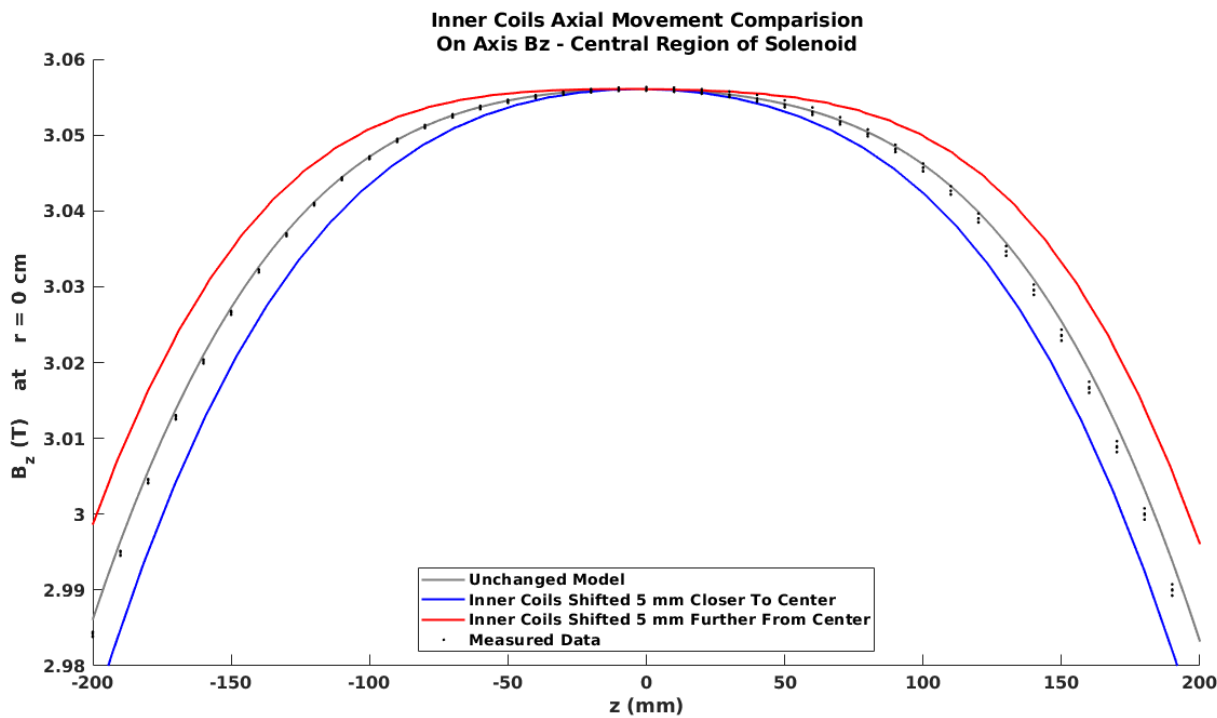


Fig 62 (a) Comparison of model and mapped data at $r=0$ cm with inner coils moved axially.

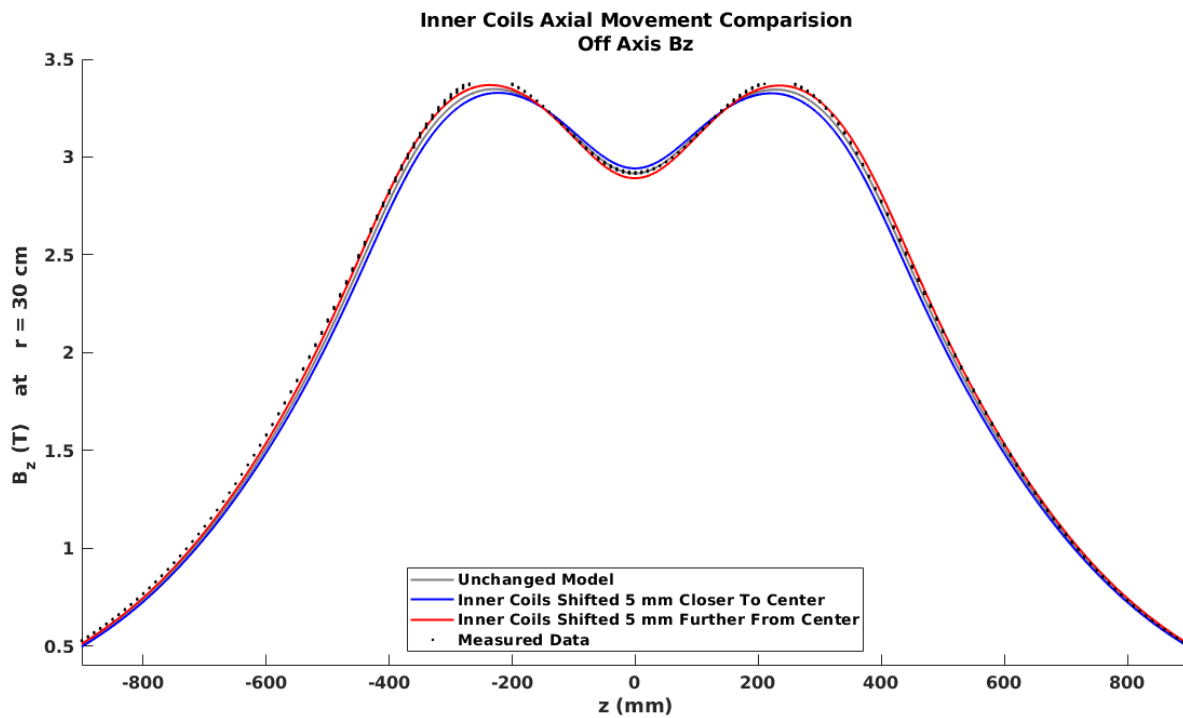


Fig 62 (b) Comparison of model and mapped axial data at $r=30$ cm with inner coils moved axially.

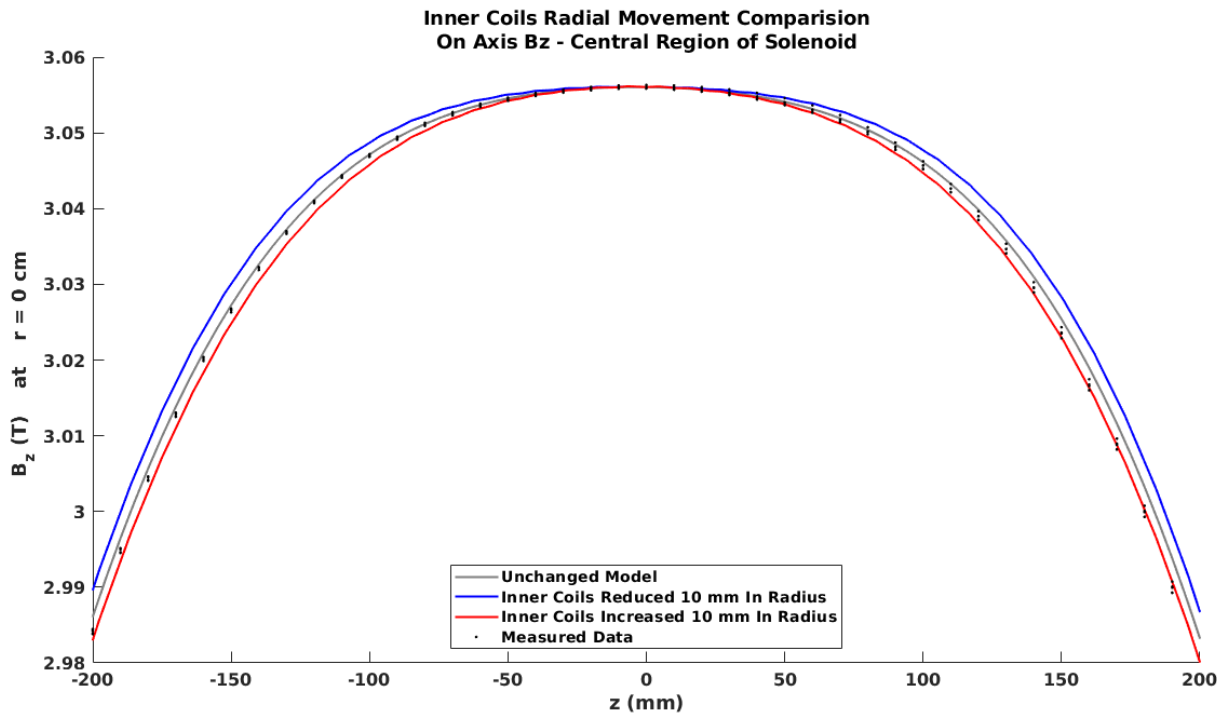


Fig 63 (a) Comparison of model and mapped data at $r=0$ cm with inner coils moved radially.

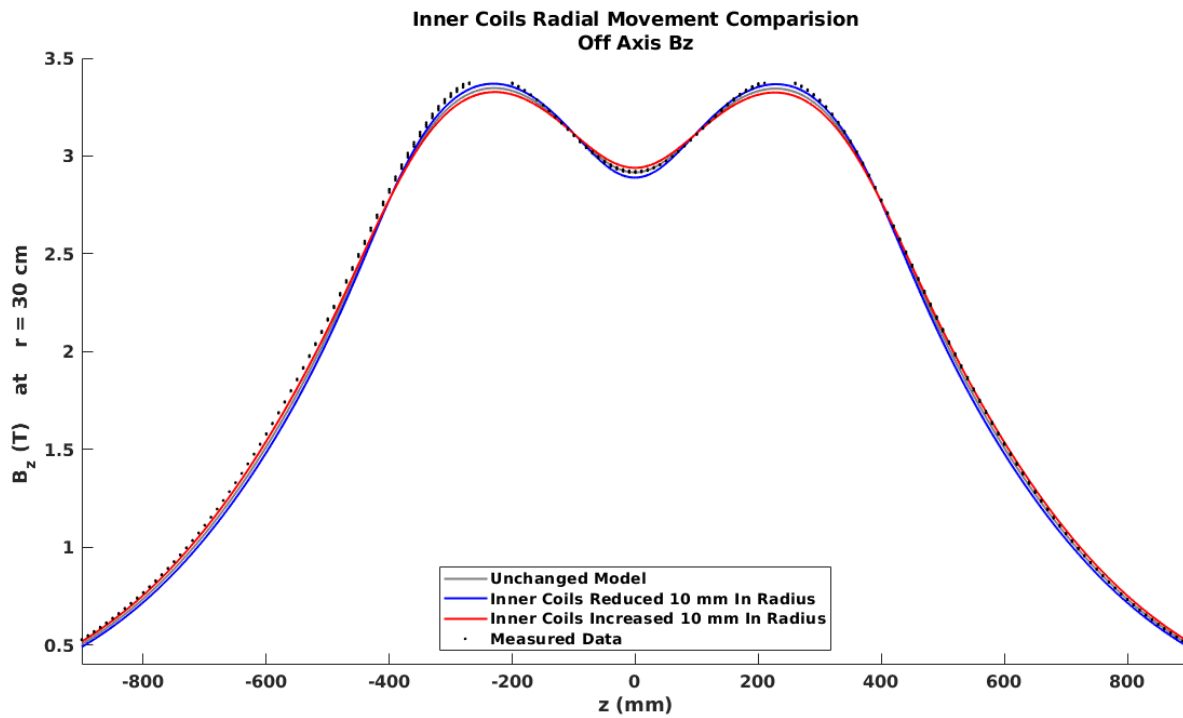


Fig 63 (b) Comparison of model and mapped axial data at $r=30$ cm with inner coils moved radially.

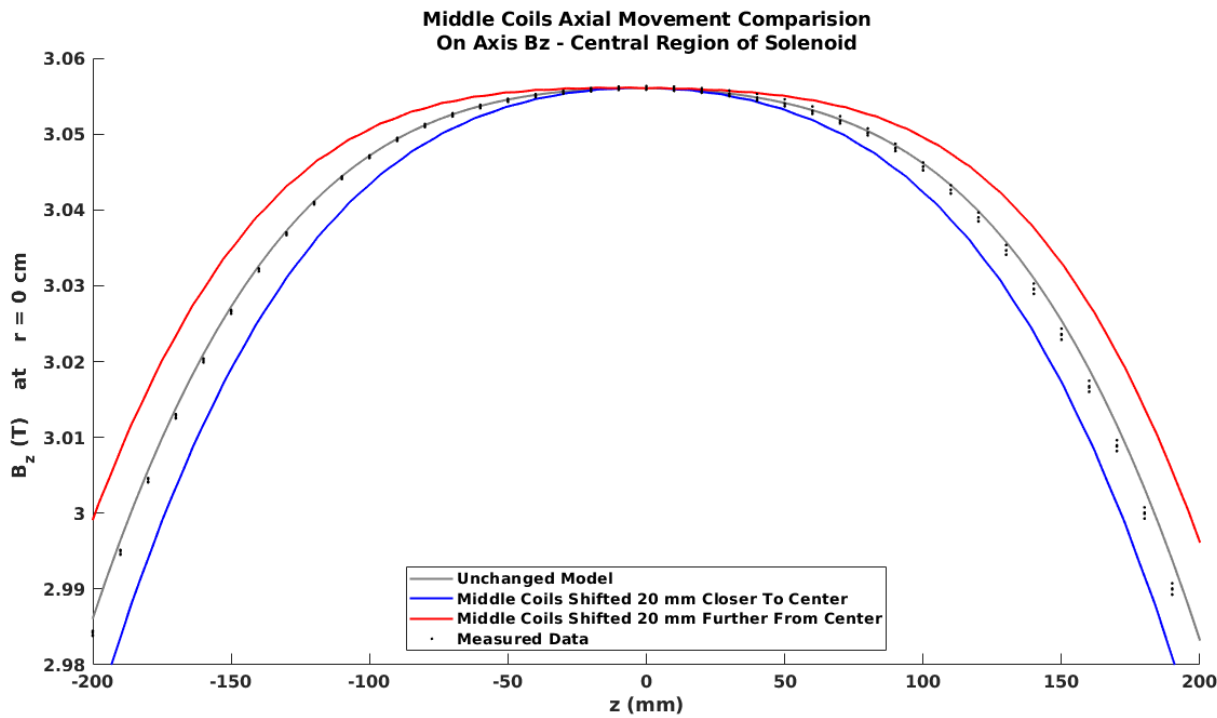


Fig 64 (a) Comparison of model and mapped data at $r=0$ cm with middle (intermediate) coils moved axially.

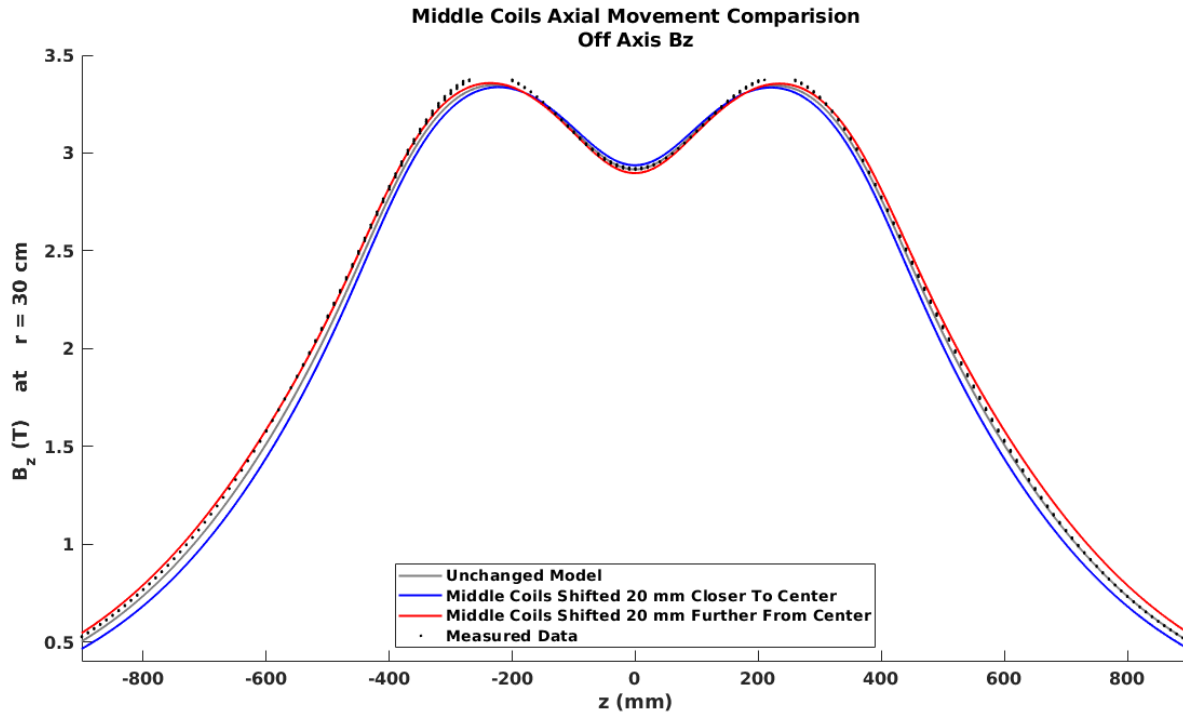


Fig 64 (b) Comparison of model and mapped axial field data at $r=30$ cm with middle (intermediate) coils moved axially.

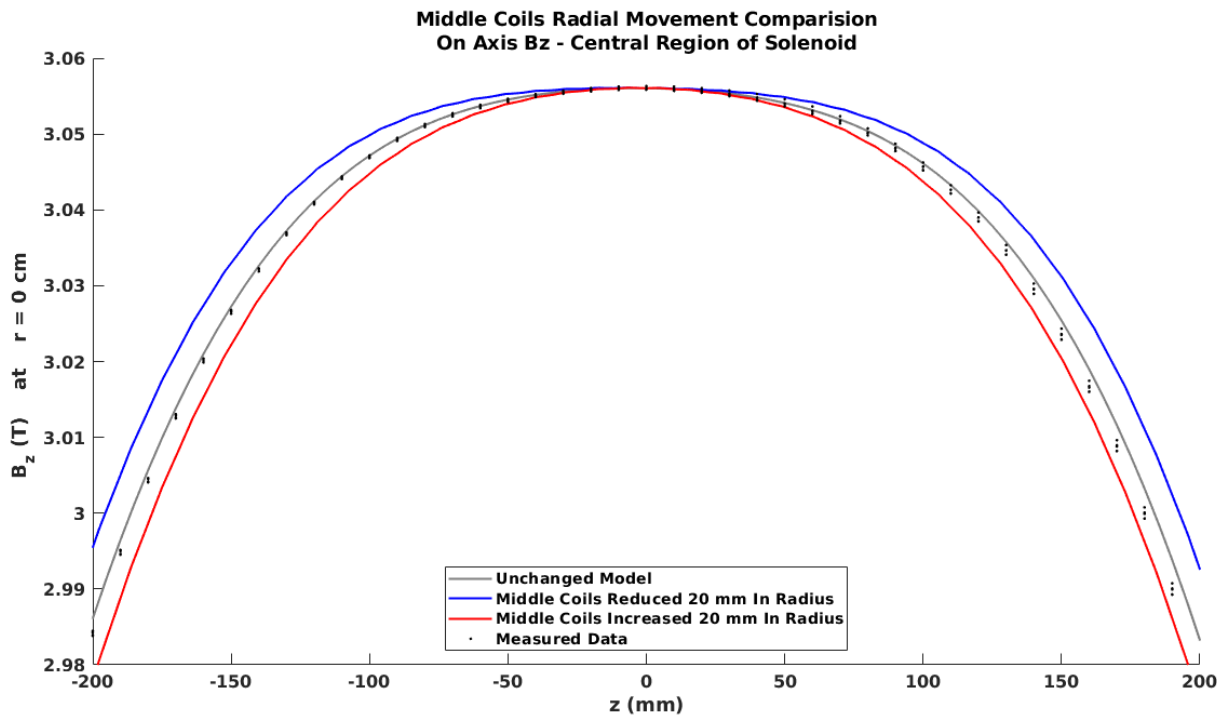


Fig 65 (a) Comparison of model and mapped data at $r=0$ cm with middle (intermediate) coils moved radially .

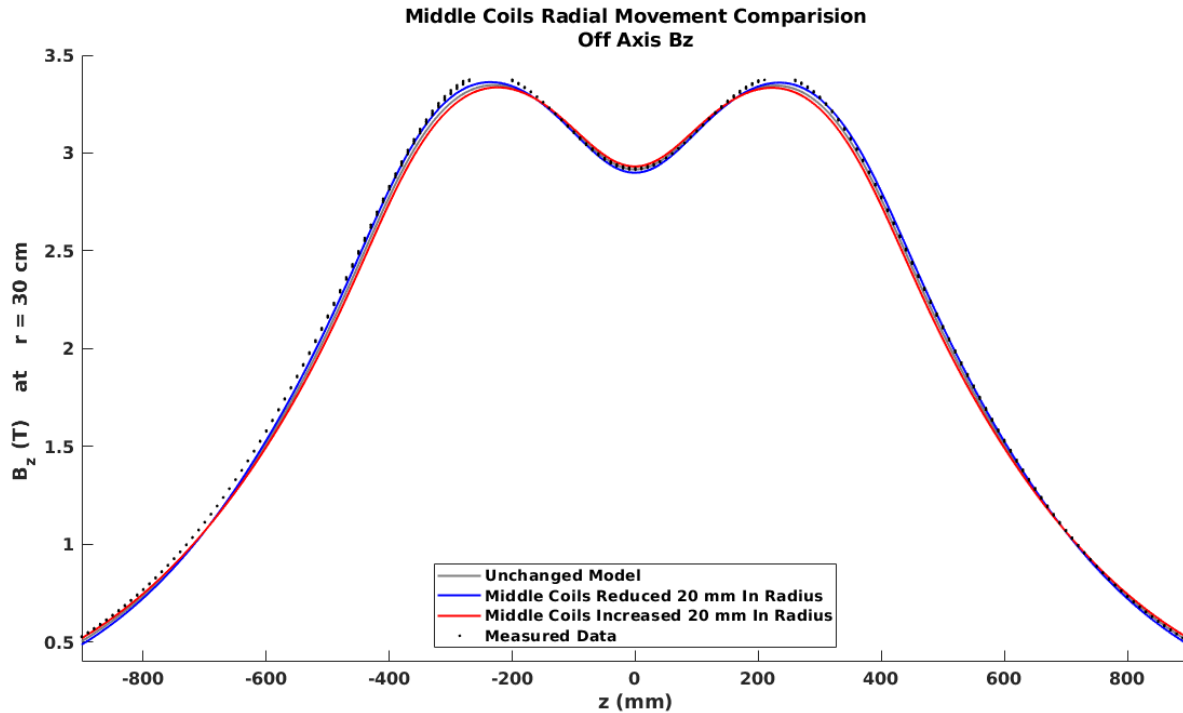


Fig 65 (b) Comparison of model and mapped radial field data at $r=30$ cm with middle (intermediate) coils moved axially.

Summary

As with any typical project, the key drivers were technical reliability, schedule, and cost. These drivers encouraged the team to adopt and extensively use the Failure Modes and Effects Analysis (FMEA) methodology for both magnets from design through to installation and commissioning. Regular reviews such as the Magnet Advisory Group review, JLab Director's Reviews, and U.S. Department of Energy Office of Project Assessment Reviews provided a clear focus and boundaries for the JLab project team. The skills, resourcefulness, and outstanding work ethic of the members of the 12 GeV Magnet Task Force, coupled with the support and commitment of other groups and departments within the laboratory, enabled the project team to flex its planning, management, and execution strategies to overcome all manner of obstacles, including sub-standard potting of torus coils, vendor quality issues on the distribution box, cool down issues involving vertical supports for the torus, and the later than expected delivery of the solenoid to name the key ones.

Ultimately both the superconducting torus and solenoid magnets developed and constructed to be used for the new CLAS12 spectrometer have met the required system specifications that will enable the full physics program to be carried out.

Acknowledgements

The authors would like to acknowledge the contributions and support from all Hall B staff, the DC Power Group, Cryogenics Group, Detector Support Group, SRF - Assembly & Test, Procurement Team, Travel, Human Resources, Planning, Finance, Information and Technology (IT), JLab management and, in particular, Allison Lung, Claus Rode, and the technicians at JLab. The authors would also like to thank reviewers, to name a few in particular, Soren Prestemon (LBNL), Bob Flora (FNAL), V. Rao Ganni (MSU), and Herman Ten Kate (CERN). This material is based upon work supported by the U.S. Department of Energy, Office of Science, Office of Nuclear Physics under contract DE-AC05-06OR23177. The U.S. Government retains a non-exclusive, paid-up, irrevocable, world-wide license to publish or reproduce the published form of this manuscript, or allow others to do so, for United States Government purposes.

REFERENCES

1. Fair, R. J. & Young, G. L., "Superconducting Magnets for the 12 GeV Upgrade at Jefferson Laboratory", *IEEE Transactions on Applied Superconductivity*, V25 (3), 2015, DOI - 10.1109/TASC.2014.2365737.
2. Luongo, C., Ballard, J., Biallas, G., Elouadrhiri, L., Fair, R., Ghoshal, P., et al., "The CLAS12 Torus Detector Magnet at Jefferson Lab.", *IEEE Transactions on Applied Superconductivity*, V26 (4), 2016, DOI - 10.1109/ TASC.2015.2510336.
3. Krave, S., Velev, G., Makarov, A., Nobrega, F., Kiemschies, O., Robotham, B., et al., "Overview of Torus magnet coil production at Fermilab for the Jefferson Lab 12-GeV Hall B upgrade", *IEEE Transactions on Applied Superconductivity*, V26 (4), 2016, DOI 10.1109/TASC.2016.2533264.
4. Ghoshal, P. K., Bachimanchi, R., Fair, R. J., Kashy, D., Rajput-Ghoshal, R., Hogan, J., Sandoval, N., Young, G., "Instrumentation and Control Selection for the 12 GeV Hall-B Magnets at Jefferson Lab", *Supercon. Sci. and Tech.*, V31 (9), 095007, 2018, DOI: 10.1088/1361-6668/aad277.
5. Ghoshal, P. K., Biallas, G., Fair, R. J., Rajput-Ghoshal, R., Schneider, W., Legg, R., et al., "FMEA on the Superconducting Torus for the Jefferson Lab 12GeV Accelerator Upgrade", *IEEE Transactions on Applied Superconductivity*, V25 (3), 4901005, 2015, DOI - 10.1109/TASC.2015.2388591.
6. Ghoshal, P., Pastor, O., Kashy, D., Schneider, W., Wiseman, M., Zarecky, M., et al., "Electromagnetic and Mechanical Analysis of the Coil Structure for the CLAS12 Torus for 12 GeV Upgrade", *IEEE Transactions on Applied Superconductivity*, V25(3), 4500705, 2015, DOI 10.1109/TASC.2014.2382604.
7. de Hoog, F. R., Coijnsen, M., Yuen, W. Y. D. and Huynh, H. N., "Predicting Winding Stresses for Wound Coils of Linear Orthotropic material", in *Proc. Instrumentation Mech. Engineers, Part C, J. Mechanical Engineering Science*, 218 (C1), 13–25, 2004.
8. Li, S and Cao, J., "A Hybrid Approach for Qualifying the Winding Process and Material Effects on Sheet Coil Deformation", *J. Engineering Materials and Technology*, V126, pp. 303-313, July 2004.
9. Knight, C. E., "Residual Stress and Strength Loss in Filament-wound Composites", *Composite Materials: Testing and Design (Eighth Conference)*, Editor: J. D. Whitcomb, ASTM, 1988.
10. Arp, V., "Stresses in Superconducting Magnets", *Journal of Applied Physics*, V48, No. 5, pp. 2026-2036, May 1977
11. Pojer, M., Devred, A & Scandale, W., "A Finite Element Model for Mechanical Analysis of LHC Main Dipole Magnet Coils", *LHC Project Report 1001, Applied Superconductivity Conference (ASC 2006)*, 2006.
12. P. K. Ghoshal, R. J. Fair, D. Hampshire, V. Hagen-Gates, D. Kashy, R. Legg, R. Rajput-Ghoshal, Y. Tsui, "Design and Evaluation of joint resistance in SSC Rutherford type cable splices for Torus magnet for the Jefferson Lab 12 GeV Upgrade," *IEEE Transactions on Applied Superconductivity*, 2016; V26(4), DOI - 10.1109/TASC.2016. 2517922

13. Kashikhin, V., Elouadheri, L., Ghoshal, P., Kashy, D., Makarov, A., Pastor, *et al.*, "Torus CLAS12-Superconducting Magnet Quench Analysis", *IEEE Transactions on Applied Superconductivity*, V24 (3), 2014, DOI - 10.1109/TASC.2014.2299531.
14. Pastor, O., Willard, T., Ghoshal, P., Kashy, D., Wiseman, M., Kashikhin, V., Young, G., Elouadrhiri, L., & Rode, C., "Structural Analysis of Thermal Shields During a Quench of a Torus Magnet for the 12 GeV Upgrade", *IEEE Transactions on Applied Superconductivity*, V25 (3), 2015, DOI-10.1109/TASC.2014.2371820.
15. Fazilleau, P., Ball, J., Hervieu, B., & Pes, C., "CLAS 12 Solenoid Magnet Technical Design Report", *Centre de Scalay, A-CRYOM-02-07-01-01-RT05*.
16. Rajput-Ghoshal, R., Ghoshal, P. K., Fair, R. J., Hogan, J., & Kashy, D, "An investigation into the electromagnetic interactions between a superconducting torus and solenoid for the Jefferson Lab 12 GeV Upgrade", *IEEE Transactions on Applied Superconductivity*, V25 (3), June 2015, DOI - 10.1109/TASC.2014.2372049.
17. Ghoshal, P. K., Bachimanchi, R., Fair, R. J., Gelhaar, D., Kumar, O., Philip, S., & Todd, M., "Superconducting Magnet Power Supply and Hard Wired Quench Protection at Jefferson Lab for 12 GeV Upgrade", *IEEE Transactions on Applied Superconductivity*, V27 (8), 4703006, 2017, DOI - 10.1109/TASC.2017.2759280.
18. Pfeffer, H., Flora, B., & Wolff, D., "Protection of Hardware: Powering Systems (Power Converter, Normal-Conducting, and Superconducting Magnets)", *US Particle Accelerator School, Batavia*, Aug 2016, DOI: 10.5170/CERN-2016-002.343
19. Neilsen, C., "Design Report USA 502337-201, Hall B Torus/Solenoid MPS", *MPS 854 - Danfysik System 8500*, www.danfysik.com, June 2014.
20. Ekelof, S., "The genesis of the Wheatstone bridge", *Engineering Science and Education Journal*, V10 (1), Feb 2001, DOI: 10.1049/esej:20010106
21. *Lakeshore Cryotronics - Cernox temperature sensor technical data* (2017). http://www.lakeshore.com/Documents/LSTC_appendixB_1.pdf, p168, Online at <http://www.lakeshore.com>
22. Compact-sized FPGA development platform for prototyping circuit designs, <http://www.terasic.com.tw/cgi-bin/page/archive.pl?Language=English&CategoryNo=139&No=593>
23. Single Resistor Gain Programmable Precision Instrumentation Amplifier, Online link information at <http://cds.linear.com/docs/en/datasheet/1167fc.pdf>
24. Designers Guide for Applying Instrument Amplifiers Effectively, <http://www.analog.com/media/en/training-seminars/designhandbooks/designers-guide-instrument-amps-chV.pdf>
25. Wiseman, M., Elementi, L., Elouadheri, L., Gabrielli, G., Gardner, T. J., Ghoshal, P. K., *et al.*, "Design and Manufacture of the Conduction Cooled Torus Coils for The Jefferson Lab 12 GeV Upgrade", *IEEE Transactions on Applied Superconductivity*, V25 (3), 2015, DOI 10.1109/TASC.2014.2376964.

26. Legg, R., Kashy, D., Fair, R., Ghoshal, P., Bachimanchi, R., Bruhwel, K., *et al.*, “Liquid Nitrogen Tests of a Torus Coil for the Jefferson Lab 12-GeV Accelerator Upgrade”, *IEEE Transactions on Applied Superconductivity*, V25 (3), 2015, DOI - 10.1109/TASC.2014.2360139.
27. Ghoshal, P. K., Biallas, G., Fair, R. J., Kashy, D., Matalevich, J., & Luongo, C., “Commissioning Validation of CLAS-12 Torus Magnet Protection and Cryogenic Safety System”, *IEEE Transactions on Applied Superconductivity*, V28 (6), 2018, DOI 10.1109/TASC.2018.2841928.
28. Wilson, M. N., “Superconducting magnets,” *Oxford University Press*, UK, 1983, pp158-198.
29. D. Kashy, R. Fair, P. K. Ghoshal, R. Rajput-Ghoshal, “An investigation of the Electromagnetic Interactions between the CLAS12 Torus & Solenoid Superconducting Magnets at JLab”, Presented at ASC2019 (paper details to be added later)
30. Fry, J. R., Ruggiero, G., Bergsma, F., “Precision Magnetic Field Mapping for CERN experiment NA62”, *IOP Publishing, J. Phys. G: Nuclear Particle Physics* 43 (2016) 125004, DOI - 10.1088/0954-3899/43/12/125004
31. Ikeda, T., Chapman, M. D., Igarashi, Y., Imazato, J., Lee, J. M., Khabibullin, M. M., *et. al.*, “High-precision magnetic field mapping with a 3D Hall probe for a T-violation experiment in $K_{\mu 3}$ decay”, Elsevier Publications, Nuclear Instruments and Methods in Physics Research, Sec A, 401, pp243-262, 1997.
32. Ghoshal, P. K., Beck, J. M., Fair, R. J., Kashy, D., Mestayer, M. D., Meyers, J., Newton, J., Rajput-Ghoshal, R., Tremblay, K., Wiggins, C. L., “Magnetic Field Mapping of the CLAS12 Torus—A Comparative Study Between the Engineering Model and Measurements at JLab”, *IEEE Transactions on Applied Superconductivity*, V29 (4), 4000310, 2019, DOI - 0.1109/TASC.2018.2884968.
33. Rajput-Ghoshal, R., Fair, R., Meyers, J., Beck, M., Brakman, D., Mestayer, M., *et al.*, “Field Mapper for Superconducting Torus Magnet for the Jefferson Lab 12GeV Upgrade”, *International Magnetic Meas. Workshop, IMMW-20*, Oxford (UK), June 2017 (Talk).